Identification of the EURO-SEIS Test Structure

Asmussen, J.C.; Andersen, P.; Brincker, Rune; Manos, G. C.

Publication date:
1996

Document Version
Early version, also known as pre-print

INSTITUTTET FOR BYGNINGSTEKNIK
DEPT. OF BUILDING TECHNOLOGY AND STRUCTURAL ENGINEERING
AALBORG UNIVERSITET • AUC • AALBORG • DANMARK

FRACTURE & DYNAMICS
PAPER NO. 76

J. C. ASMUSSEN, P. ANDERSEN, R. BRINCKER & G. C. MANOS
IDENTIFICATION OF THE EURO-SEIS TEST STRUCTURE
MARCH 1996 ISSN 1395-7953 R9612

The FRACTURE AND DYNAMICS papers are issued for early dissemination of research results from the Structural Fracture and Dynamics Group at the Department of Building Technology and Structural Engineering, University of Aalborg. These papers are generally submitted to scientific meetings, conferences or journals and should therefore not be widely distributed. Whenever possible reference should be given to the final publications (proceedings, journals, etc.) and not to the Fracture and Dynamics papers.

Printed at Aalborg University

FRACTURE AND DYNAMICS PAPERS

PAPER NO. 64: P. S. Skjærbæk, S. R. K. Nielsen, A. Ş. Çakmak: *Assessment of Damage in Seismically Excited RC-Structures from a Single Measured Response.* ISSN 1395-7953 R9528.

PAPER NO. 65: J. C. Asmussen, S. R. Ibrahim, R. Brincker: *Random Decrement and Regression Analysis of Traffic Responses of Bridges.* ISSN 1395-7953 R9529.

PAPER NO. 66: R. Brincker, P. Andersen, M. E. Martinez, F. Tallavó: *Modal Analysis of an Offshore Platform using Two Different ARMA Approaches.* ISSN 1395-7953 R9531.

PAPER NO. 67: J. C. Asmussen, R. Brincker: *Estimation of Frequency Response Functions by Random Decrement.* ISSN 1395-7953 R9532.

PAPER NO. 68: P. H. Kirkegaard, P. Andersen, R. Brincker: *Identification of an Equivalent Linear Model for a Non-Linear Time-Variant RC-Structure.* ISSN 1395-7953 R9533.

PAPER NO. 69: P. H. Kirkegaard, P. Andersen, R. Brincker: *Identification of the Skirt Piled Gullfaks C Gravity Platform using ARMAV Models.* ISSN 1395-7953 R9534.

PAPER NO. 70: P. H. Kirkegaard, P. Andersen, R. Brincker: *Identification of Civil Engineering Structures using Multivariate ARMAV and RARMAV Models.* ISSN 1395-7953 R9535.

PAPER NO. 71: P. Andersen, R. Brincker, P. H. Kirkegaard: *Theory of Covariance Equivalent ARMAV Models of Civil Engineering Structures.* ISSN 1395-7953 R9536.

PAPER NO. 72: S. R. Ibrahim, R. Brincker, J. C. Asmussen: *Modal Parameter Identification from Responses of General Unknown Random Inputs.*ISSN 1395-7953 R9544.

PAPER NO. 73: S. R. K. Nielsen, P. H. Kirkegaard: *Active Vibration Control of a Monopile Offshore Structure. Part One - Pilot Project.* ISSN 1395-7953 R9609.

PAPER NO. 74: J. P. Ulfkjær, L. Pilegaard Hansen, S. Qvist, S. H. Madsen: *Fracture Energy of Plain Concrete Beams at Different Rates of Loading.* ISSN 1395-7953 R9610.

PAPER NO 75: J. P. Ulfkjær, M. S. Henriksen, B. Aarup: *Experimental Investigation of the Fracture Behaviour of Reinforced Ultra High Strength Concrete.* ISSN 1395-7953 R9611.

PAPER NO. 76: J. C. Asmussen, P. Andersen: *Identification of EURO-SEIS Test Structure.* ISSN 1395-7953 R9612.

PAPER NO. 77: P. S. Skjærbæk, S. R. K. Nielsen, A. Ş. Çakmak: *Identification of Damage in RC-Structures from Earthquake Records - Optimal Location of Sensors.* ISSN 1395-7953 R9614.

Department of Building Technology and Structural Engineering
Aalborg University, Sohngaardsholmsvej 57, DK 9000 Aalborg
Telephone: +45 98 15 85 22 Telefax: +45 98 14 82 43

FRACTURE AND DYNAMICS PAPERS

PAPER NO. 47: P. H. Kirkegaard & A. Rytter: *Use of Neural Networks for Damage Assessment in a Steel Mast.* ISSN 0902-7513 R9340.

PAPER NO. 48: R. Brincker, M. Demosthenous & G. C. Manos: *Estimation of the Coefficient of Restitution of Rocking Systems by the Random Decrement Technique.* ISSN 0902-7513 R9341.

PAPER NO. 49: L. Gansted: *Fatigue of Steel: Constant-Amplitude Load on CCT-Specimens.* ISSN 0902-7513 R9344.

PAPER NO. 50: P. H. Kirkegaard & A. Rytter: *Vibration Based Damage Assessment of a Cantilever using a Neural Network.* ISSN 0902-7513 R9345.

PAPER NO. 51: J. P. Ulfkjær, O. Hededal, I. B. Kroon & R. Brincker: *Simple Application of Fictitious Crack Model in Reinforced Concrete Beams.* ISSN 0902-7513 R9349.

PAPER NO. 52: J. P. Ulfkjær, O. Hededal, I. B. Kroon & R. Brincker: *Simple Application of Fictitious Crack Model in Reinforced Concrete Beams. Analysis and Experiments.* ISSN 0902-7513 R9350.

PAPER NO. 53: P. H. Kirkegaard & A. Rytter: *Vibration Based Damage Assessment of Civil Engineering Structures using Neural Networks.* ISSN 0902-7513 R9408.

PAPER NO. 54: L. Gansted, R. Brincker & L. Pilegaard Hansen: *The Fracture Mechanical Markov Chain Fatigue Model Compared with Empirical Data.* ISSN 0902-7513 R9431.

PAPER NO. 55: P. H. Kirkegaard, S. R. K. Nielsen & H. I. Hansen: *Identification of Non-Linear Structures using Recurrent Neural Networks.* ISSN 0902-7513 R9432.

PAPER NO. 56: R. Brincker, P. H. Kirkegaard, P. Andersen & M. E. Martinez: *Damage Detection in an Offshore Structure.* ISSN 0902-7513 R9434.

PAPER NO. 57: P. H. Kirkegaard, S. R. K. Nielsen & H. I. Hansen: *Structural Identification by Extended Kalman Filtering and a Recurrent Neural Network.* ISSN 0902-7513 R9433.

PAPER NO. 58: P. Andersen, R. Brincker, P. H. Kirkegaard: *On the Uncertainty of Identification of Civil Engineering Structures using ARMA Models.* ISSN 0902-7513 R9437.

PAPER NO. 59: P. H. Kirkegaard & A. Rytter: *A Comparative Study of Three Vibration Based Damage Assessment Techniques.* ISSN 0902-7513 R9435.

PAPER NO. 60: P. H. Kirkegaard, J. C. Asmussen, P. Andersen & R. Brincker: *An Experimental Study of an Offshore Platform.* ISSN 0902-7513 R9441.

PAPER NO. 61: R. Brincker, P. Andersen, P. H. Kirkegaard, J. P. Ulfkjær: *Damage Detection in Laboratory Concrete Beams.* ISSN 0902-7513 R9458.

PAPER NO. 62: R. Brincker, J. Simonsen, W. Hansen: *Some Aspects of Formation of Cracks in FRC with Main Reinforcement.* ISSN 0902-7513 R9506.

PAPER NO. 63: R. Brincker, J. P. Ulfkjær, P. Adamsen, L. Langvad, R. Toft: *Analytical Model for Hook Anchor Pull-out.* ISSN 0902-7513 R9511.

INSTITUTTET FOR BYGNINGSTEKNIK
DEPT. OF BUILDING TECHNOLOGY AND STRUCTURAL ENGINEERING
AALBORG UNIVERSITET • AUC • AALBORG • DANMARK

FRACTURE & DYNAMICS
PAPER NO. 76

J. C. ASMUSSEN, P. ANDERSEN, R. BRINCKER & G. C. MANOS
IDENTIFICATION OF THE EURO-SEIS TEST STRUCTURE
MARCH 1996
ISSN 1395-7953 R9612

Identification of the EURO-SEIS Test Structure

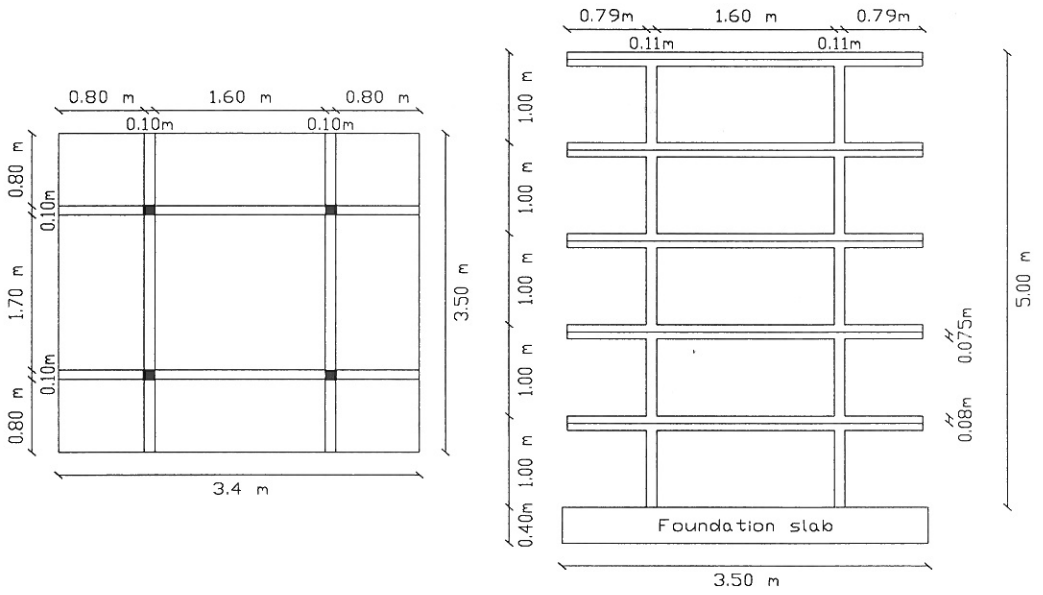

J.C. Asmussen, P. Andersen & R. Brincker

Department of Building Technology and Structural Engineering
Aalborg University
DK-9000 Aalborg, Denmark.

G.C. Manos

Department of Civil Engineering
Aristotle University
GR-54006 Thessaloniki, Greece.

March 1996

CONTENTS

PREFACE

In the summer of 1995 the Ph.D.-students John Christian Asmussen and Palle Andersen from the Department of Building Technology and Structural Engineering, Aalborg University, Denmark, visited the Department of Civil Engineering, Aristotle University of Thessaloniki, Greece.

During this period, they were attached to the EURO SEISTEST project under guidance of Professor G.C. Manos (Aristotle University) and Professor R. Brincker (Aalborg University). The aim of the work was system identification of the EURO SEISTEST test structure, located at the Volvi test site in Greece. This report presents the results from identification of the structure using four different approaches.

All figures and tables of chapters 1-3 and 5 are presented in the text. All figures related to the actual measurements and results of chapter 2 and 4 are presented in appendix A.

ABBRIVATIONS AND ACRONYMS

AR(n)	Auto-Regressive (univariate) model of order n
ARV(n)	Auto-Regressive Vector (multivariate) model of order n
ARMA(n,m)	Auto-Regressive Moving Average (univariate) model of order n in the auto regressive polynomial, and of order m in the moving average polynomial.
ARMAV(n,m)	Auto-Regressive Moving Average Vector (multivariate) model of order n in the autoregressive matrix polynomial, and of order m in the moving average matrix polynomial.

1 INTRODUCTION

1.1 Description of EURO SEISTEST

This section describes the EURO SEISTEST project and the test site model structure. It includes the general objectives of the project, the location of the test site, a technical description of the structure, and the instrumentation. Furthermore, the purpose of the analysis is presented.

1.1.1 General Objectives of the EURO SEISTEST

The primary objectives of EURO SEISTEST project are to establish a European test site for engineering seismology and earthquake engineering. A test-site, where high-quality seismic recordings can be gathered over a long period of time, in a very well-defined seismological, geological, geotechnical, and structural environment.

One of the general objectives is the improvement of seismic hazard assessment through a careful monitoring of the local seismicity and of its consequences on ground motion in a well-known geophysical environment. Another objective is the improvement of seismic design and analysis criteria for typical structures in earthquake prone areas, in order to mitigate the damage and losses from future earthquake events. It is expected that during the monitoring period of the test structure at least one earthquake greater than Ms=5.0 will occur.

1.1.2 Location of Test Site

The test site is located at a sediment-filled valley 30 km north-east of Thessaloniki (Greece) at the village Stivos between the lakes Agios Vassilios and Volvi. This test area fulfils three major requirements: Wide accessibility, significant seismic activity, and representative soil conditions.

1.1.3 Technical Description of Test Structure

The test site structure is a model of a 5-storey building in scale 1:3. The final structure is symmetrical consisting of reinforced concrete columns, reinforced concrete slabs, and with masonry infill between the columns. The overall height is 5 m (each storey is 1 m), and it is founded on a concrete slab, see figure 1.1.

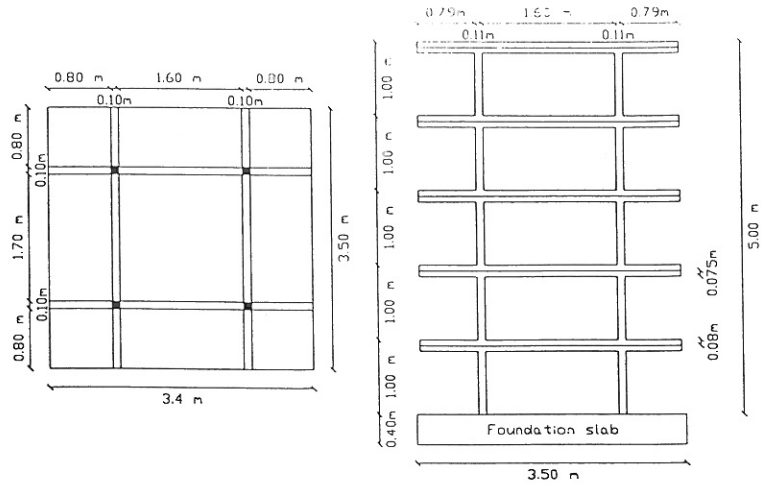

Figure 1.1: The test site structure, plan and cross section.

The data used in this report are measured during the period before the masonry infill was constructed. Three cases are considered: The first case is the naked (symmetrical virginal) structure, consisting only of the reinforced concrete columns and reinforced concrete slabs, see figure 1.2a. In the second case steel diagonals have been attached between the columns on all storeys (symmetrical structure), see figure 1.2b. Finally, in the third case, half of the diagonals on each storey have been removed (unsymmetrical structure), see figure 1.2a. Section two provides a clear description of the actual measurements performed in each of the three cases. For further description of the structure, see Manos et al. [1].

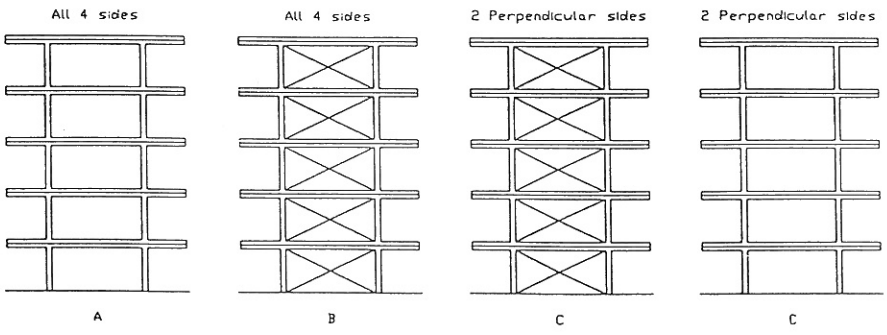

Figure 1.2: a) Naked (virginal) structure. b) Diagonals on all sides of each storey.
c) Half of the diagonals of each storey has been removed.

1.1.4 Instrumentation

The structure is permanently instrumented with sixteen accelerometers. Each storey has three accelerometers installed, one in the x-directional centre line, one in the y-directional center line, and one on the edge pointing in the x-direction, see figure 1.3. References to the coordinate system in figure 1.3 will be made during the report.

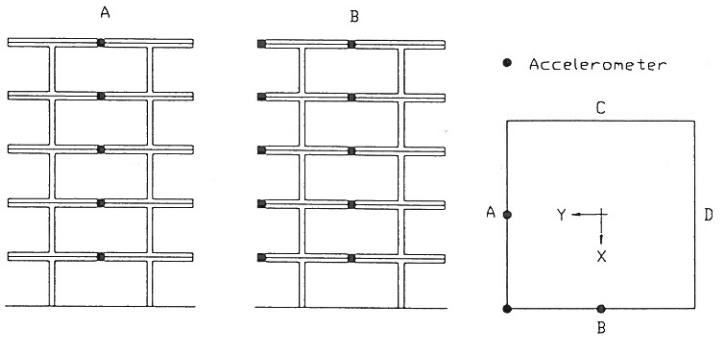

Figure 1.3: Positions of accelerometers on the structure.

An additional accelerometer is mounted on the foundation block, in order to measure the ground motion. This accelerometer is not plotted on the figure since it is not used in the analysis. All accelerometers are connected to a multi-channel acquisition board, operating on a continuous-time basis at the test site. When the response of any of the sixteen channels exceeds a triggering level corresponding to 7% g, the whole system is triggered, and the response of all channels is recorded and stored permanently. A sampling rate equal to 1000 Hz makes it unnecessary to use analog anti-aliasing filters.

1.2 Purpose of Analysis

The purpose of the present analysis is to obtain as good knowlegde about the dynamic behaviour of the structure as possible from the experimental obtained data. This information is of great importance for e.g. validation of a finite element model of the structure. Three different construction states are considered in order to evaluate the sensitivity of the dynamic properties of the structure. First of all, there is a virginal state, only consisting of the concrete slabs, beams, and columns. Secondly, steel diagonals is mounted on two perpendicular sides between the concrete columns, and finally steel diagonals are mounted on all sides.

2 DESCRIPTION OF MEASUREMENTS

This chapter describes the measurements of the structural response. They were conducted at three different states during construction of the structure: Naked symmetrical structure, unsymmetrical structure with diagonals and symmetrical structure with diagonals, as described in figure 1.2.

2.1 Excitation, Measurements, and Data-Preprocessing

In order to excite all structural modes, two different excitation types are used: Pull-out at the centre of the structure and pull-out at the edge of the structure. The two different excitation methods are illustrated in figure 2.1. The figure shows the ideal pull-out methods, which were used in the x-direction. The tests were made by Prof. Manos.

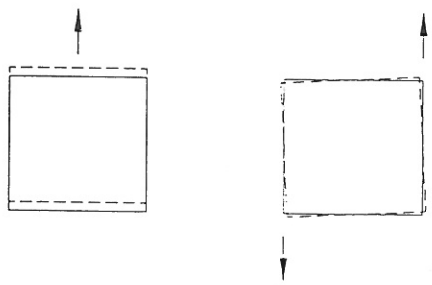

Figure 2.1: Ideal pull-out methods.

If the structure is symmetrical and linear, centre pull out should only excite translational modes, while edge pull-out should only excite rotational modes. Since, in practice, the ideal pull-outs are difficult to perform the edge pull-out migth also excite translational modes. Also, non-linear stiffness relation migth cause energy exchange between the different modes. This can especially occur for closely spaced modes, see Tso [2]. For each pull out the acceleration response of the structure is measured at 16 different points on the structure. 8450 points were measured at a sampling rate of 1000 Hz. The responses were not filtered before they were converted to a digital signal. Instead the responses are highly oversampled to avoid aliasing and low-pass filtered digitally. Before the time series were analysed they were decimated 10 times for the FFT analysis and the single mode filtering approach, and 15 times for the analysis using hybrid ARMA and ARMAV models. In the first case, the decimation reduced the actual number of points to 845 in every measured response, and the sampling frequency to 100 Hz. In the second case the number of data points was reduced to 564, and the sampling frequency to 67 Hz. Since the highest frequency is at approximately 20 Hz this procedure does not remove any structural information from the data.

2.2 Symmetrical Virginal Structure

The symmetrical virginal (naked) structure only consists of the concrete plates, beams and columns. The reason for calling these measurements virginal is to distinguish between these measurements and the measurements described in section 2.3 and 2.4. The state of the structure will in this case also be referred to as the naked state. The reason for this is that during the measurements no steel diagonal was mounted on the structure. The responses from 10 different pull outs were measured: 5 centre pull-outs, one at each storey and 5 edge pull outs, one at each storey.

2.3 Unsymmetrical Structure

The unsymmetrical structure consists of the naked structure, see section 2.2, with diagonals on two sides perpendicular to each other. This makes the structure unsymmetrical. The responses from 10 different pull outs were measured: 5 centre pull-outs, one at each storey and 5 edge pull-outs, one at each storey. So the same amount of data is available for the unsymmetrical structure as for the naked structure

2.4 Symmetrical Structure

The symmetrical structure with diagonals consists of the naked structure where the stiffness has been increased by 8 steel diagonals at each storey from the ground floor to the fifth storey. The purpose of these measurements is to determine how much this increase of stiffness influences the eigenfrequencies. Only response measurements from one centre pull-out and one edge pull-out were measured in this case. Both pull-outs were made at the third storey.

2.5 Coupling of Translational and Rotational Modes

This section deals with the effect of energy transfer between rotational and translational modes for symmetrical structures. The effect has been investigated in Tso [2]. If the rotational and translational modes are closely spaced (about equal eigenfrequencies), then an energy transfer can take place due to non-linear stiffness, Tso [2]. The energy transfer will take place some time after the excitation of the structure. As seen from the results in chapter 4, the rotational and translational eigenfrequencies are nearly identical. If the symmetrical structure e.g. is excited by centre pull-out then excitation of translational modes only is expected. If the energy transfer takes place, the rotational modes also will be excited after some time. This effect is investigated in this section. Consider the symmetrical structure without diagonals. The response at the fifth storey from centre step excitation at all 5 storeys is considered. If the excitation is ideal and no energy transfer takes place, then the response at the centre of the structure and at the edge of the structure should be identical. Figure 2.2-2.6 shows the response at the fifth storey due to centre step

excitation at the first to the fifth storey. Each figure shows the centre response, the edge response and the difference of the two responses. From the figures it is seen that during the first 1-1.5 seconds the difference of the responses looks like noise. After that time the difference seems to be structural response with increasing amplitudes until the fourth or fifth second and then with decreasing amplitudes. Figures 2.7-2.11 show the Fourier transformation of the responses from figures 2.2-2.6. [_____] signifies centre response,, [- - - - -] signifies edge response and [.....] signifies centre response subtracted from edge response.

Especially from the third mode it is seen that the frequency from the difference of the responses is lower than the frequency of the responses. As will be shown in section 4.1, the rotational eigenfrequencies are lower than the translational eigenfrequency. Figure 2.12 shows the magnitude of the Fourier transformation of all responses from figures 2.2-2.6 put in one vector. The figure shows the third eigenfrequency more clearly.

It is concluded, that an energy transfer between translational and rotational modes takes place. This effect will not be taken into consideration during the analysis in chapter 4. One of the consequences can be an overestimation of the damping ratios, since energy is transferred from one mode to another and not dissipated.

3 DESCRIPTION OF IDENTIFICATION METHODS

Four different methods used for identification of the EUROSEIS TEST structure are described in this chapter. The Fast Fourier Transform, and Auto-Regressive Moving Average Vector (ARMAV) are used to identify the structure in all three states. The single mode filtering is not used to identify the unsymmetrical structure, since the modes are too closely spaced. The hybrid ARMA method is only tested on the naked symmetrical structure.

3.1 Fast Fourier Transform

Fast Fourier Transformations (FFT) are used to estimate the transfer functions from the free decays of the structure. From the transfer functions, the mode shapes and corresponding eigenfrequencies are extracted, see Ewins [3]. No advanced curve fitting procedures were used to estimate all modal parameters. Also it is chosen not to estimate the damping ratios from the peaks of the absolute values of the transfer functions.

To have as precise estimates of the eigenfrequencies as possible, all the response is stacked in one vector. The FFT of this vector constitutes the basis for estimating the eigenfrequencies. The eigenfrequencies are identified as the frequency corresponding to the maximum value of a peak in the power spectrum (magnitude). The mode shapes are estimated by taking the value of the transfer function at the estimated eigenfrequencies.

3.2 Single-Mode Filtering

The purpose of this analysis is to isolate the individual modes by filtering, to validate the earlier observed values for the eigenfrequencies and to obtain estimates for the damping ratios.

To filter out the single modes, Finite Impulse Filters (FIR) with about 100 filter constants were used, see Oppenheim et al. [4]. The filters were applied both forwards and backwards to eliminate time delay, and to increase filter steepness.

After filtering, the eigenfrequencies and damping ratios are estimated from the single mode free decays. It has been chosen to use an Auto Regressive model of order 2, see Pandit [5]. The modal parameters are determined in a least squares sense to minimize the differences between the actual free decay and the predicted free decay of the model. Since the amount of data from the symmetrical structure with diagonals is small, it has been chosen also to use a visual least squares fit.

3.3 Hybrid ARMA

The hybrid ARMA approach is a two-stage approach. First all data records are stacked in one vector, in order to get maximum information about the eigenfrequencies and damping ratios (the discrete-time eigenvalues that are related to the system dynamics). To do this, a high-order univariate ARMA-model is calibrated to the vector of measurements, and the discrete-time eigenvalues of the model are calculated.

The second step is to construct a regression problem involving the eigenvalues and some lagged covariance matrices of the response. These covariance matrices are calculated using an unbiased FFT approach. The unknown parameters of this regression problem are the modal weight matrices, that relate the eigenvalues to the covariance function of the response, see Pandit [5].

The final step is to extract the modal parameters. The eigenfrequencies and damping ratios are extracted from the eigenvalues, and the mode shapes from the modal weight matrices. For a more complete description of the approach, see Brincker et al. [6].

3.4 ARMAV

The ARMAV model can be shown to be the covariance equivalent discrete-time model to a continuous-time second-order mechanical system excited by Gaussian white noise, see Andersen et al. [7]. This approach is well-proved and has been used for many different dynamic analyses, see e.g. Pandit [3], Kirkegaard et al. [8] and Kirkegaard et al. [9]. The dynamics of the system is modelled by the autoregressive term, whereas the noise present in the measurements is modelled by the moving average term of the model. In other words, the modal parameters are extracted using a spectral decomposition of the auto regressive term.

The model is calibrated using a non-linear least squares algorithm that uses a Gauss-Newton search criterion. This kind of algorithm is very efficient near optimum, because of its quadratic convergence properties. However, for efficiency purposes, it needs good initial estimates. This is secured through a fast two-stage iterative linear least squares algorithm.

4 ANALYSIS OF MEASUREMENTS

4.1 Procedures for Symmetrical Virginal Structure

The data consists of 16 acceleration response measurements from each excitation. The structure were excited at the center and at the edge of each floor, which means 10 excitations were performed. The translational modes are estimated from the center step response measurements, and the rotational modes are estimated from the edge step response measurements. The measurements in the y-direction are not used.

4.1.1 Fast Fourier Transform

To identify the translational modes all responses from the center step excitation were put in one vector. The power spectrum of this vector is shown in figure 4.1. The x-axis shows the natural frequency and the identified frequency at the five modes is indicated. The eigenfrequencies were identified as the frequencies corresponding to the maximum value in a peak.

The rotational modes were identified by the same procedure, except that the edge step response were used. The center responses ere subtracted from the edge response in order to remove eventually translational modes. The power spectrum of the vector including all measurements are shown in figure 4.2. The identified frequency are indicated.

The response at each storey from each excitation are put in one vector. This gives five vectors with responses. The FFT of these vectors constitutes the basis for estimation mode shapes. The magnitude of the mode shapes are estimated from the absolute value of the FFT at the frequency value. The phase of the mode shapes are estimated from the complex value of the FFT at the frequency value. This procedure were applied to the responses from the center step and the edge step excitation. The magnitude of the translational mode shapes are shown in figure 4.3, while the magnitude of the rotational mode shapes are shown in figure 4.4. The sign of the magnitude were determined from the complex of the FFT.

4.1.2 Single-Mode Filtering

The responses from edge step excitation are used to estimate the rotational modes. To make sure that the edge response from edge step excitation only consists of rotational modes, the corresponding center response is subtracted. The translational modes are estimated from the center response excited by center step. All the responses from translational are put in one vector and all the responses from rotational modes are put in one vector. The power spectral density of these to vectors constitutes the basis for filtering out the individual modes, since the filter is designed from these power spectral density functions. Figure 4.5 and figure 4.6 shows the power

spectral density of the translational modes and the rotational modes, respectively. Furthermore, the characteristic of the filter designed to pick out the first mode is shown.

By filtering the decays corresponding to rotational and translational modes, 25 different decays for each rotational and translational mode are obtained. Before using an analytical model to estimate the damping coefficient and the eigenfrequency the decays are averaged. This is done by using the maximum value in every decay as the starting point. Figures 4.7-4.11 and figures 4.12-4.16 show the resulting free decays for translational and rotational modes, respectively.

By using an AR(2) model the damping coefficient and eigenfrequency is estimated in a least squeares sense. For the translational modes the sensitivity of the modal parameters to the filter bandwidth is investigated. First, the filter bandwidth is chosen as 4 Hz and then as 4.5 Hz. Tabel 4.1 shows the estimated modal parameters for the two different filter bandwidths.

Bandwidth	Parameter	1st mode	2nd mode	3rd mode	4th mode	5th mode
4.0 Hz	f [Hz]	2.425	7.250	12.42	15.95	20.35
	ζ [%]	1.60	1.30	1.90	2.30	2.60
4.5 Hz	f [Hz]	2.428	7.250	12.43	15.95	20.37
	ζ [%]	1.70	1.40	1.90	2.40	2.60

Tabel 4.1: Sensitivities of modal parameters of translational modes. Singel mode filtering.

From the results of the two different analysis it is concluded that a filter bandwidth of 4 Hz is appropriate. So this filter bandwidth is also used for the rotational modes. The results are shown in tabel 4.2

Bandwidth	Parameter	1st mode	2nd mode	3rd mode	4th mode	5th mode
4.0 [Hz]	f [Hz]	2.405	6.800	11.69	14.65	18.30
	ζ [%]	1.40	1.80	2.10	2.90	2.60

Tabel 4.2: Modal parameters of rotational modes. Single mode filtering.

4.1.3 Hybrid ARMA

The x-directional center step excited response measurements of the centre accelerometers are used to calculate the translational modes. The response measurements of all five pull-outs is stacked into one vector. The performance of three different models has been tested. These models are: ARMA(10,9), ARMA(12,11), and ARMA(14,13). From the Akaike Final Prediction Error

criterion, see e.g. Ljung [10], the optimal model was verified to be an ARMA(12,11). The modal parameters obtained from the physical eigenvalues of this model can be seen in table 4.3, and the mode shapes can be seen in figure 4.17. The autospectral densities are shown in figure 4.18.

Parameter	1st mode	2nd mode	3rd mode	4th mode	5th mode
f [Hz]	2.434	7.227	12.460	15.799	20.317
ζ [%]	2.09	1.46	2.27	6.47	3.32

Table 4.3: Eigenfrequencies and damping ratios of translational modes. HARMA.

The response measurements from the x-directional edge step excitation are used to estimate the rotational modes. In order to eliminate influence of the translational modes the response measurements of the centre x-directional accelerometers are subtracted from the measurements of the edge accelerometers. By analysing the Akaike Final Prediction Error criterion it is verified that again the optimal model is an ARMA(12,11) model. The modal parameters obtained from the physical eigenvalues are shown in table 4.4 and the mode shapes in figure 4.19. The autospectral densities are shown in figure 4.20.

Parameter	1st mode	2nd mode	3rd mode	4th mode	5th mode
f [Hz]	2.397	6.801	11.706	14.622	18.276
ζ [%]	1.50	2.04	2.45	4.27	4.86

Table 4.4: Eigenfrequencies and damping ratios of rotational modes. Harma.

4.1.4 ARMAV

The x-directional center step excited response measurements of the centre accelerometers are used to calculate the translational modes. The response measurements of all five pull-outs are stacked into one vector. The performance of four different models has been tested. These models are: ARV(4), ARMAV(2,1), ARMAV(4,3), and ARMAV(6,5). From the Akaike's Final Prediction Error criterion the optimal model was verified to be an ARMAV(4,3). This is also expected because the number of measurement channels equals the number of degrees of freedom present in the measurements, see Andersen et al. [7]. The modal parameters obtained from calibration of this model to the data can be seen in table 4.5, and the mode shapes can be seen in figure 4.21. The autospectral densities obtained from the model are shown in figure 4.22.

Parameter	1st mode	2nd mode	3rd mode	4th mode	5th mode
f [Hz]	2.429	7.222	12.389	16.049	20.628
ζ [%]	2.35	1.25	1.89	4.97	4.61

Table 4.5: Eigenfrequencies and damping ratios of translational modes. ARMAV.

The response measurements from the x-directional edge step excitation are used to estimate the rotational modes. In order to eliminate influence of the translational modes the response measurements of the centre x-directional accelerometers are subtracted from the measurements of the edge accelerometers. By analysing the Akaike Final Prediction Error criterion it is verified that again the optimal model is an ARMAV(4,3) model. The modal parameters obtained from the calibration are shown in table 4.6 and the mode shapes in figure 4.23. The autospectral densities obtained from the model are shown in figure 4.24.

Parameter	1st mode	2nd mode	3rd mode	4th mode	5th mode
f [Hz]	2.387	6.803	11.694	14.821	18.717
ζ [%]	1.47	1.93	2.93	4.44	4.72

Table 4.6: Eigenfrequencies and damping ratios of rotational modes. ARMAV.

4.2 Procedures for Unsymmetrical Structure

The unsymmetrical structure is excited at each storey by centre and edge pull-out. Since the structure is unsymmetrical, the mode shapes are expected to be a combination of rotational and translational displacement. So the modes cannot be separated into purely rotational and purely translational modes. The modes of the structure are estimated corresponding to both centre and edge pull-out.

4.2.1 Fast Fourier Transform

Figure 4.25 shows the power spectral density of a vector where all response measurements are stacked in one vector. In order to detect the eigenfrequencies several different vectors are used to calculate the power spectral densities. As an example, three different power spectral densities are calculated from the response to centre step excitation. First, all measurements in the x-direction are used, second only centre response measurements are used, and third only edge response measurements in the x-direction are used. Table 4.7 shows all combinations of response and loads and the detected eigenfrequencies. Furthermore, the final eigenfrequencies are indicated. The argument for this procedure is that the different excitation will give different initial conditions, which results in different excitation of the modes.

Load	Respons	Mode 1	Mode 2	Mode 3	Mode 4	Mode 5	Mode 6
All	All	2.54	7.03	7.32	12.0	12.6	13.1
Centre	All-X	2.54	7.03	7.32	12.0	12.6	13.1
Centre	Centre	2.54	7.03	7.52	-	12.7	13.2
Centre	Edge	2.44	7.03	7.32	12.0	-	-
Edge	All-X	2.44	-	7.32	12.0	12.6	13.1
Edge	Centre	2.54	-	7.52	-	12.7	13.2
Edge	Edge	2.44	7.03	7.32	12.0	-	-
Centre	Y	2.54	7.03	7.42	12.0	12.7	-
Edge	Y	2.54	7.03	7.42	12.0	12.7	-
All	Y	2.54	7.03	7.42	12.0	12.7	-
Final	result	2.54	7.03	7.42	12.0	12.6	13.1
Load	Respons	7	8	9	10	11	
All	All	15.2	16.0	16.5	18.3	20.7	
Centre	All-X	15.2	16.0	-	18.3	20.5	
Centre	Centre	-	16.0	16.5	18.3	20.7	
Centre	Edge	15.2	16.0	-	18.3	20.4	
Edge	All-X	15.2	16.0	16.5	18.3	20.5	
Edge	Centre	-	16.0	16.5	18.3	20.7	
Edge	Edge	15.2	16.0	-	18.3	20.4	
Edge	Y	-	-	16.5	-	20.8	
Centre	Y	-	-	16.5	-	20.7	
All	Y	-	-	16.5	-	20.7	
Final	result	15.2	16.0	16.5	18.3	20.7	

Table 4.7: Final result for detected eigenfrequencies of unsymmetrical structure.

The mode shapes are estimated using the complex value of the Fourier transformation of the measurements at the above indicated eigenfrequencies. The mode shapes are shown in figures

4.26-4.47. In the plotting procedure it has been assumed that the concrete slabs are infinitely stiff. The figures show the 3-dimensional mode shape and the undeformed structure. From the fifth to the first storey a 2-dimensional plot of the mode shape and the undeformed concrete slabs are shown. Furthermore, in the top, the mode shape has been projected on the axis where the accelerometers have measured the response.

4.2.3 ARMAV

In the present case, where the structure is unsymmetrical, the analysis has been divided into two parts. The centre and edge step excitations has been used separately in each of the two parts. In each case, the response measurements of all five pull-outs are stacked into one vector. The performance of three different models has been tested. These models are; ARV(4), ARMAV(2,1), and ARMAV(4,3). From the Akaike Final Prediction Error criterion the optimal model was verified to be an ARMAV(2,1) in both cases. This is also expected because the number of measurement channels approximately equals the number of degrees of freedom present in the measurements. The modal parameters of the first 13 dynamic modes, obtained from calibration of these models to the data, can be seen in table 4.8. The mode shapes can be seen in figures 4.38-4.73. Both in the table and the figures the results obtained from centre- and edge excitation are shown separately.

	Centre pull-out		Edge pull-out	
Mode	f [Hz]	ζ [%]	f[Hz]	ζ [%]
1	2.534	4.78	2.528	4.62
2	2.551	10.24	2.537	8.86
3	7.015	3.49	7.014	3.46
4	7.302	3.17	7.308	3.17
5	7.545	3.56	7.537	3.53
6	12.00	2.01	12.01	2.01
7	13.03	5.51	13.02	5.46
8	13.11	12.96	13.08	12.82
9	15.47	5.70	15.45	5.79
10	16.95	5.84	16.91	5.73
11	19.39	26.68	18.88	26.34
12	20.17	3.37	20.35	2.83
13	21.06	5.55	21.28	7.83

Table 4.8: Eigenfrequencies and damping ratios of the first 13 dynamic modes.

4.3 Procedures for Symmetrical Structure

4.3.1 Fast Fourier Transform

To identify the translational modes all responses from center step excitation were stacked in one vector. The power spectrum of this vector is shown in figure 4.74. The frequencies are identified as the frequency corresponding to the maximum value in a peak. The identified frequencies are indicated.

The rotational modes were identified by the same procedure, except that the edge step response was used. The centre response was subtracted from the edge response measurements. The power spectrum of the vector containing these corrected measurements is shown in figure 4.75, where the identified frequencies are indicated.

The mode shapes were estimated from the complex value of the Fourier transform of the individual responses at the eigenfrequencies. The magnitude of the translational and rotational modes is shown in figure 4.76 and figure 4.77.

4.3.2 Single-Mode Filtering

The data preparation follows the same procedure as in section 4.3.1. Figure 4.78 and figure 4.79 show the the power spectrum of the translational modes and the rotational modes, respectively. Furthermore, the characteristics of the filter designed to pick out the first mode is shown.

From the resulting or averaged free decays the eigenfrequencies and damping rations are estimated by fitting an AR(2)-model and by using a visual best fit approach. Figures 4.80 and 4.81 show the theoretical fitted free decays from visual fit and the measured free decays for the first translational and rotational mode, respectively. To investigate the influence the filter bandwidth is varied from 4 to 4.5 Hz on the translational modes. The influence is negligible, so only a filter bandwidth equal to 4 Hz is used on the rotational modes. The results are shown in table 4.9 and table 4.10.

Method	Param.	Mode 1	Mode 2	Mode3	Mode 4	Mode 5
Filter Bandwidth = 4 Hz	f (VI)	2.560	7.600	12.89	16.60	21.50
	f (AR)	2.582	7.623	12.87	16.56	21.36
	ζ (VI)	0.800	1.800	1.200	0.800	1.200
	ζ (AR	0.500	2.180	1.250	1.200	0.920
Filter Bandwidth = 4.5Hz	f (VI)	2.580	7.600	12.85	16.60	21.50
	f (AR)	2.588	7.637	12.86	16.55	21.40
	ζ (VI)	0.800	1.000	1.100	0.800	1.000
	ζ (AR)	0.510	1.950	0.940	1.020	0.830

Table 4.9: Identified modal parameters of translational modes using AR-models and Visual regression. Damping ratios in %, frequency in Hz. Single mode filtering.

Method	Parameter	Mode 1	Mode 2	Mode 3	Mode 4	Mode 5
Filter Bandwidth = 4 Hz	f (VI)	2.600	7.450	12.40	16.20	19.40
	f (AR)	2.608	7.428	12.40	16.17	19.26
	ζ (VI)	0.900	0.900	0.700	0.700	1.200
	ζ (AR)	0.420	2.42	1.160	1.430	0.600

Table 4.10: Identified modal parameters of rotational modes using AR-models and Visual regression. Damping ratios in %, frequency in Hz. Single mode filtering.

4.3.3 ARMAV

The x-directional response measurements of the centre accelerometers, due to the edge step excitation of the third storey, are used to calculate the translational modes. The performance of three different models has been tested. These models are; ARV(4), ARMAV(2,1), and ARMAV(4,3). From the Akaike Final Prediction Error criterion the optimal model was verified to be an ARMAV(2,1). This is again also expected because the number of measurement channels equals the number of degrees of freedom present in the measurements. The modal parameters obtained from calibration of this model to the data can be seen in table 4.11, and the mode shapes can be seen in figure 4.82. The autospectral densities obtained from the model are shown in figure 4.83.

Parameter	1st mode	2nd mode	3rd mode	4th mode	5th mode
f [Hz]	2.502	7.329	13.403	16.711	21.091
ζ [%]	2.95	15.00	13.02	12.23	8.57

Table 4.11: Eigenfrequencies and damping ratios of translational modes.

The response measurements from the x-directional edge step excitation are used to estimate the rotational modes. In order to eliminate influence of the translational modes the response measurements of the centre x-directional accelerometers are subtracted from the measurements of the edge accelerometers. By analysing the Akaike Final Prediction Error criterion it is verified that the optimal model is an ARMAV(2,1) model. The modal parameters obtained from the calibration are shown in table 4.12 and the mode shapes in figure 4.84. The autospectral densities obtained from the model are shown in figure 4.85.

Parameter	1st mode	2nd mode	3rd mode	4th mode	5th mode
f [Hz]	2.575	7.415	12.520	16.809	19.628
ζ [%]	5.55	1.31	12.27	27.41	5.73

Table 4.12: Eigenfrequencies and damping ratios of rotational modes.

5 CONCLUSION

The conclusion is based on a comparison of the results from the different approaches. In each case all estimated modal parameters will be listed and commented on.

Naked symmetrical structure

Tables 5.1 and 5.2 show the estimated eigenfrequencies using the different approaches for translational and rotational modes, respectively. The averages are shown in the last row in each of the tables.

FFT	2.441	7.227	12.40	15.92	20.41
SMF	2.425	7.250	12.42	15.95	20.35
hARMA	2.434	7.227	12.46	15.80	20.32
ARMAV	2.429	7.222	12.39	16.05	20.63
Average	2.432	7.232	12.42	15.93	20.43

Table 5.1: Eigenfrequenies for translational modes.

FFT	2.344	6.836	11.72	14.65	18.36
SMF	2.405	6.800	11.69	14.65	18.30
hARMA	2.397	6.801	11.71	14.62	18.28
ARMAV	2.387	6.803	11.69	14.82	18.72
Average	2.383	6.810	11.70	14.69	18.42

Table 5.2: Eigenfrequencies for rotational modes.

The results from all 4 approaches show a good agreement of all eigenfrequencies. The ARMAV estimate of the fourth eigenfrequency, both for the translational as well as the rotational modes, seems to be higher than for rest of the methods. The uncertainty of this eigenfrequency can also be seen by looking at the corresponding damping ratios.

Tables 5.3 and 5.4 show the estimated damping ratios in %. The averages are shown in the last row in each of the tables.

SMF	1.70	1.40	1.90	2.40	2.60
hARMA	2.09	1.46	2.27	6.47	3.32
ARMAV	2.35	1.25	1.89	4.97	4.61
Average	2.05	1.32	2.02	4.61	3.51

Table 5.3 Damping ratios in % for translational modes.

FFT	1.40	1.80	2.10	2.90	2.60
hARMA	1.50	2.04	2.45	4.27	4.86
ARMAV	1.47	1.75	1.89	4.97	4.61
Average	1.46	1.86	2.15	4.05	4.02

Table 5.4 Damping ratios in % for rotational modes.

Especially for the three lowest eigenfrequencies reasonable agreement between the damping ratios is obtained. For the two highest modes the damping ratios fluctuate.

Figures 5.1 and 5.2 show the estimated translational mode shapes and figures 5.3 and 5.4 show the estimated rotational mode shapes. The FFT estimates are shown by [_._._._._.], the bybrid ARMA estimates are shown by [_ _ _ _ _ _ _], the ARMAV estimates are shown by [.....] and the estimates from a Finite Element model are shown by [_____].

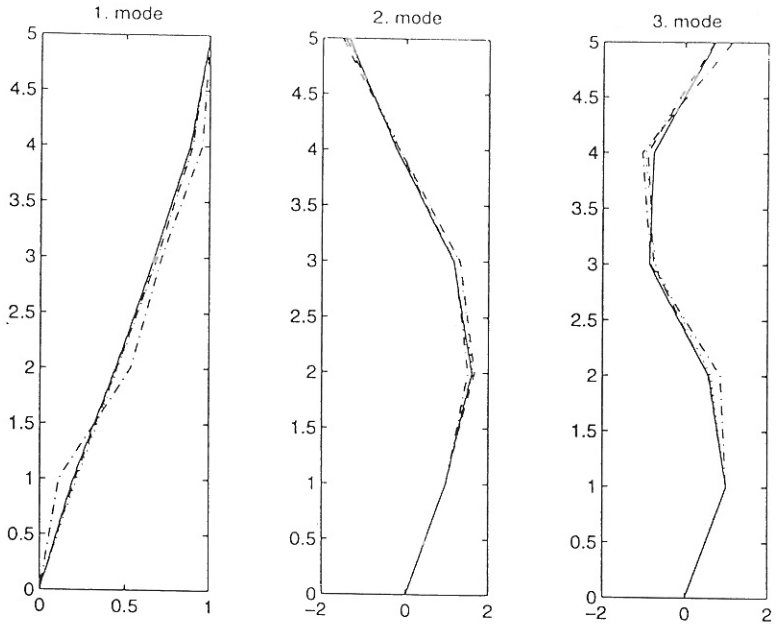

Figure 5.1: Translational mode shapes.

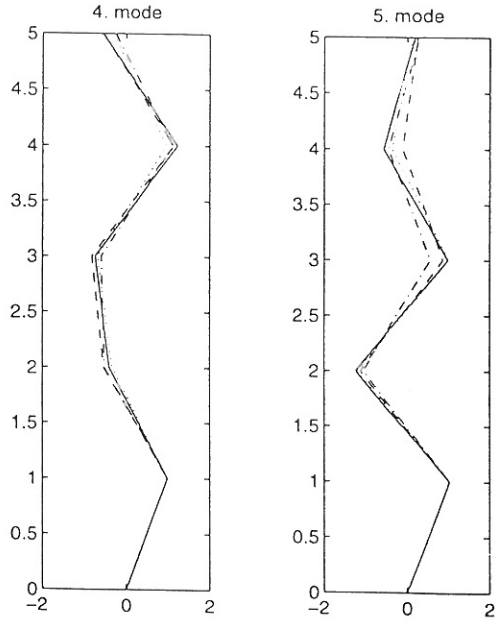

Figure 5.2: Translational mode shapes.

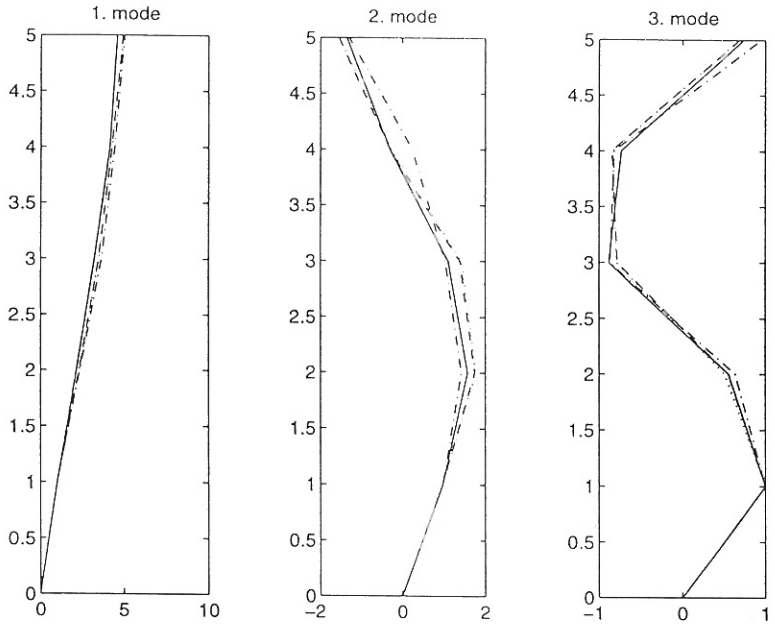

Figure 5.3: Rotational mode shapes.

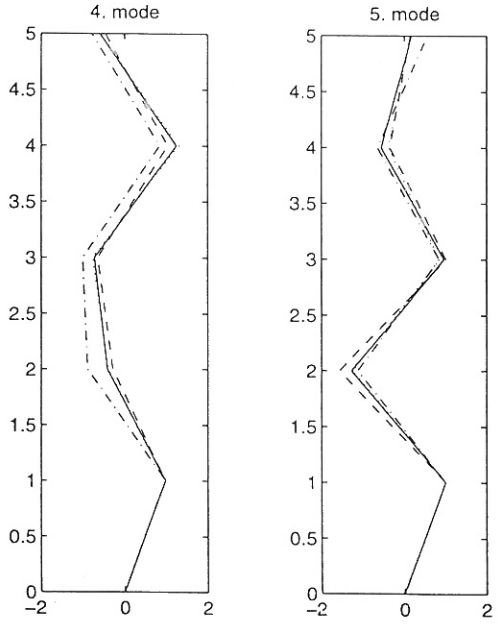

Figure 5.4: Rotational mode shapes.

The results show a good agreement between all estimates. This is expected, since there is a large amount of data. Furthermore, the structure is symmetrical with well separated eigenfrequencies and low damping, i.e. the modes can be assumed to be decoupled. The Finite Element model and the FFT approach both assumes that all modes are decoupled.

Unsymmetrical Structure

Since the structure is unsymmetrical, translational and rotational modes are expected to be coupled. If the eigenfrequencies are closely spaced the FFT approach may not give accurate results since decoupling of modes is assumed. This assumption is not necessary for the ARMAV model. Table 5.5 shows the estimated eigenfrequencies for the FFT approach and for the ARMAV model, where centre and edge pull-out response have been treated separately.

Mode	1	2	3	4	5	6	7
FFT	2.54	-	7.03	7.42	-	12.0	12.6
ARMAc	2.53	2.55	7.02	7.30	7.55	12.0	13.0
ARMAe	2.53	2.54	7.01	7.31	7.54	12.0	13.0
Average	2.53	2.55	7.02	7.34	7.55	12.0	12.9
Mode	8	9	10	11	12	13	14
FFT	13.1	15.2	16.0	16.5	18.3	20.7	-
ARMAc	13.1	15.5	-	17.0	19.4	20.2	21.1
ARMAe	13.1	15.5	-	16.9	18.9	20.4	21.3
Average	13.1	15.4	16.0	16.8	18.9	20.4	21.2

Table 5.5: Estimated eigenfrequencies. ARMAc = center pull out, ARMAe = edge pull out.

The table reveals a good agreement for all estimates of eigenfrequencies of all methods, though the FFT method seems to have encountered a mode (mode number 10) which none of the other methods have detected.

Symmetrical structure with diagonals

In the case with pull-outs only at the third storey the estimated eigenfrequencies of the three methods applied to the data are shown in table 5.6 and table 5.7 for the translational and rotational modes, respectively.

	Mode 1	Mode 2	Mode 3	Mode 4	Mode5
FFT	2.54	7.62	12.9	16.6	21.5
SMF	2.58	7.62	12.9	16.6	21.4
ARMAV	2.50	7.32	13.4	16.7	21.1
Average	2.54	7.52	13.1	16.6	21.3

Table 5.6: Estimated eigenfrequencies for translational modes

	Mode 1	Mode 2	Mode 3	Mode 4	Mode 5
FFT	2.54	7.42	12.5	16.0	19.3
SMF	2.60	7.43	12.4	16.2	19.3
ARMAV	2.58	7.41	12.5	16.8	19.6
Average	2.57	7.42	12.5	16.3	19.4

Table 5.7 Estimated eigenfrequencies for rotational modes.

Even though the amount of data is very limited, there seems to be a good agreement between the estimates of the different methods. In tables 5.8 and 5.9 the damping ratios in % are shown for the translational and rotational modes, respectively.

	Mode 1	Mode 2	Mode 3	Mode 4	Mode 5
SMF	0.500	2.180	1.250	1.200	0.920
ARMAV	2.950	15.00	13.02	12.23	8.570
Average	1.725	8.59	7.135	6.715	4.745

Table 5.8: Estimated damping ratios for translational modes in %.

	Mode 1	Mode 2	Mode 3	Mode 4	Mode 5
SMF	0.420	2.420	1.160	1.430	0.600
ARMAV	5.550	1.310	12.27	27.41	5.730
Average	2.990	1.865	6.715	14.42	3.165

Table 5.9 Estimated damping ratios for rotational modes in %.

In this case the influence of the limited amount of data is very significant. There is no correspondence between any of the damping ratios.

Figures 5.5 and 5.6 show the estimated translational mode shapes and figures 5.7 and 5.8 show the estimated rotational mode shapes. The FFT estimates are shown by [_.._.._.._.], the FFT estimates (From Prof. G.C. Manos) are shown by [_ _ _ _ _ _ _], the ARMAV estimates are shown by [.....] and the estimates from a Finite Element model are shown by [_____].

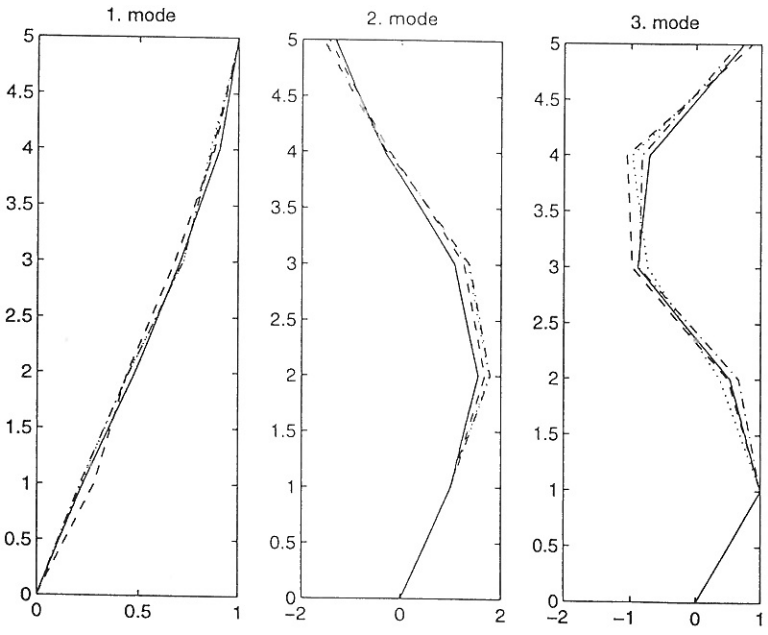

Figure 5.5: Translational mode shapes.

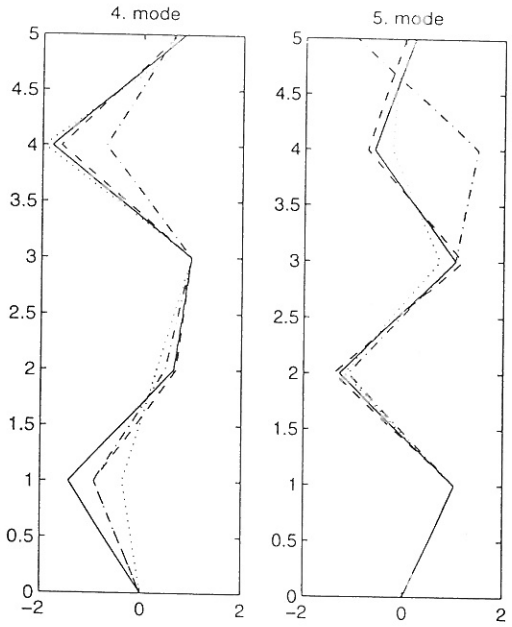

Figure 5.6 Translational mode shapes.

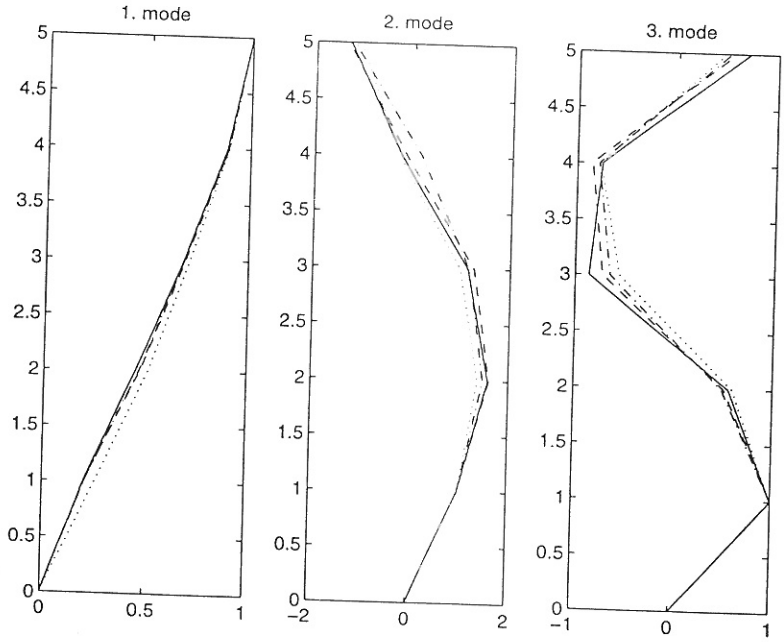

Figure 5.7: Rotational mode shapes.

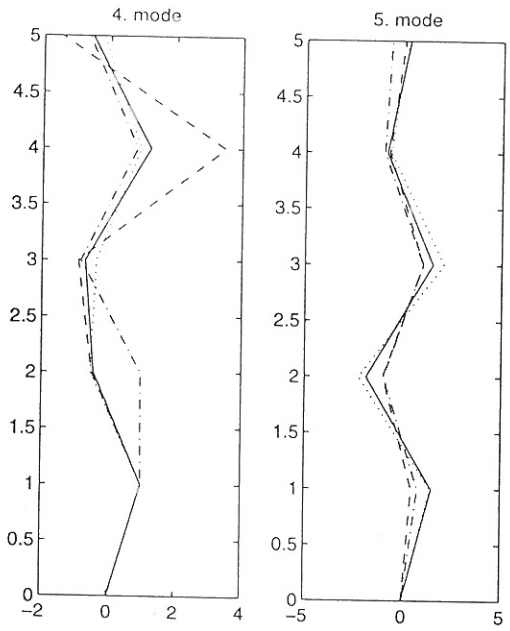

Figure 5.8: Rotational mode shapes.

For all three cases the mode shape and eigenfrequency estimates seem to agree very well. This is, however, not the case for the damping ratios. In order for the ARMA and ARMAV models to give good estimates of the damping the amount of data must very large. In this case, the time series are so short, that bias on the damping estimates might be introduced.

The overall result of the analysis is, however ,satisfying. The analysis gives clear indications of the dynamic behaviour of the structure during the three different states observed.

REFERENCES

[1] Manos, G.C., M. Demosthenous, M. Triamataki, B. Yasin & P. Skalkos: *Construction and Instrumentation of a 5-Storey Masonry Infilled R.C. Building at the Volvi-Thessaloniki EURO-SEISTEST site. Correlation of Measured and Numerically Predicted Dynamic Properties.*

[2] Tso, W.K.: *Induced Torsional Oscillations in Symmetrical Structures.* Earthquake Engineering and Structural Cynamics, Vol. 3, pp.337-346 (1975).

[3] Ewins, D.J: *Modal Testing: Theory and Practice*, Research Studies Press, 19984.

[4] Oppenheim, A.V & R.W. Schafer: *Discrete-Time Signal Processing*, Prentice-Hall,1989.

[5] Pandit, S.M: *Modal and Spectrum Analysis: Data Dependent Systems in State Space*, John Wiley, 1991.

[6] Brincker, R., P. Andersen, M.E. Martinez & F. Tallavó: *Modal Analysis of an Offshore Platform using two Different ARMA Approaches*, Proceedings of the 14th International Modal Analysis Conference, Dearborn, Michigan, USA, 1996.

[7] P. Andersen, R. Brincker & P.H. Kirkegaard: *Theory of Covariance Equivalent ARMAV Models of Civil Engineering Structures*, Proceedings of the 14th International Modal Analysis Conference, Dearborn, Michigan, USA, 1996.

[8] Kirkegaard P.H., P. Andersen & R. Brincker: *Identification of Civil Engineering Structures using Multivariate ARMAV and RARMAV Models*, Proceedings of the International Conference on Identification in Engineering Systems, Swansea, UK, 1996.

[9] Kirkegaard P.H., P. Andersen & R. Brincker: *Identification of the Skirt Piled Gullfaks C Gravity Platform using ARMAV Models*, Proceedings of the 14th International Modal Analysis Conference, Dearborn, Michigan, USA, 1996.

[10] Ljung, L: *System Identification - Theory for the User*, Prentice-Hall, 1987.

APPENDIX A

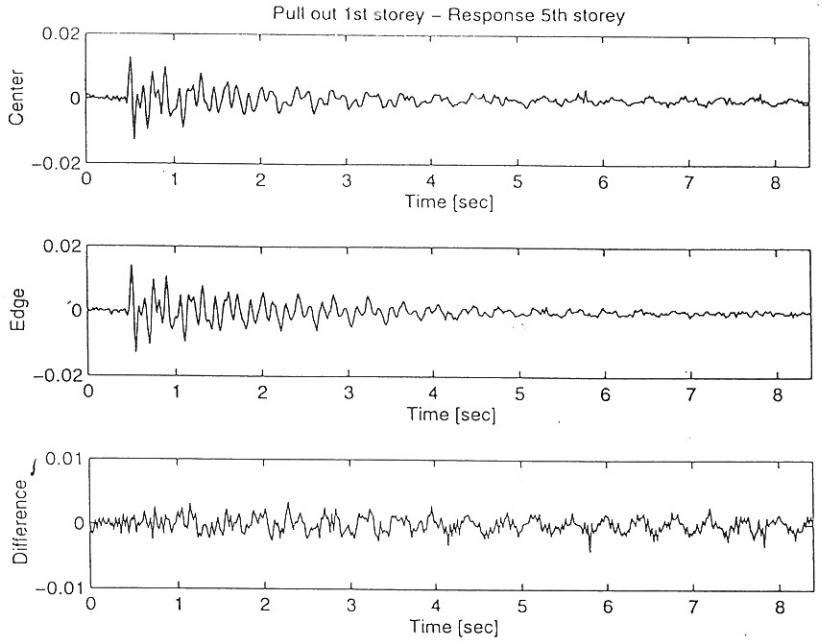

Figure 2.2: Centre, edge, and subtracted response due to centre step-excitation at 1st storey.

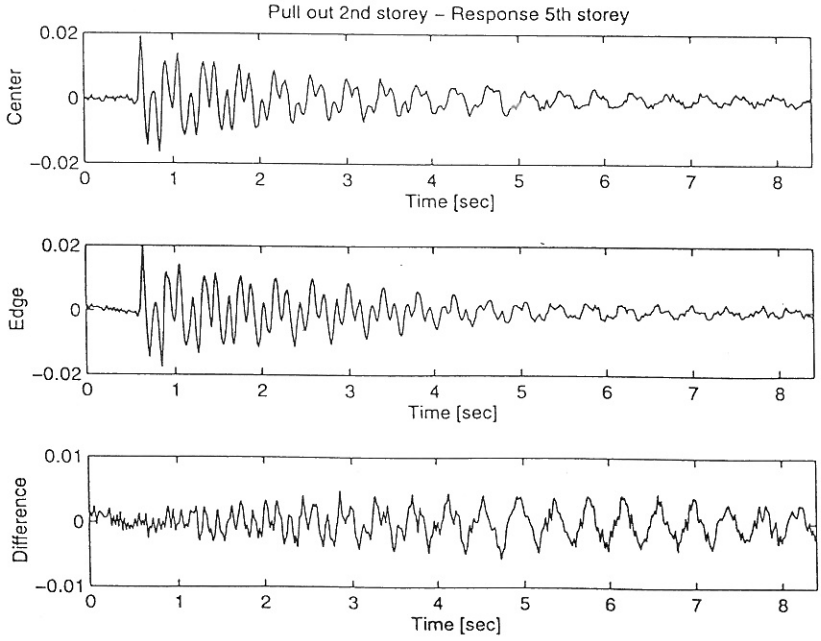

Figure 2.3: Centre, edge, and subtracted response due to centre step-excitation at 2nd storey.

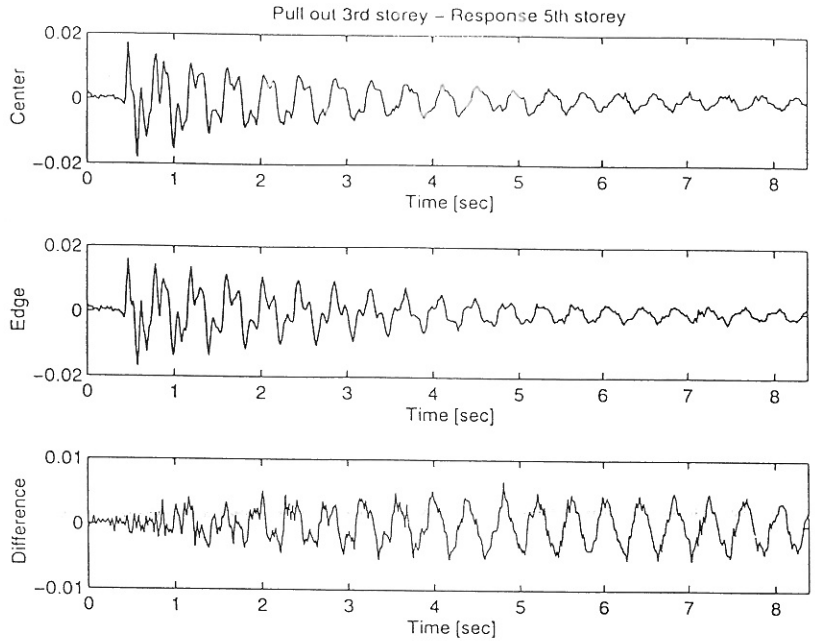

Figure 2.4: Centre, edge, and subtracted response due to centre step-excitation at 3rd storey.

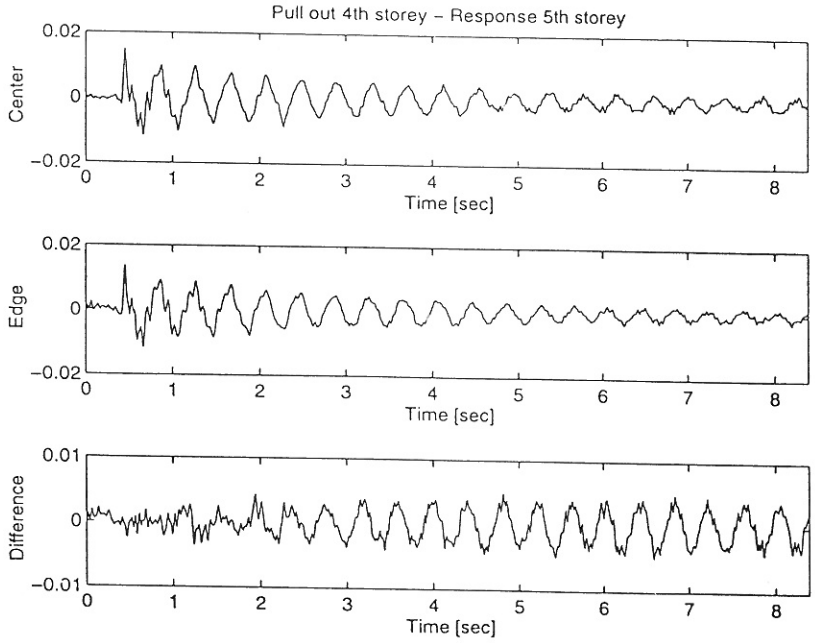

Figure 2.5: Centre, edge, and subtracted response due to centre step-excitation at 4th storey.

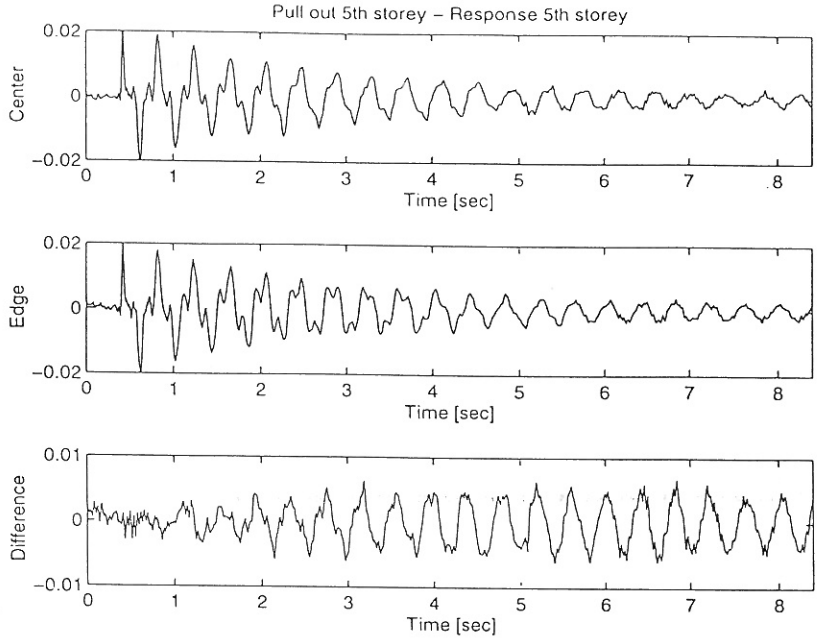

Figure 2.6: Centre, edge, and subtracted response due to centre step-excitation at 5th storey.

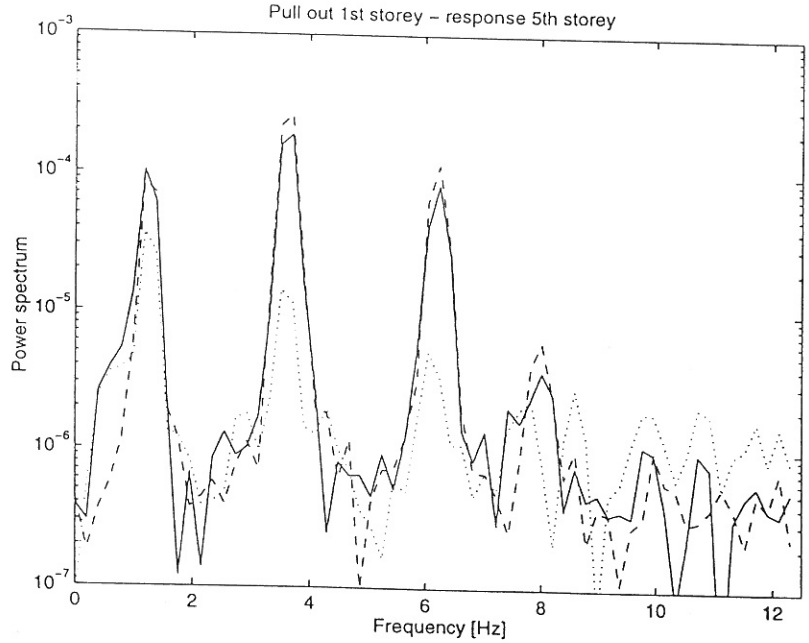

Figure 2.7: Fourier transform of centre, edge, and subtracted response due to centre step-excitation at 1st storey.

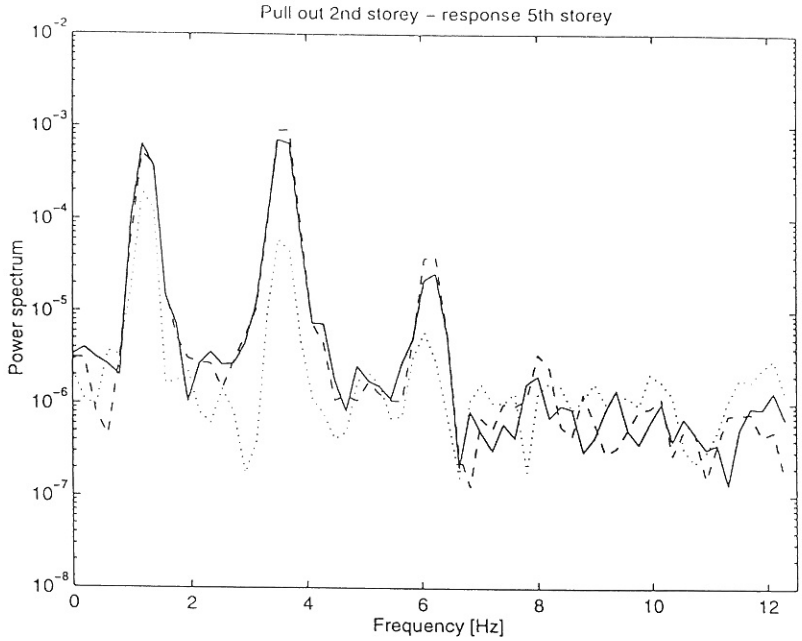

Figure 2.8: Fourier transform of centre, edge, and subtracted response due to centre step-excitation at 2nd storey.

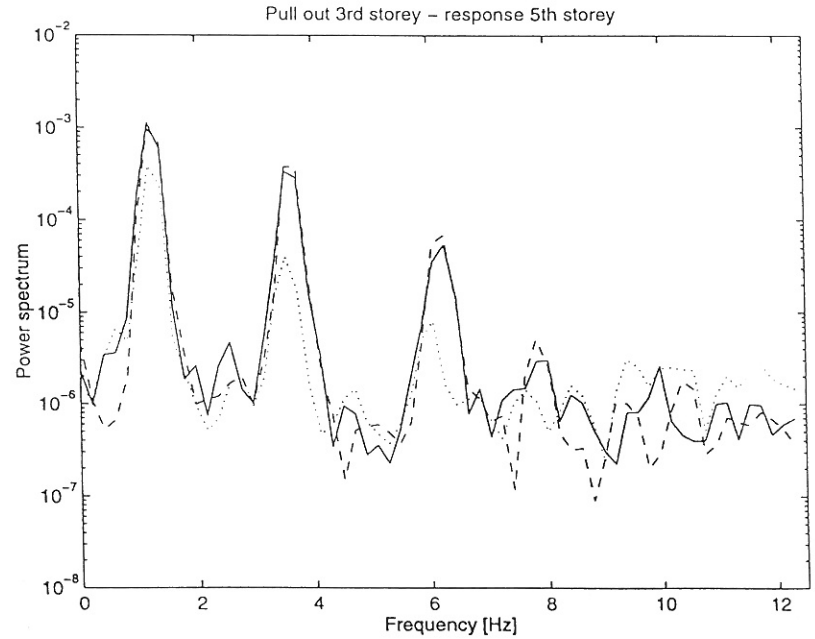

Figure 2.9: Fourier transform of centre, edge, and subtracted response due to centre step-excitation at 3rd storey.

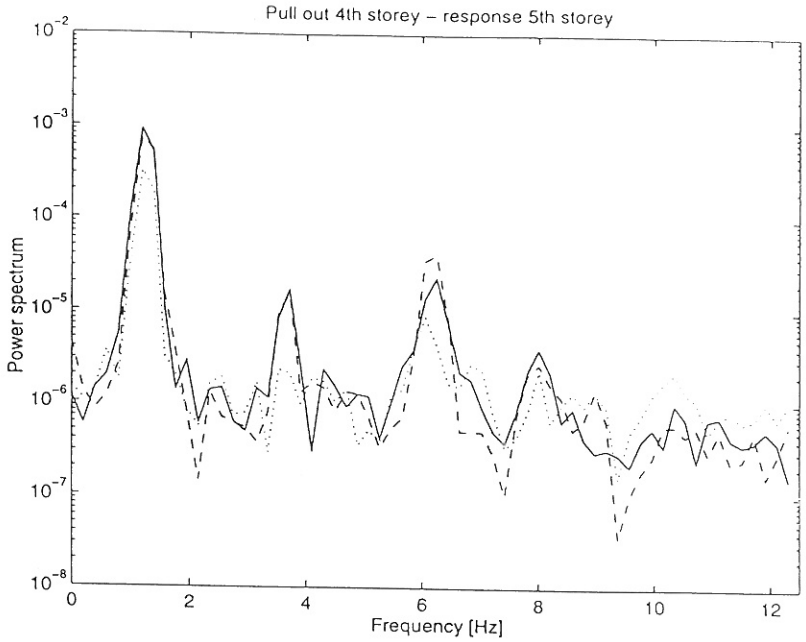

Figure 2.10: Fourier transform of centre, edge, and subtracted response due to centre step-excitation at 4th storey.

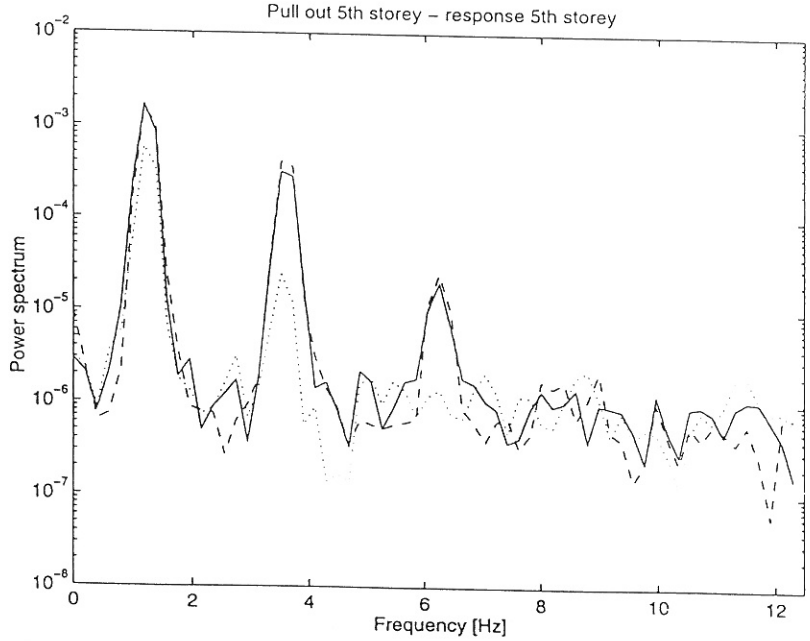

Figure 2.11: Fourier transform of centre, edge, and subtracted response due to centre step-excitation at 5th storey.

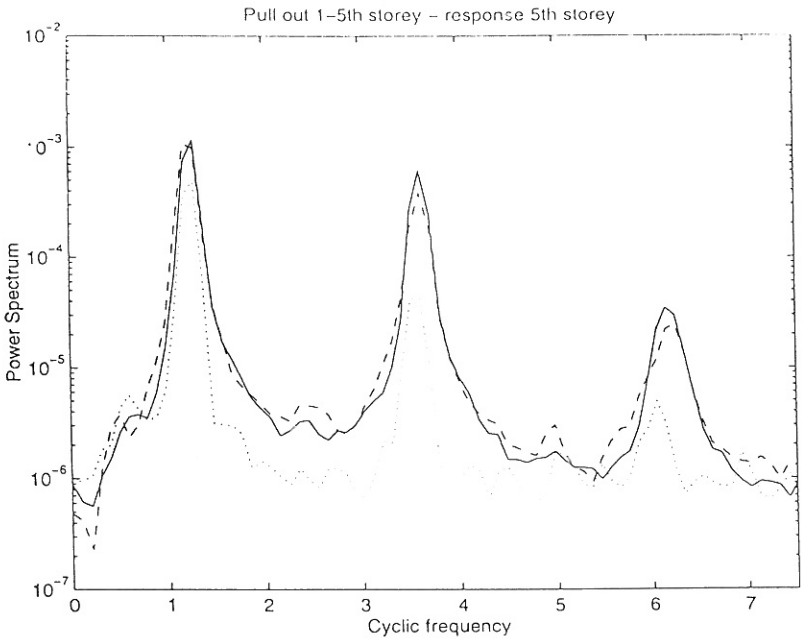

Figure 2.12: Fourier transform of all measurements.

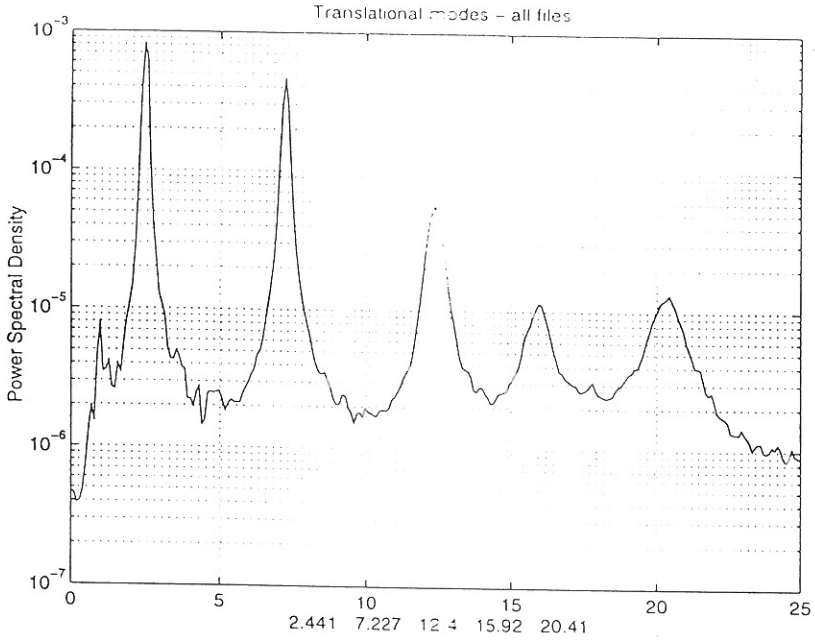

Figure 4.1: Power spectrum translational modes.

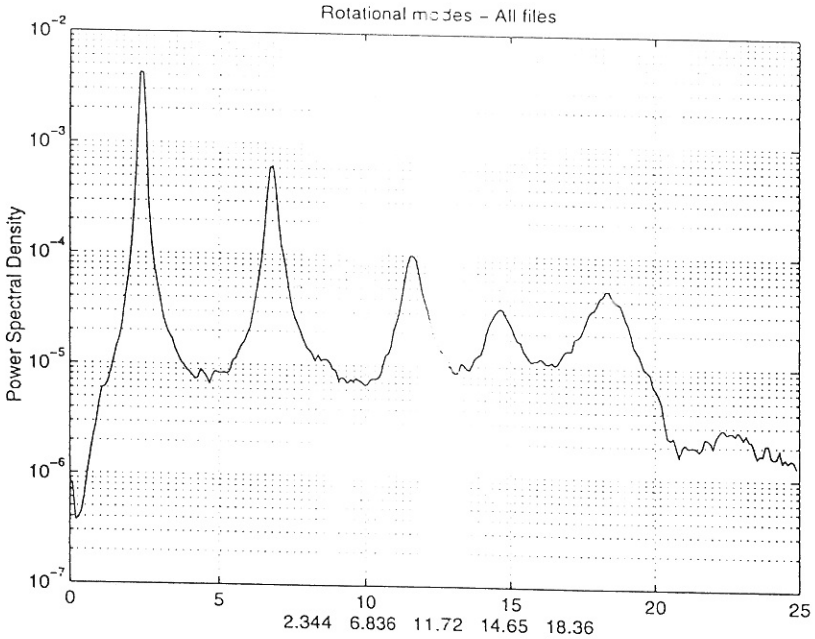

Figure 4.2: Power spectrum rotational modes.

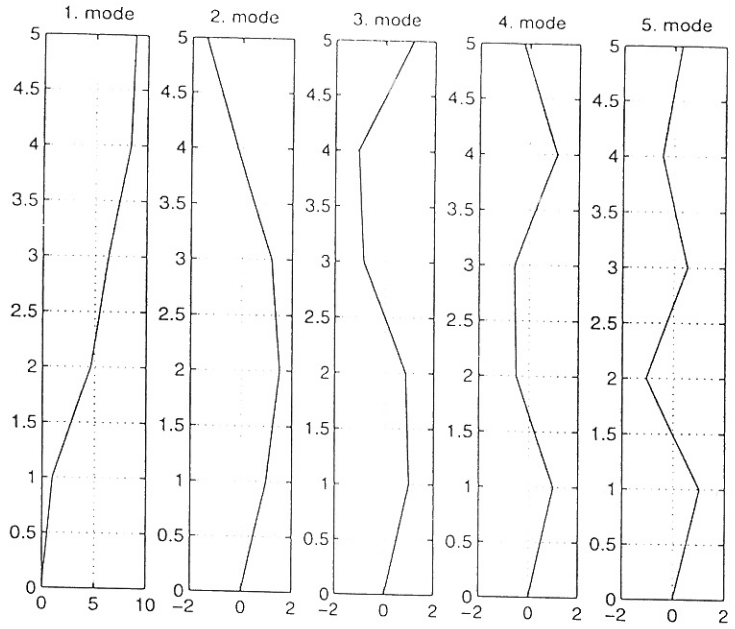

Figure 4.3: Magnitude Translational mode shapes.

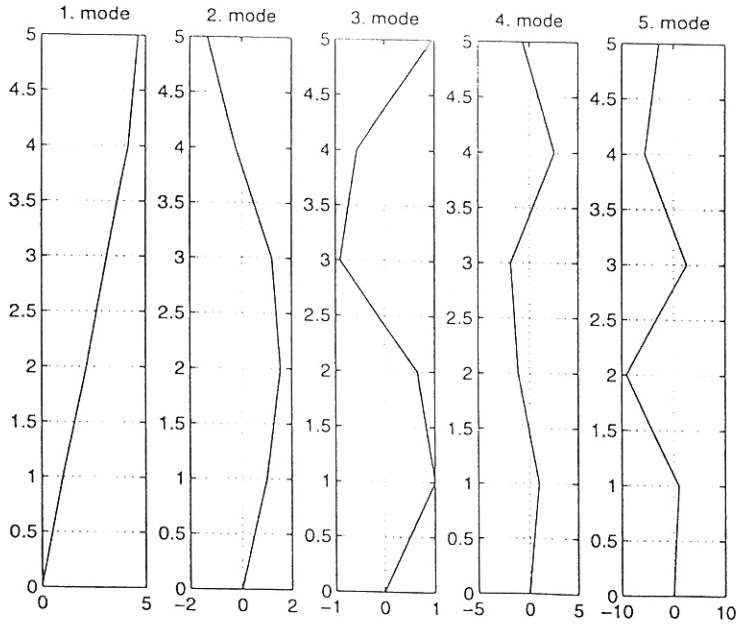

Figure 4.4: Magnitude Rotational mode shapes.

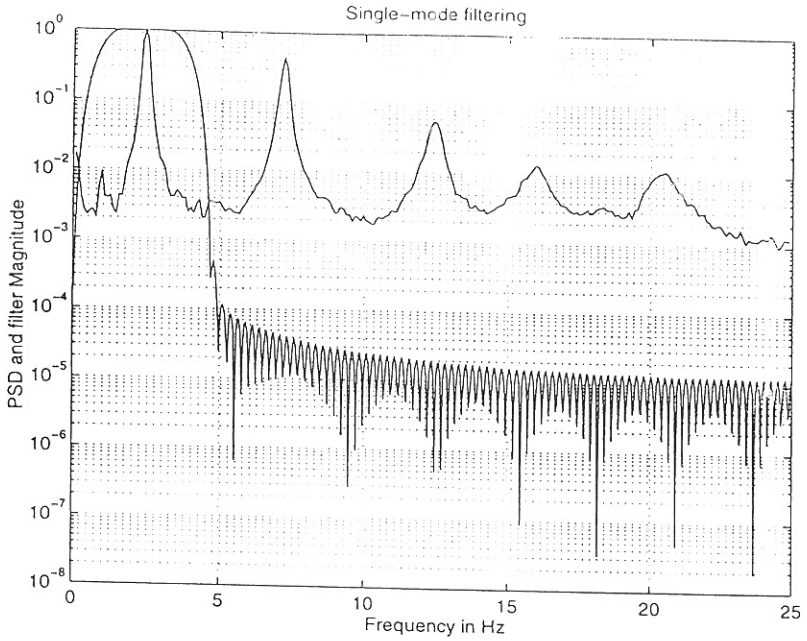

Figure 4.5: Filter magnitude used to pick out the first mode and the power spectral density of the measurements. Translational modes.

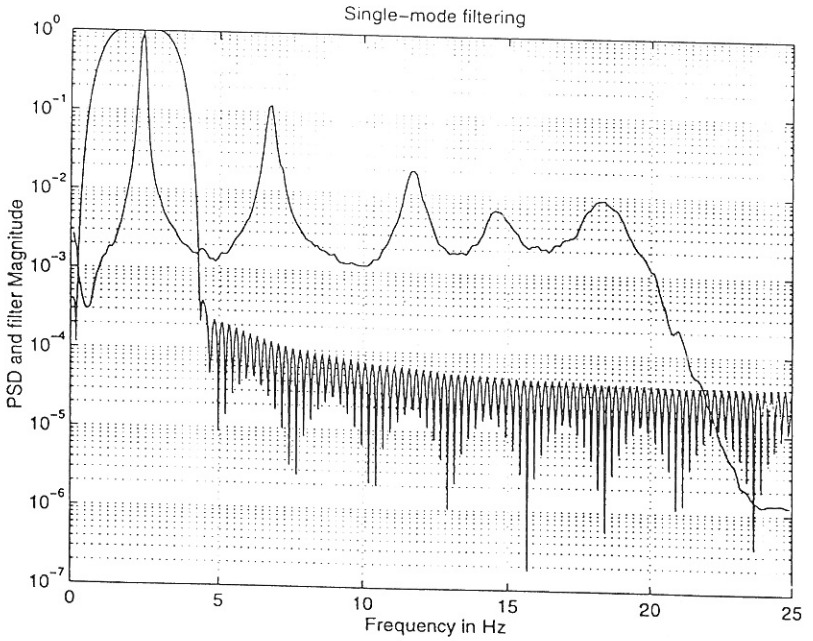

Figure 4.6: Filter magnitude used to pick out the first mode and the power spectral dentisy of the measuremnts. Rotational modes.

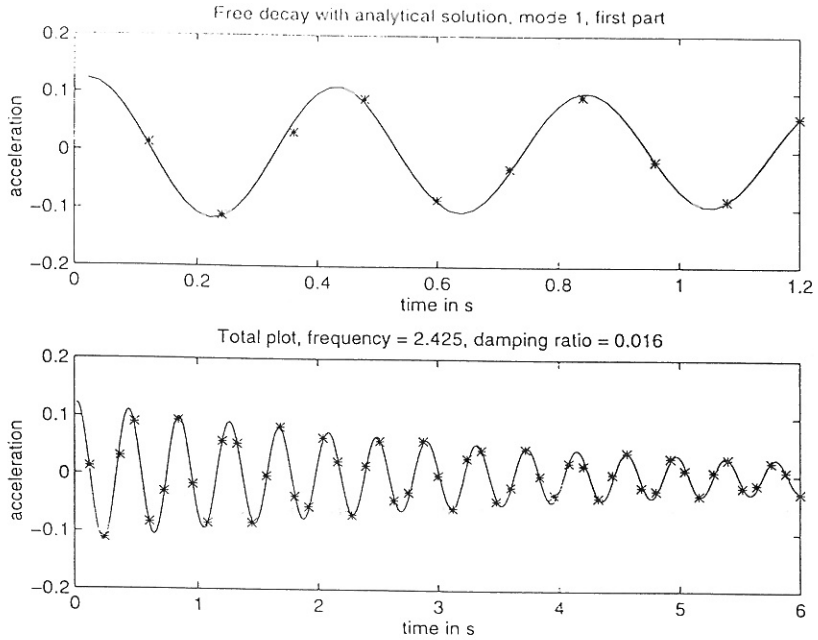

Figure 4.7: Resulting free decay of the 1st translational mode.

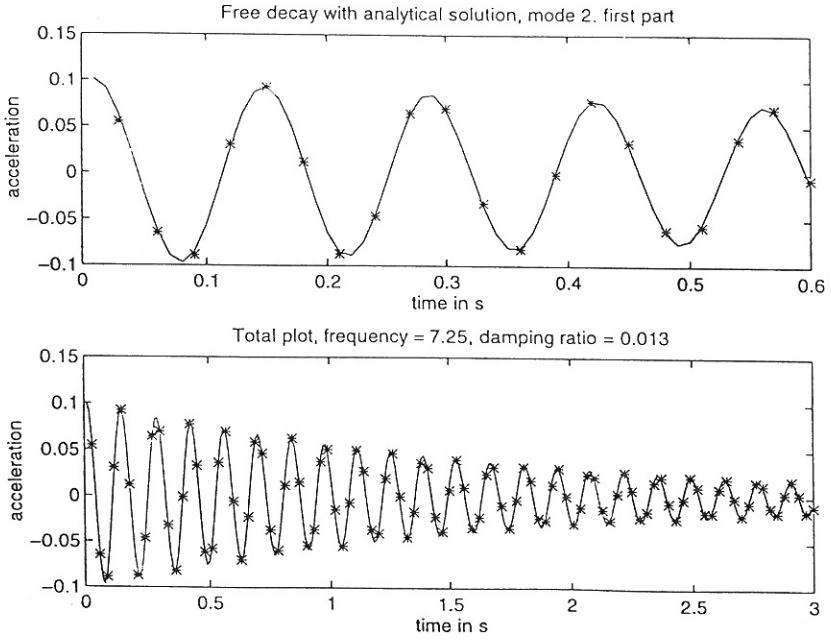

Figure 4.8: Resulting free decay of the 2nd translational mode.

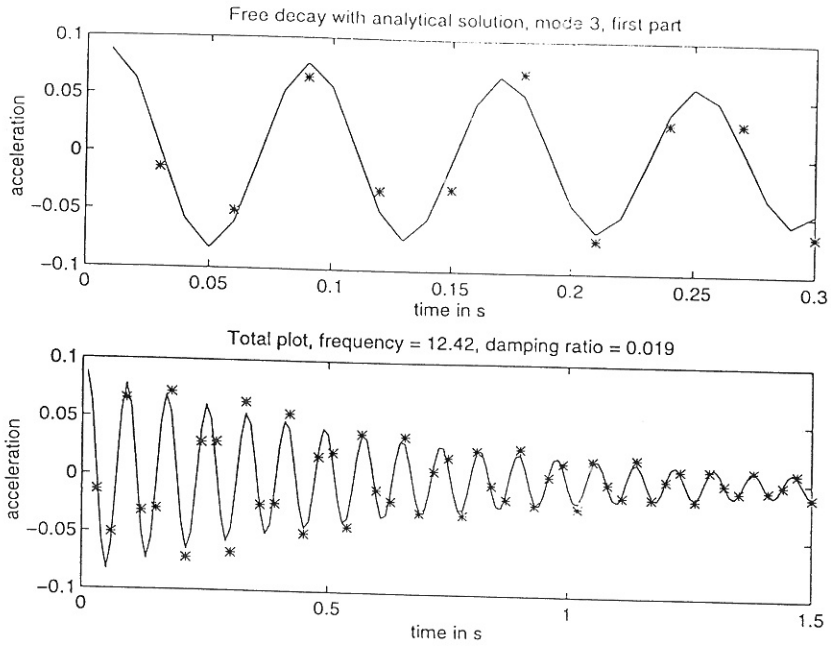

Figure 4.9: Resulting free decay of the 3rd. translational mode.

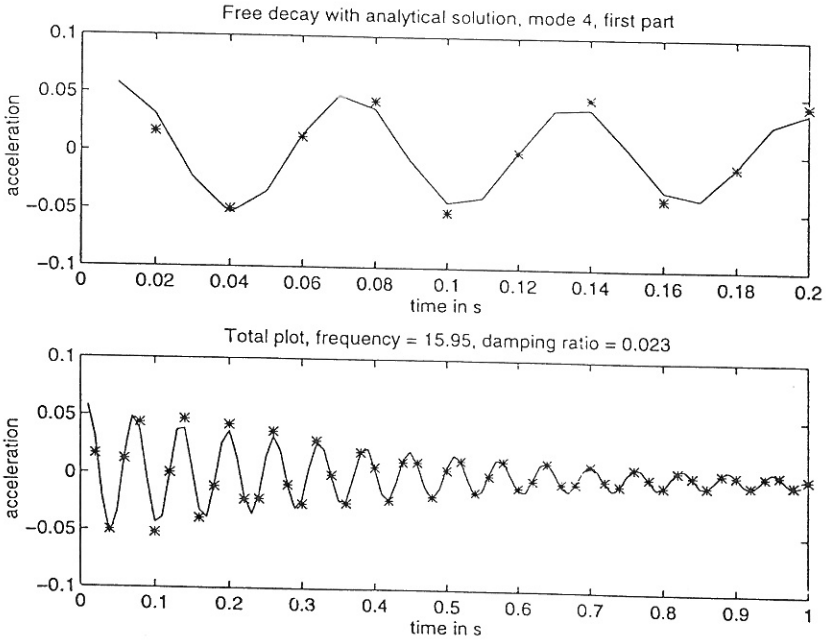

Figure 4.10: Resulting free decay of the 4th. translational mode.

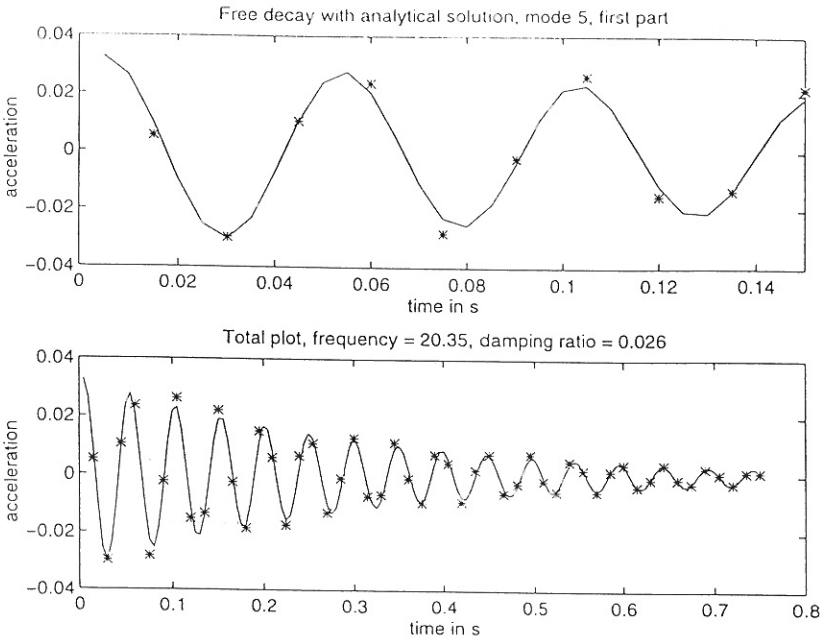

Figure 4.11: Resulting free decay of the 5th translational mode.

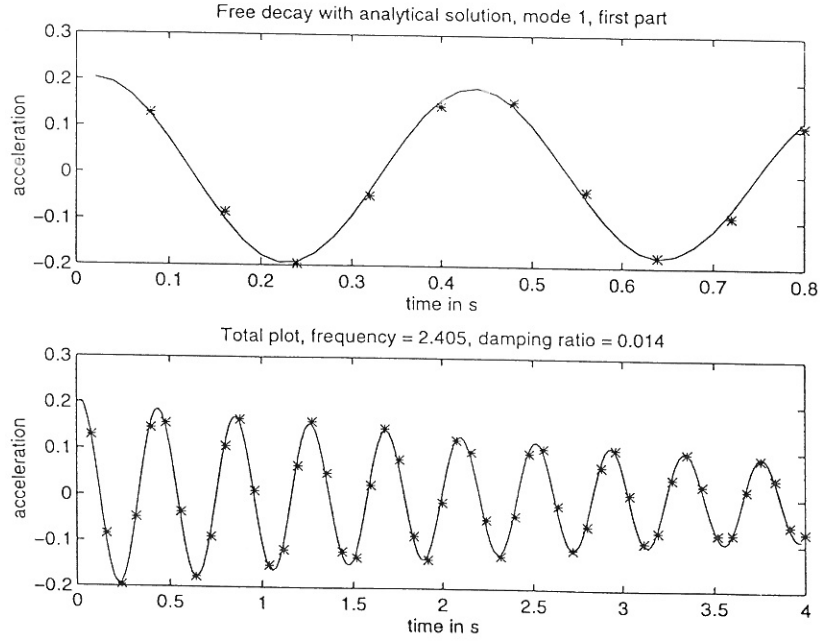

Figure 4.12: Resulting free decay of the 1st rotational mode.

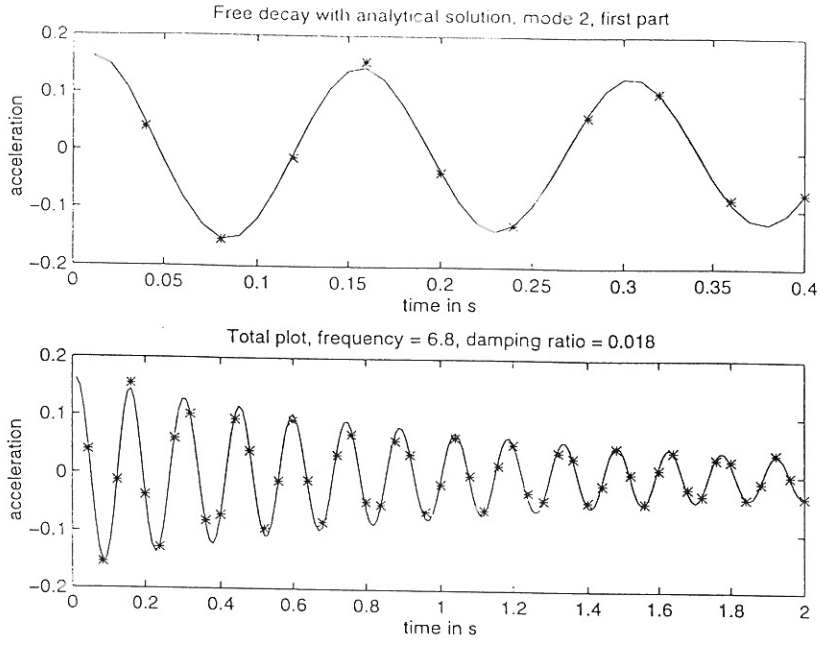

Figure 4.13: Resulting free decay of the 2nd rotational mode.

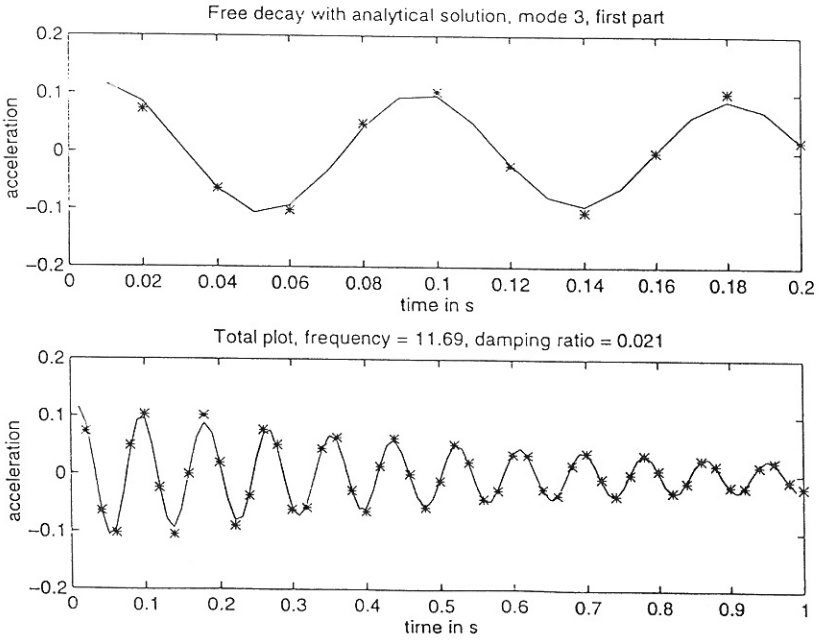

Figure 4.14: Resulting free decay of the 3rd rotational mode.

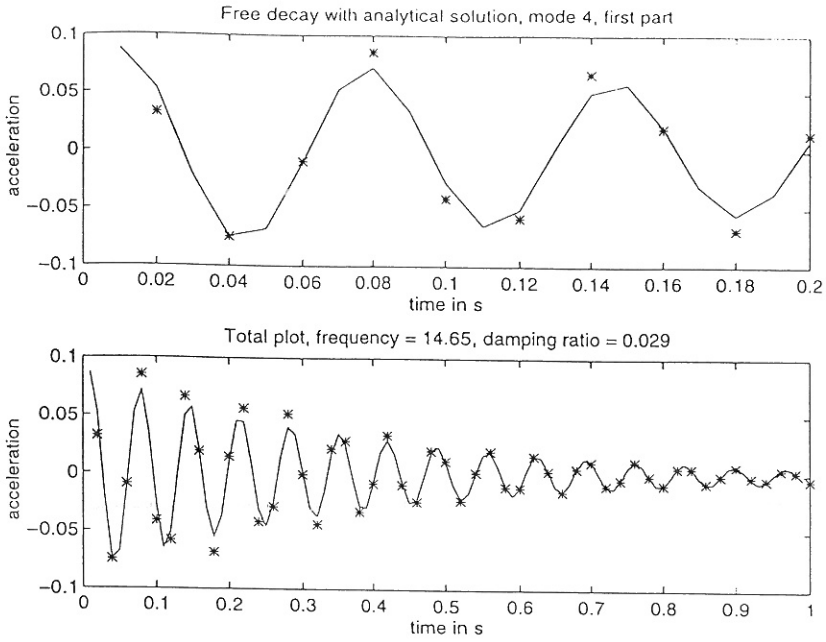

Figure 4.15: Resulting free decay of the 4th rotational mode.

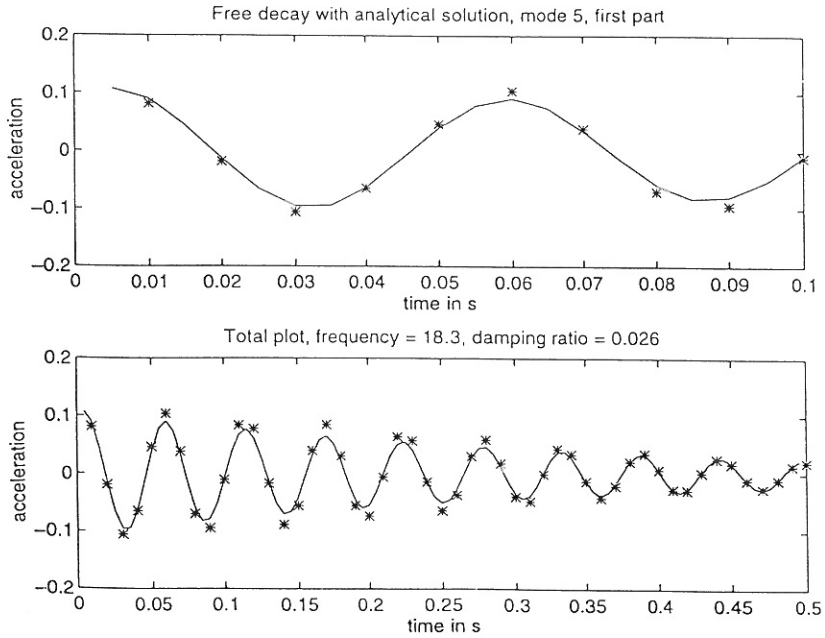

Figure 4.16: Resulting free decay of the 5th rotational mode.

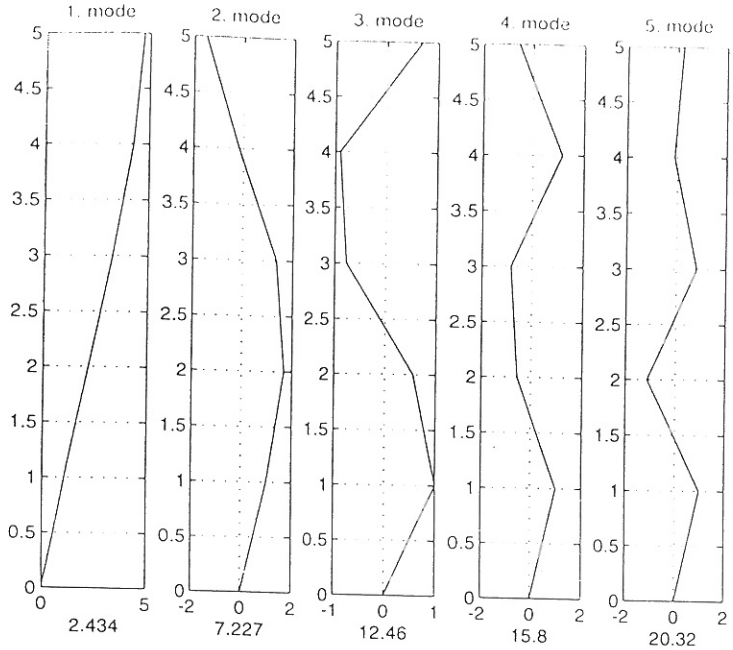

Figure 4.17: Mode shapes of translational modes.

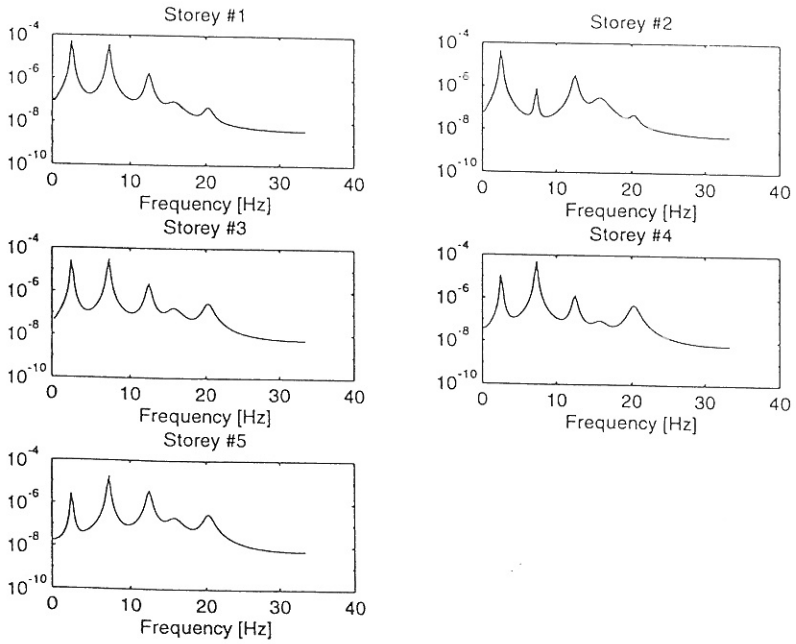

Figure 4.18: Autospectral densities obtained from the hybrid approach.

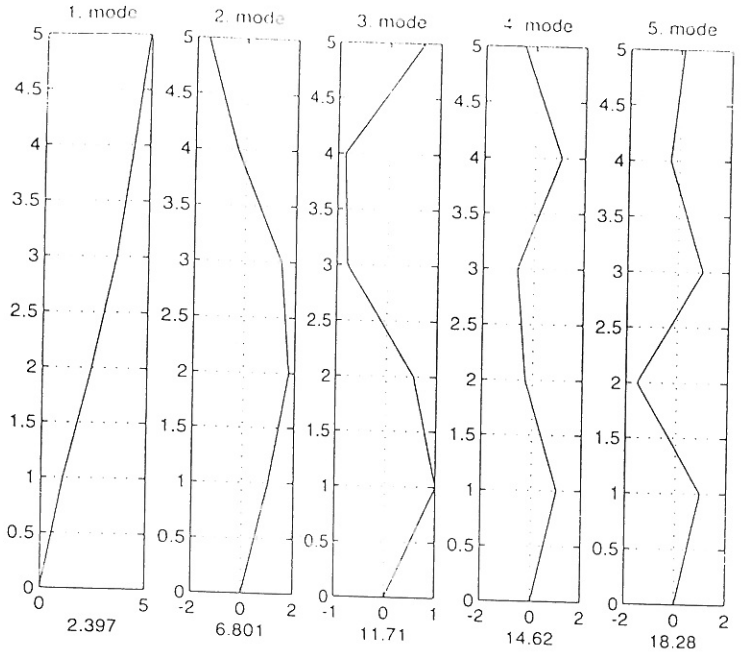

Figure 4.19: Mode shapes of rotational modes.

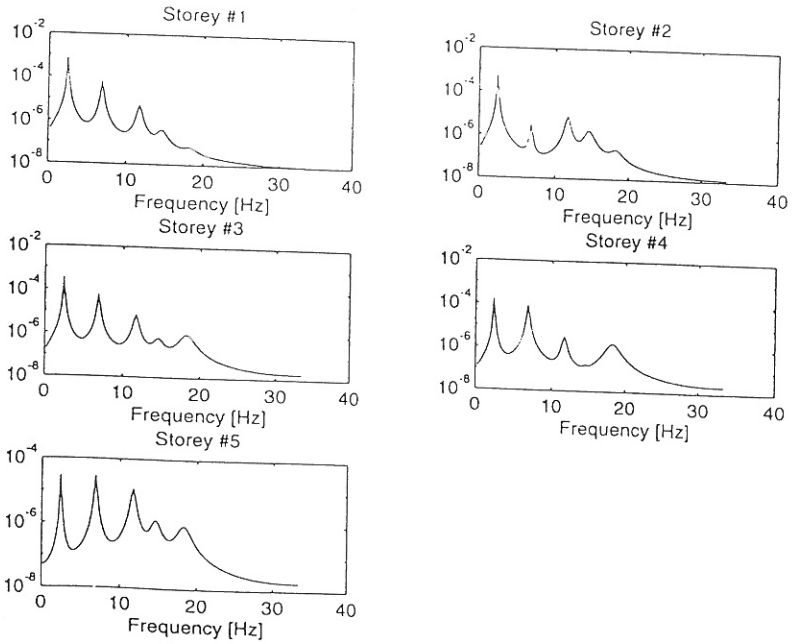

Figure 4.20: Autospectral densities the hybrid approach.

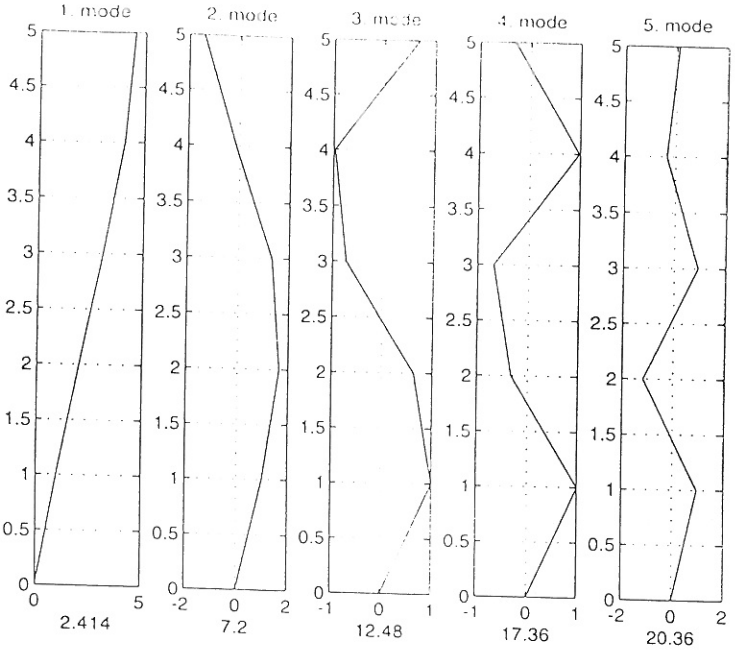

Figure 4.21: Mode shapes of translational modes.

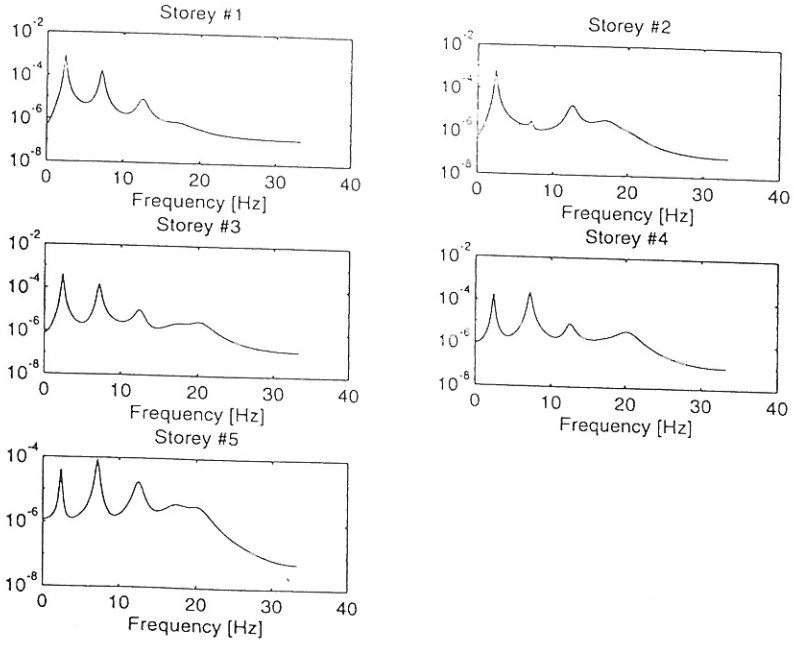

Figure 4.22: Autospectral densities obtained from the model.

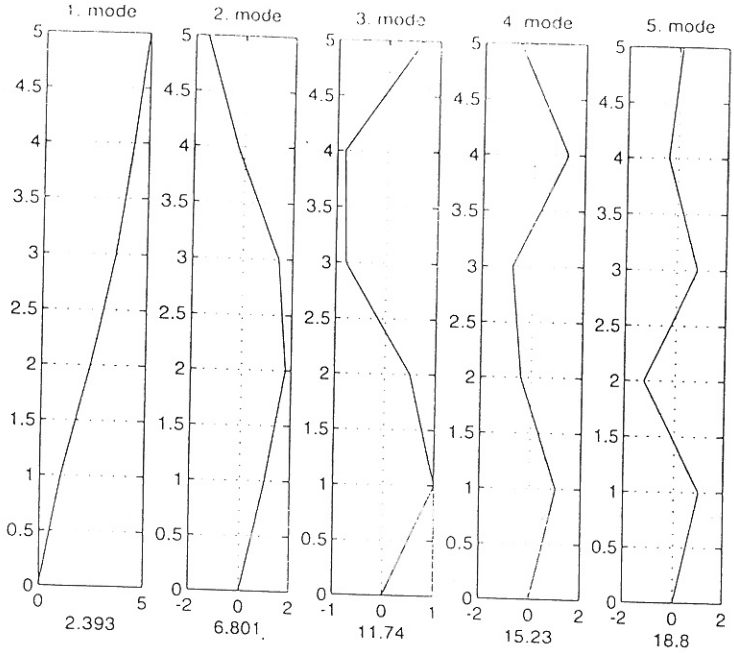

Figure 4.23: Mode shapes of rotational modes.

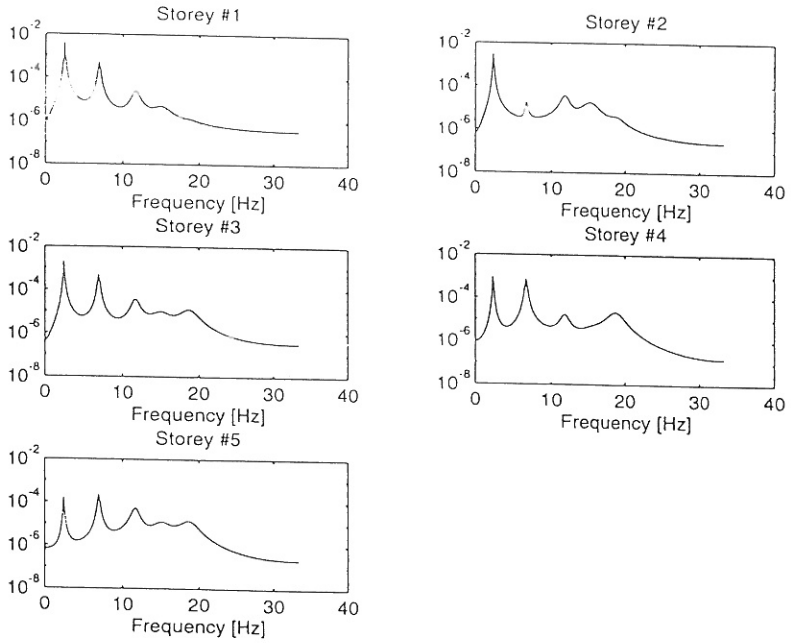

Figure 4.24: Autospectral densities obtained from the model.

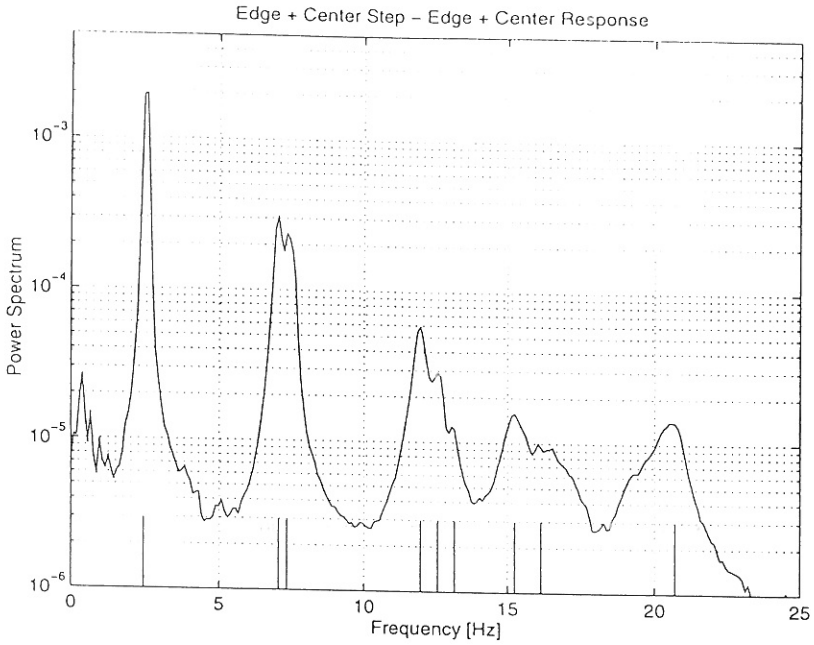

Figure 4.25: Power spectral density of all measurements.

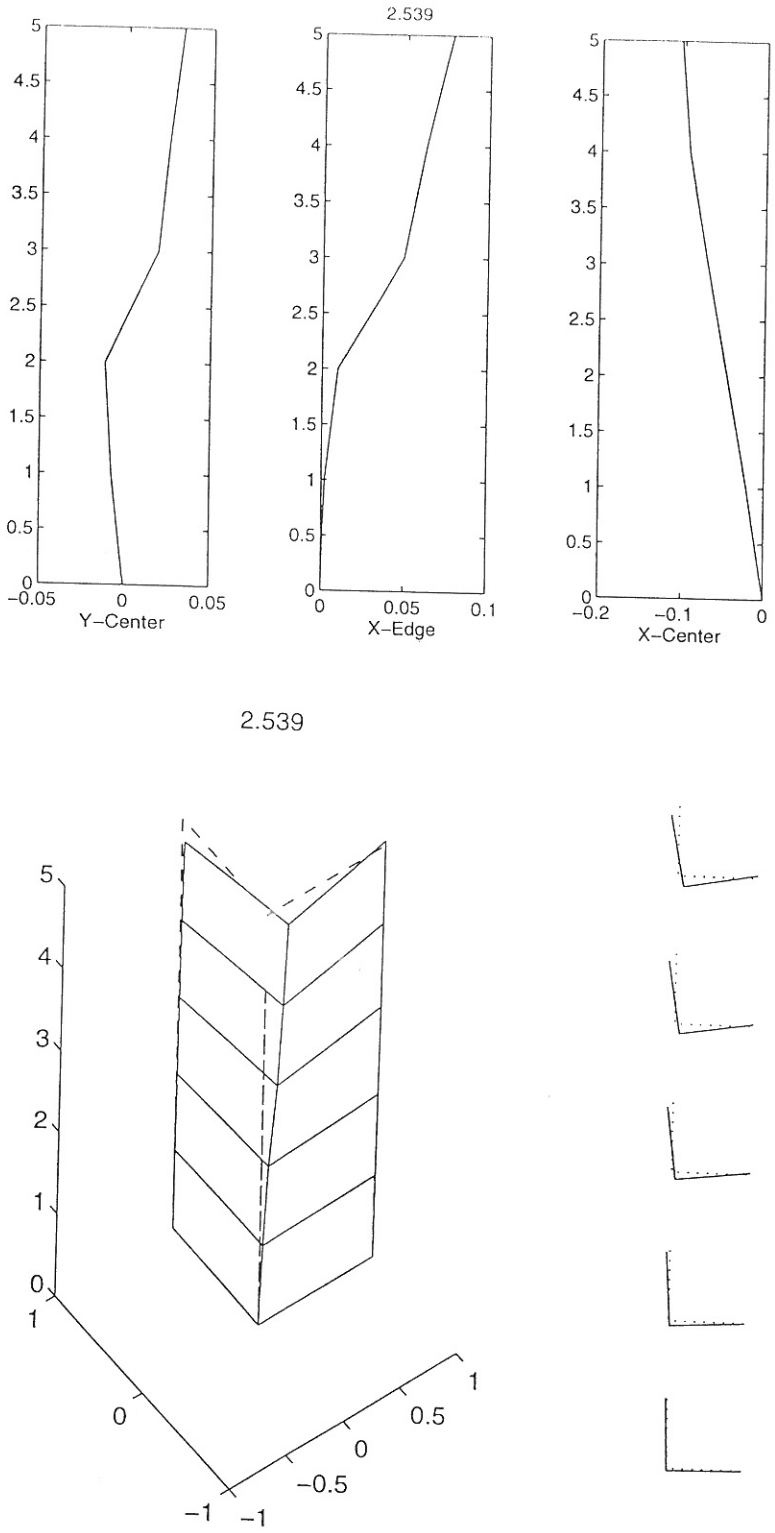

Figure 4.26: 1st mode shape estimated from center pull-out (FFT).

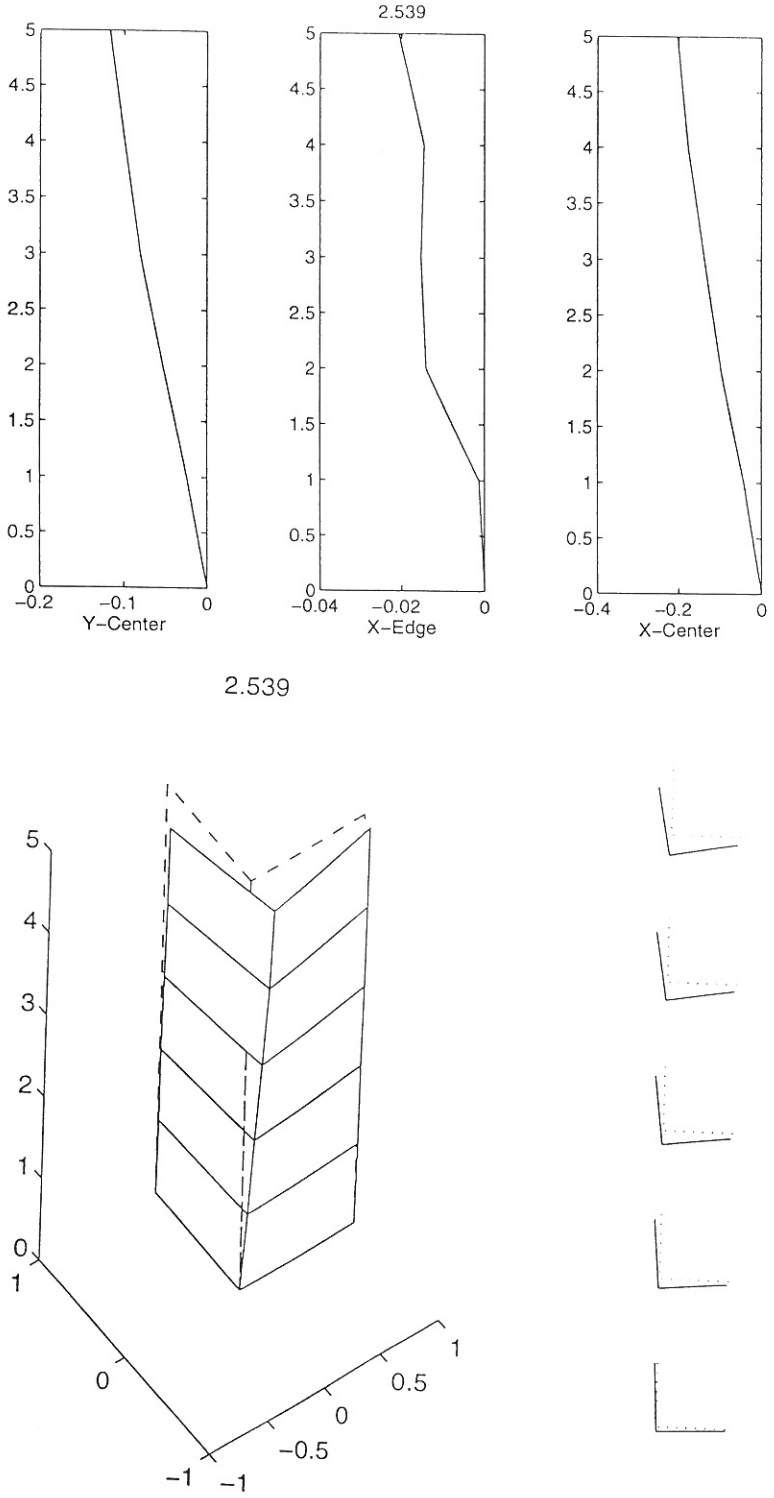

Figure 4.27: 1st mode shape estimated from edge pull-out (FFT).

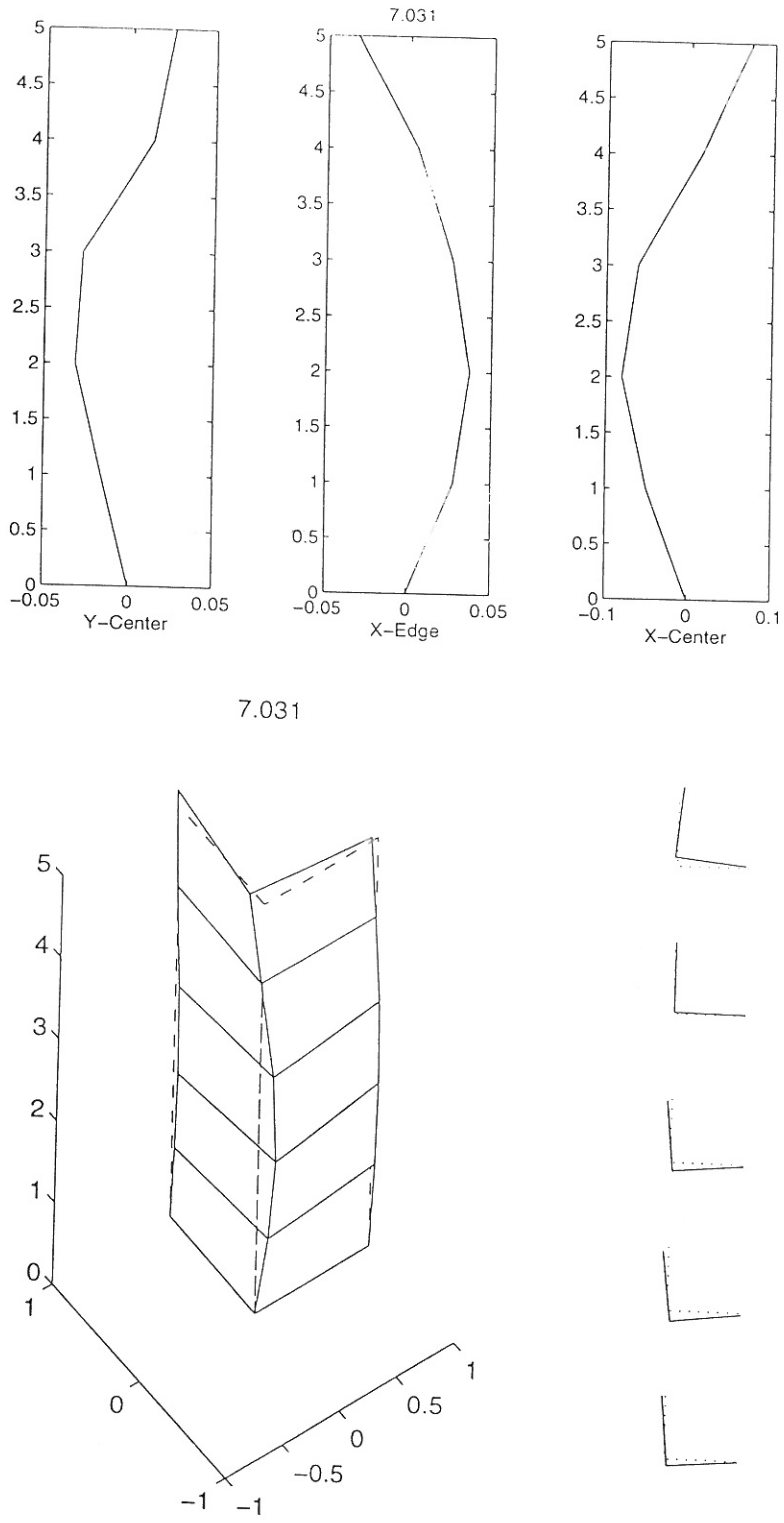

Figure 4.28: 2nd mode shape estimated from center pull-out (FFT).

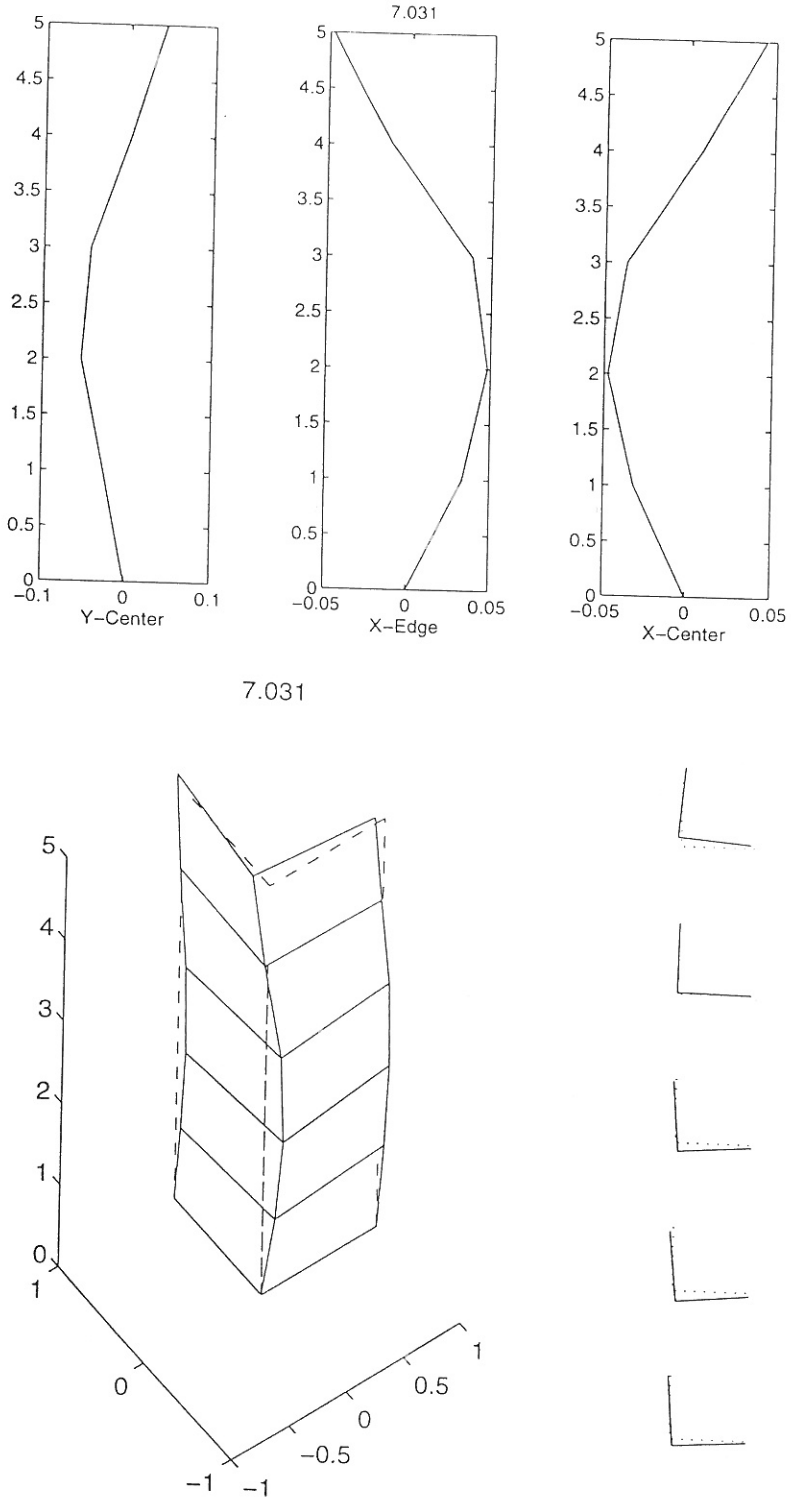

Figure 4.29: 2nd mode shape estimated from edge pull-out (FFT).

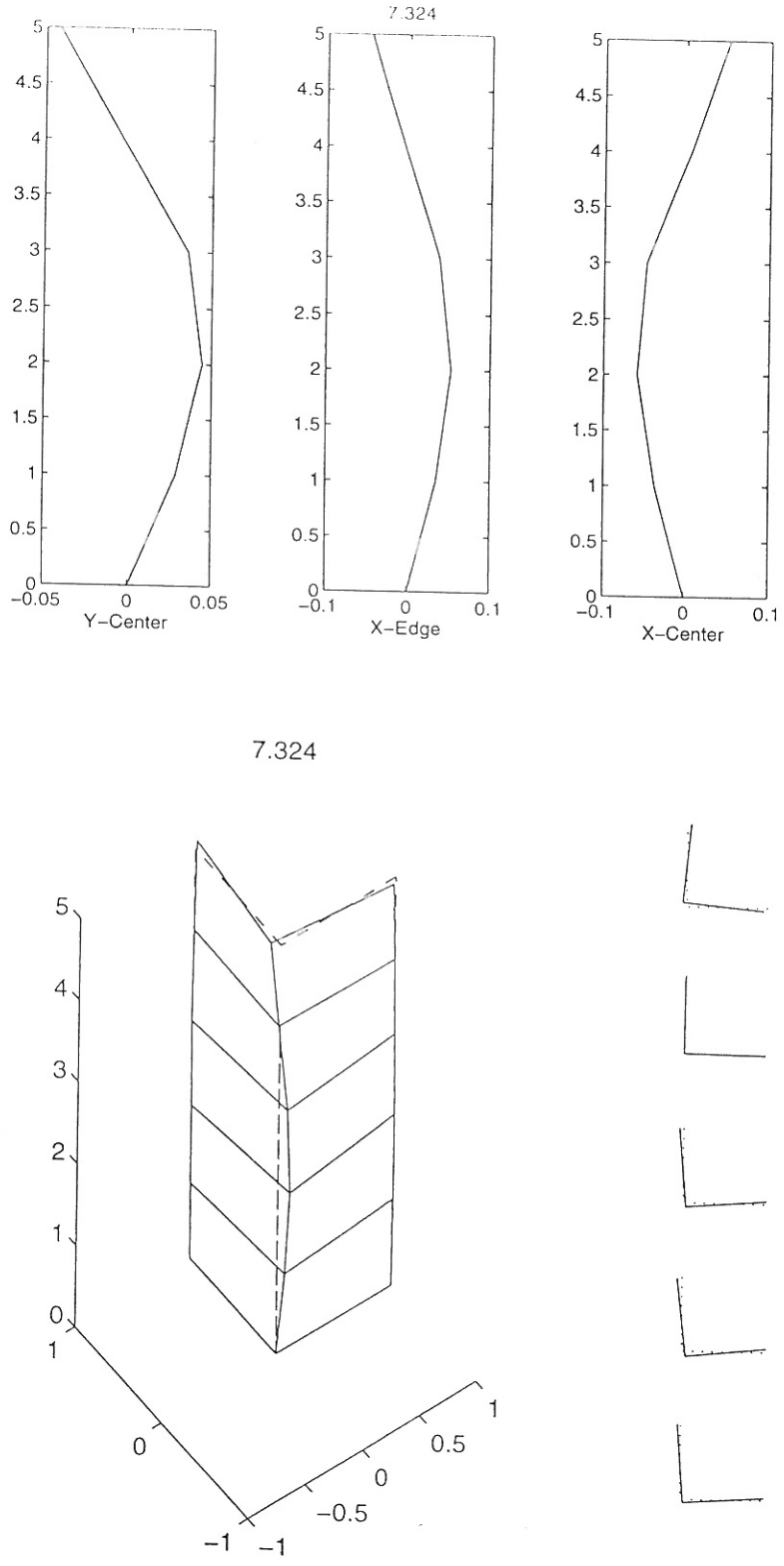

Figure 4.30: 3rd mode shape estimated from centre pull-out.

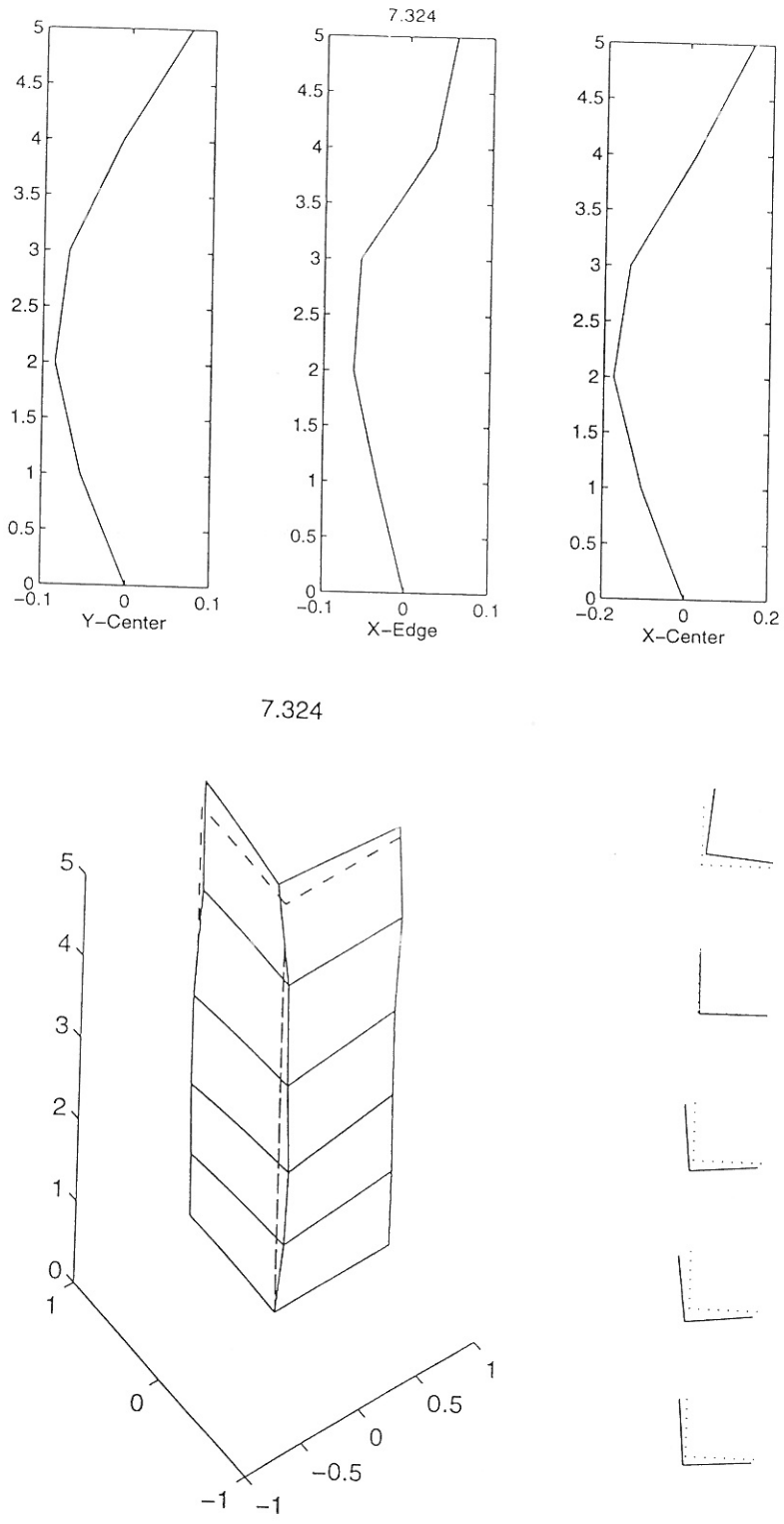

Figure 4.31: 3rd mode shape estimated from edge pull-out (FFT).

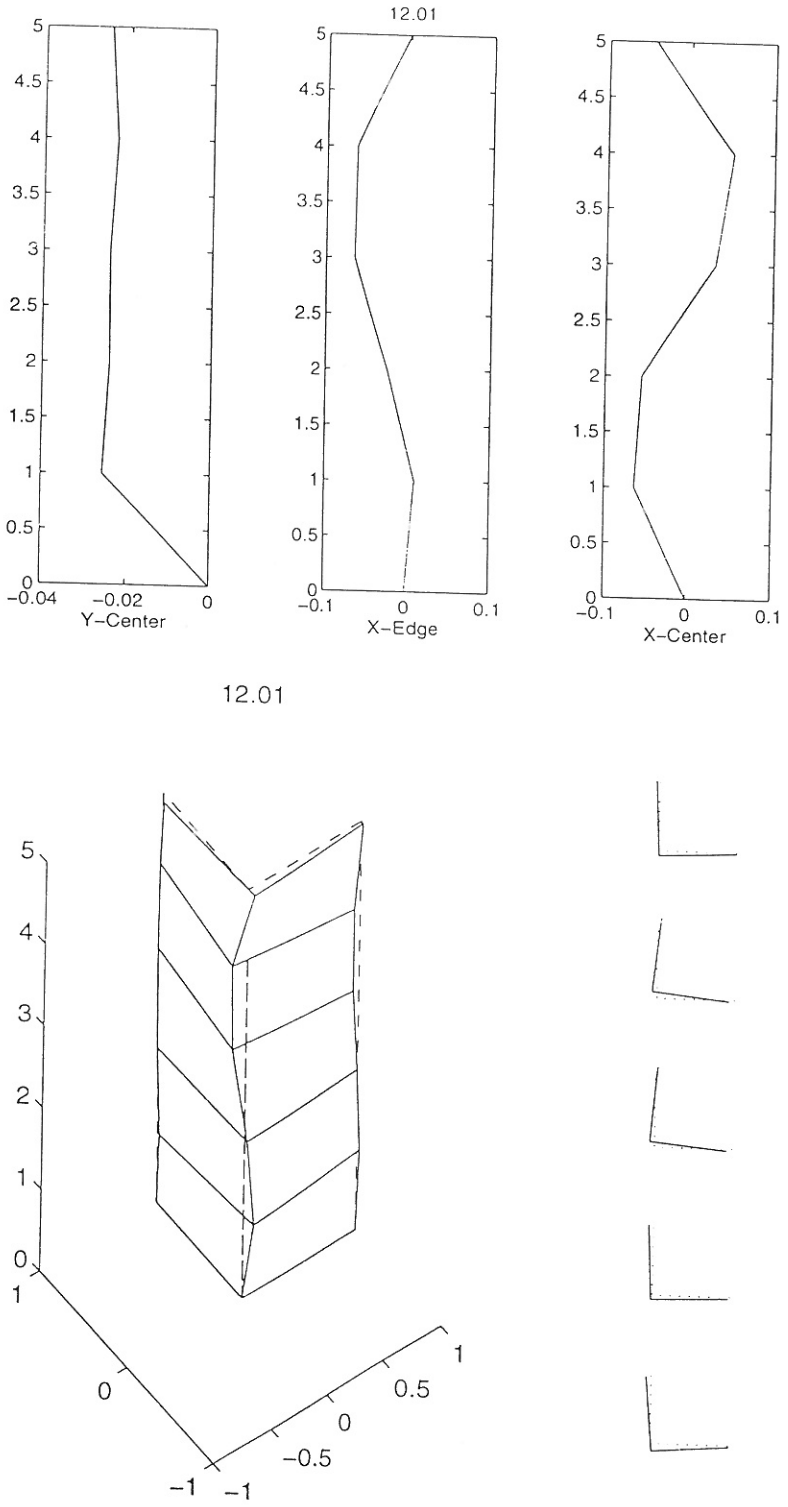

Figure 4.32: 4th mode shape estimated from centre pull-out.

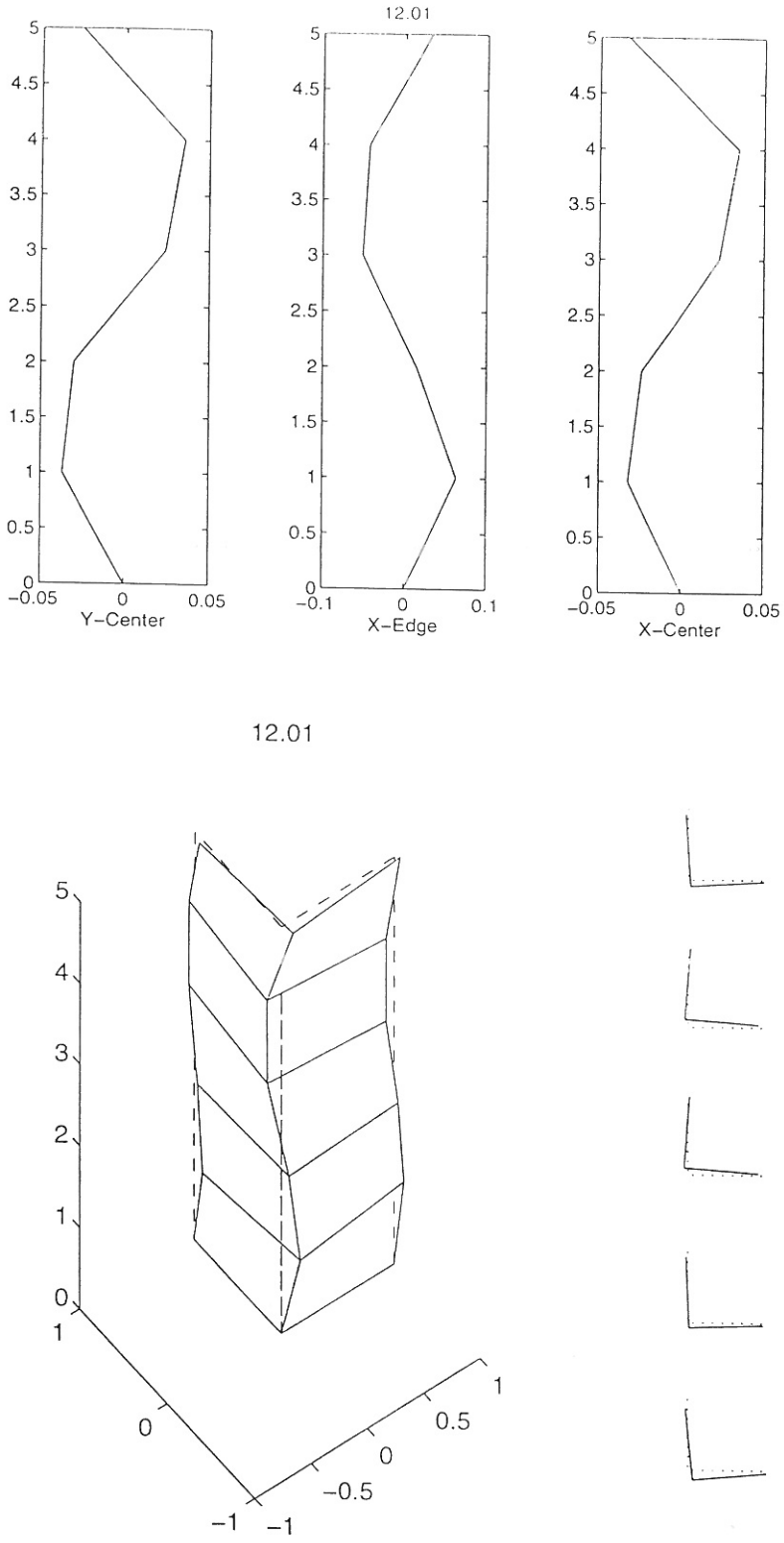

Figure 4.33: 4th mode shape estimated from edge pull-out (FFT).

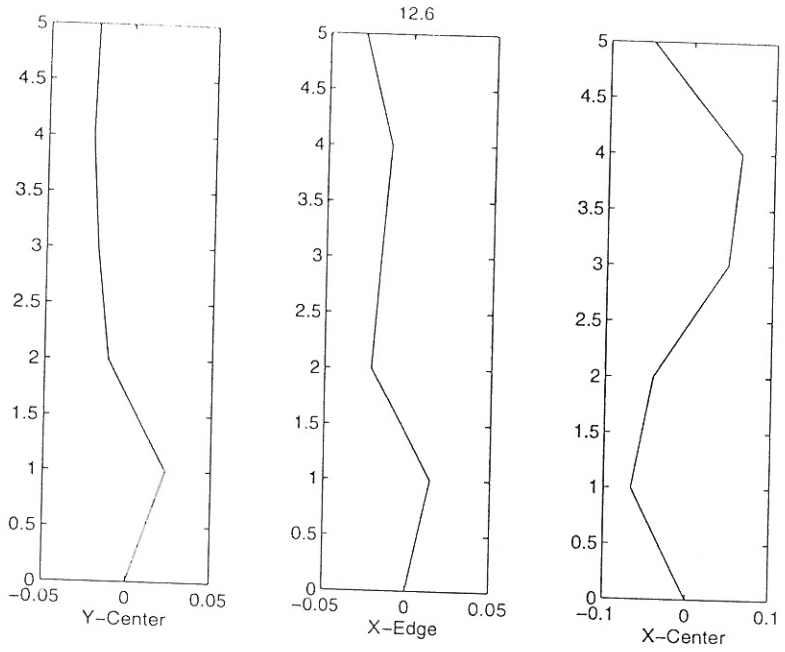

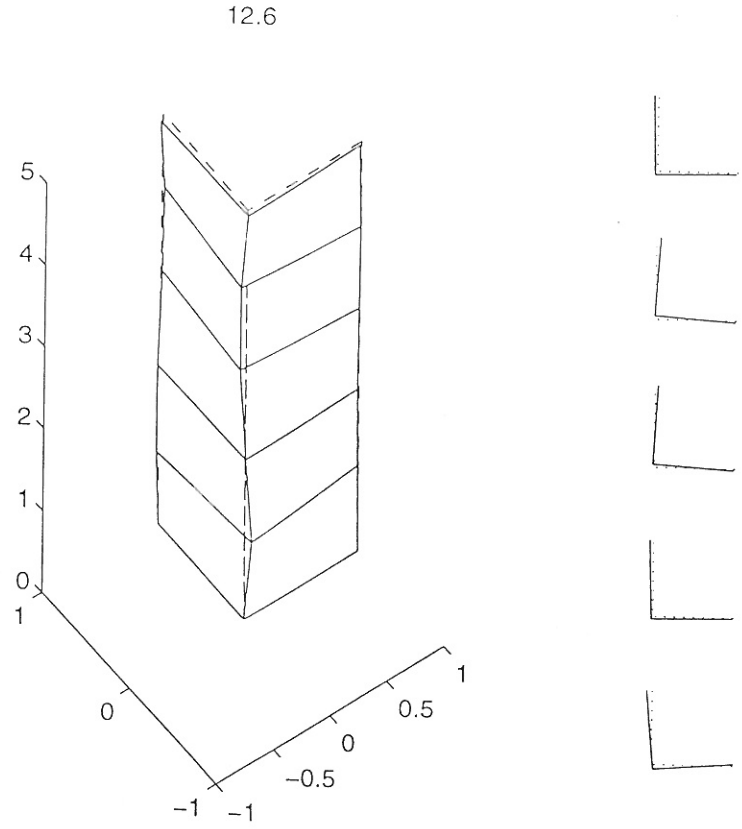

Figure 4.34: 5th mode shape estimated from centre pull-out (FFT).

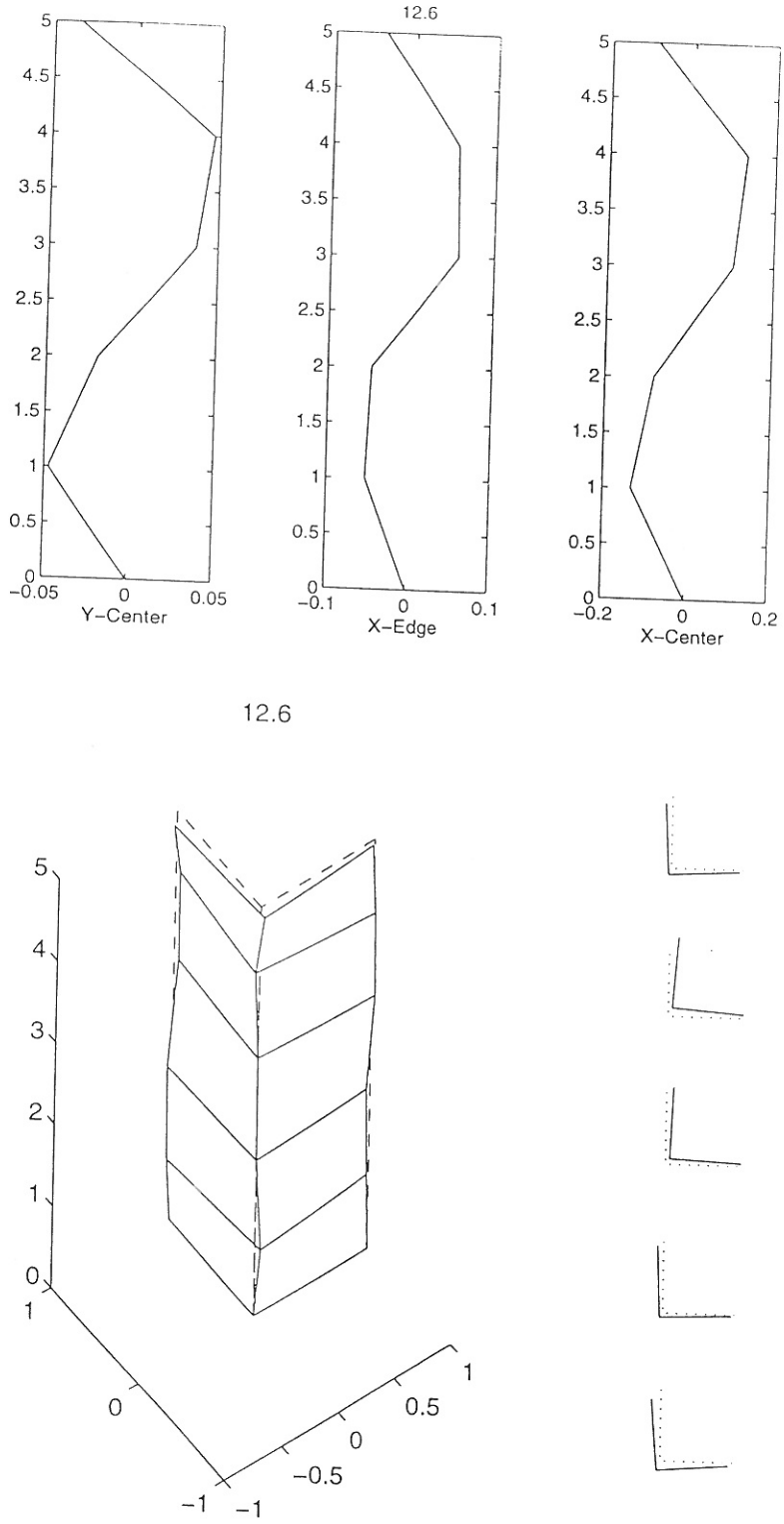

Figure 4.35: 5th mode shape estimated from edge pull-out (FFT).

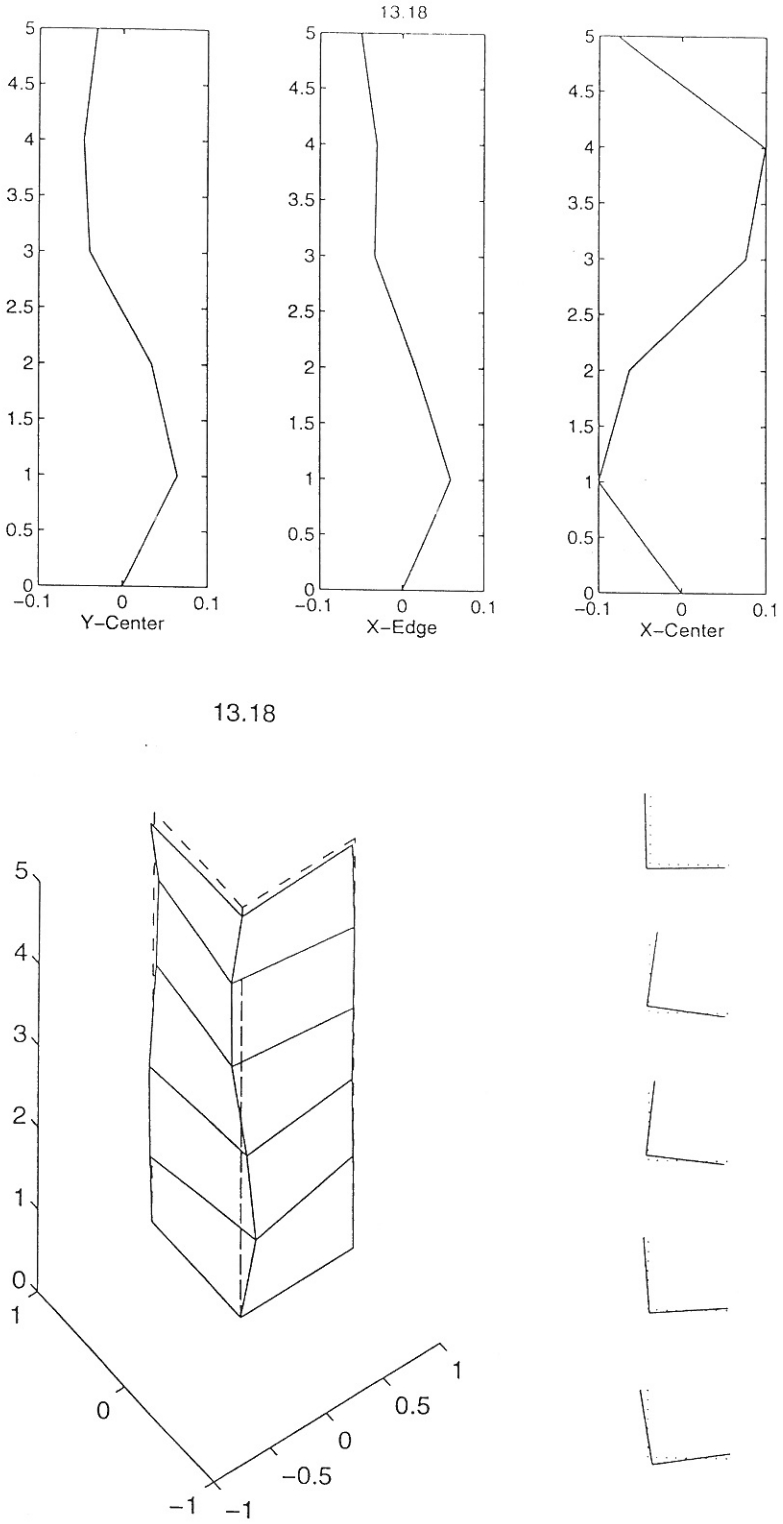

Figure 4.36: 6th mode shape estimated from centre pull-out (FFT).

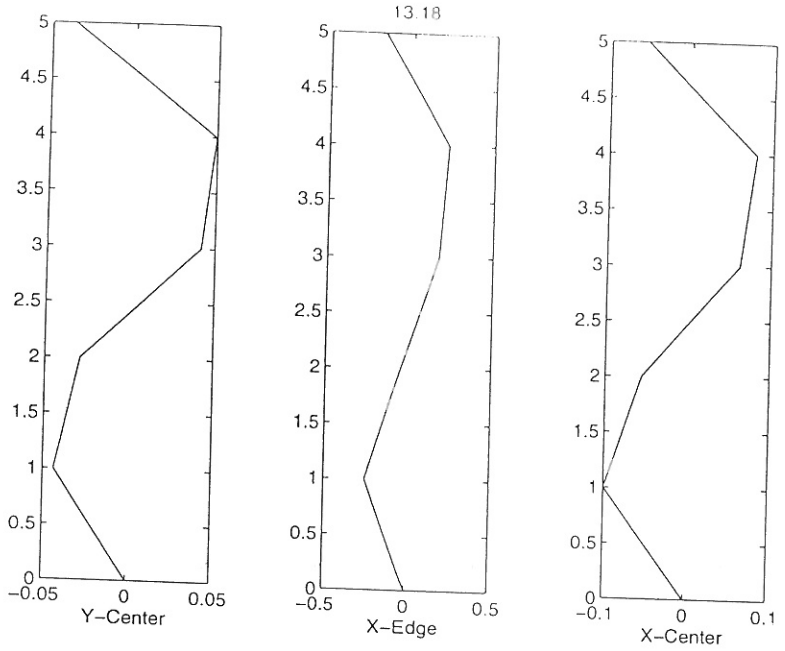

13.18

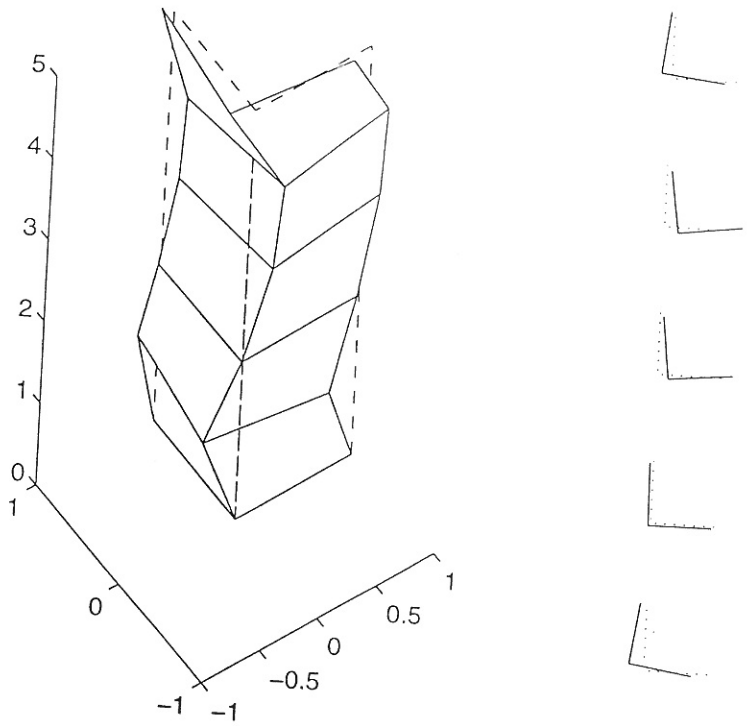

Figure 4.37: 6th mode shape estimated from edge pull-out (FFT).

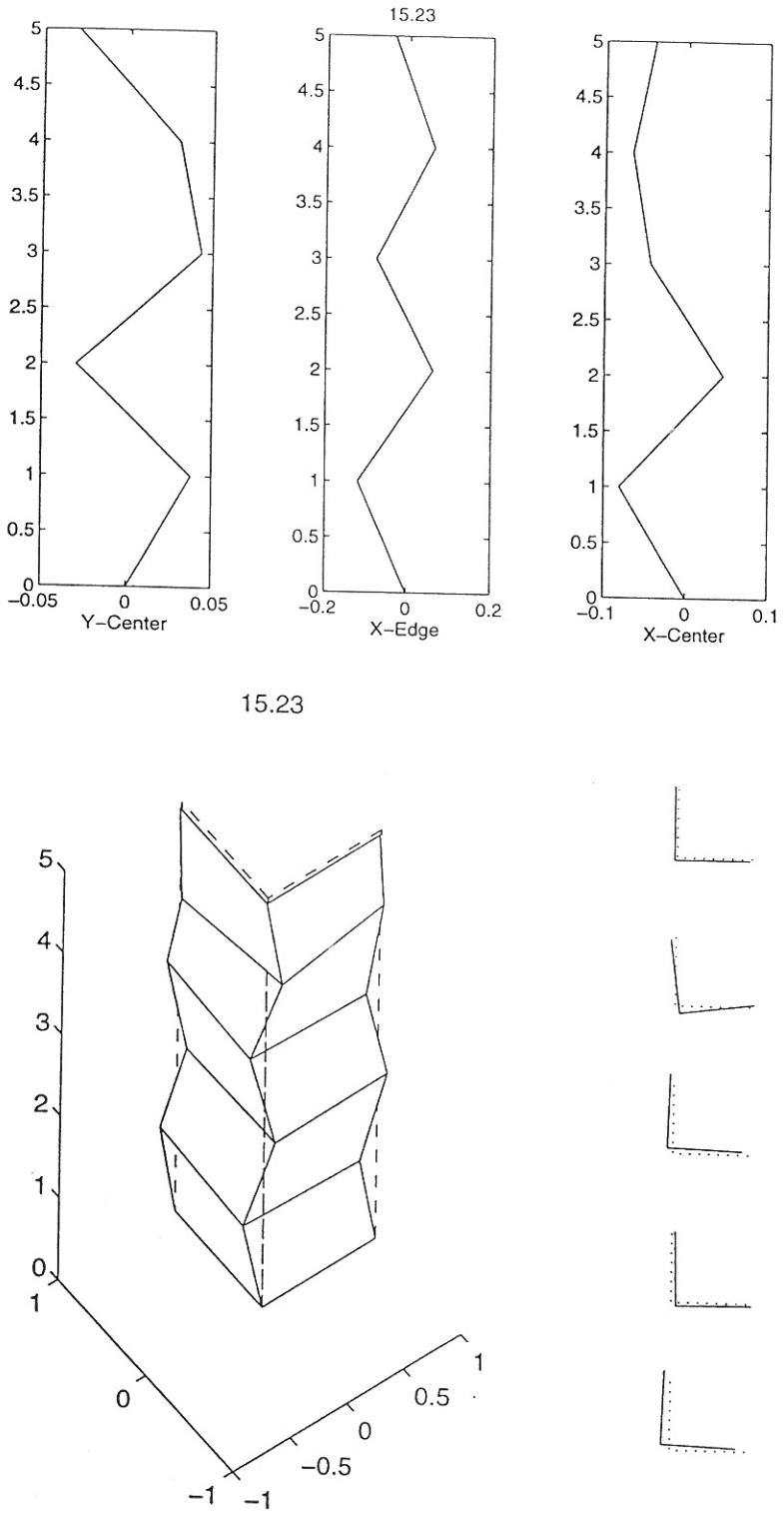

Figure 4.38: 7th mode shape estimated from centre pull-out (FFT).

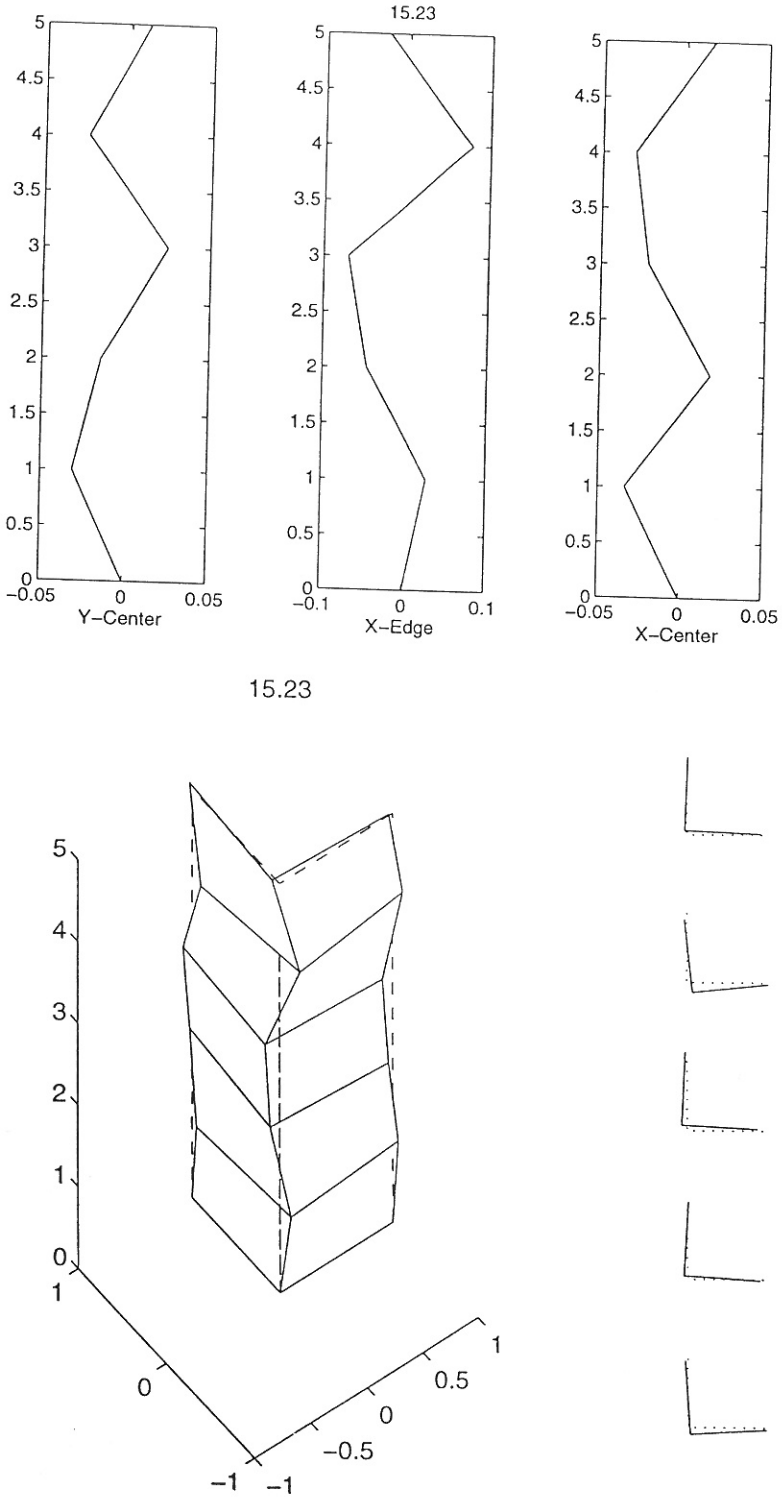

Figure 4.39: 7th mode shape estimated from edge pull-out (FFT).

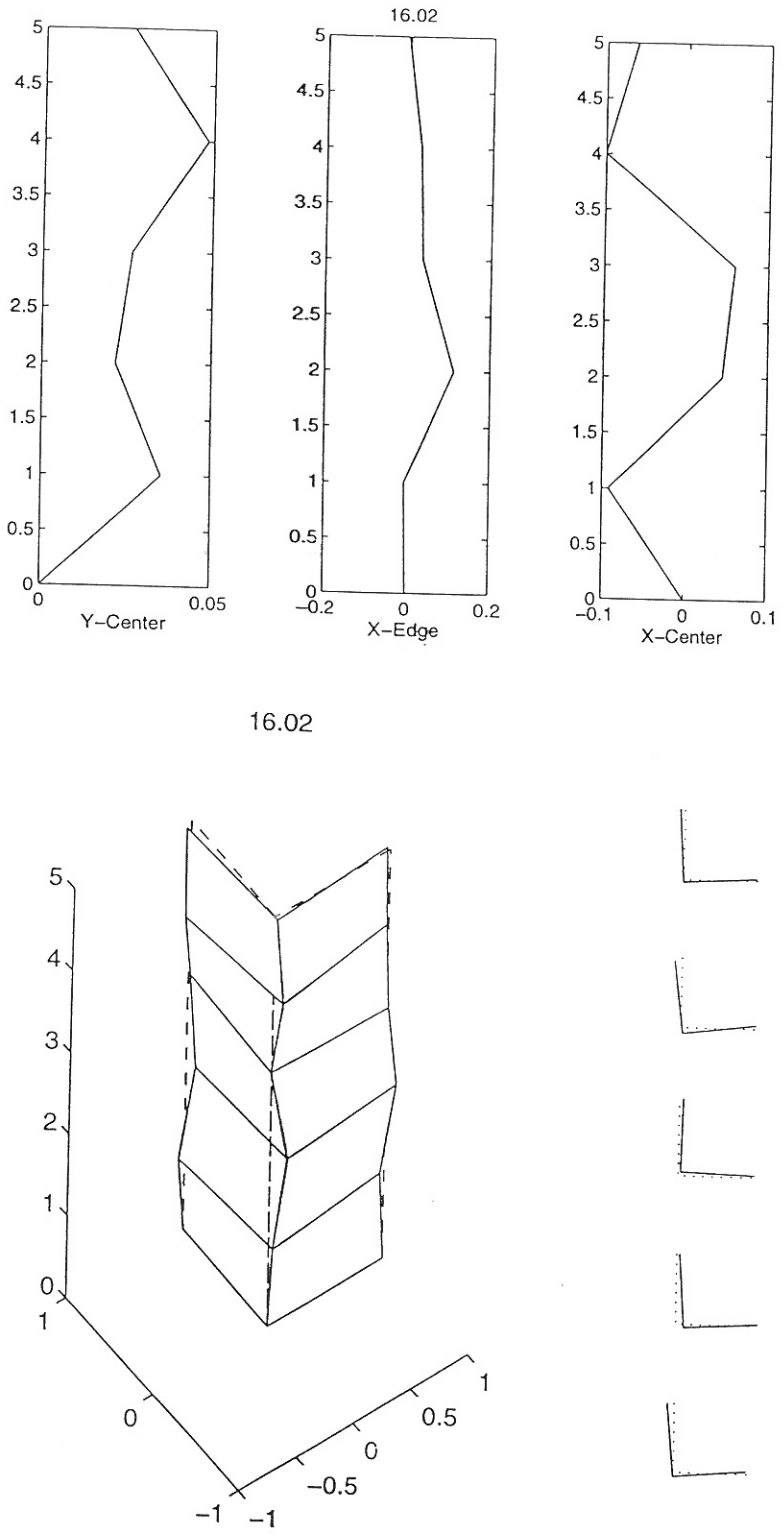

Figure 4.40: 8th mode shape estimated from centre pull-out (FFT).

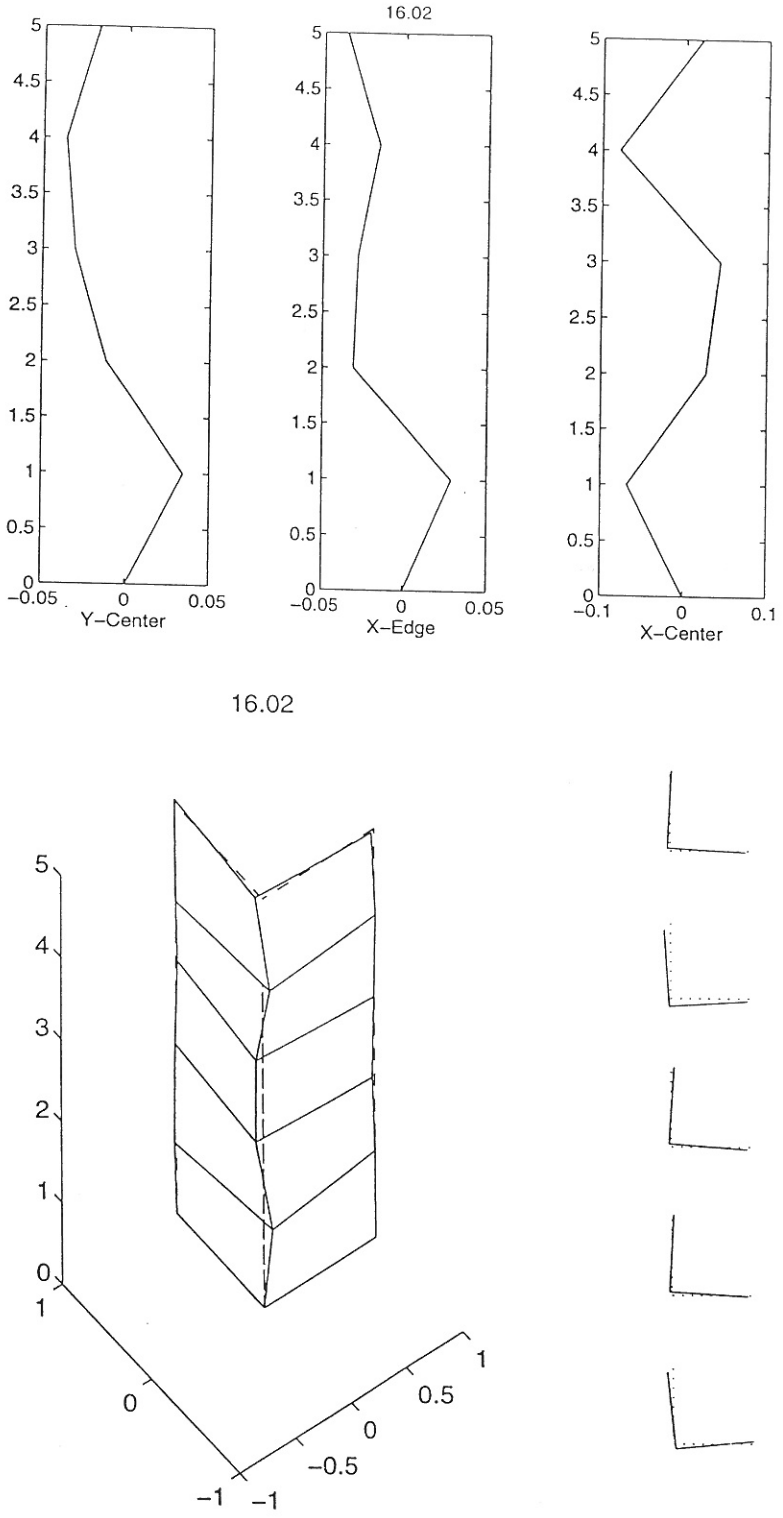

Figure 4.41: 8th mode shape estimated from edge pull-out (FFT).

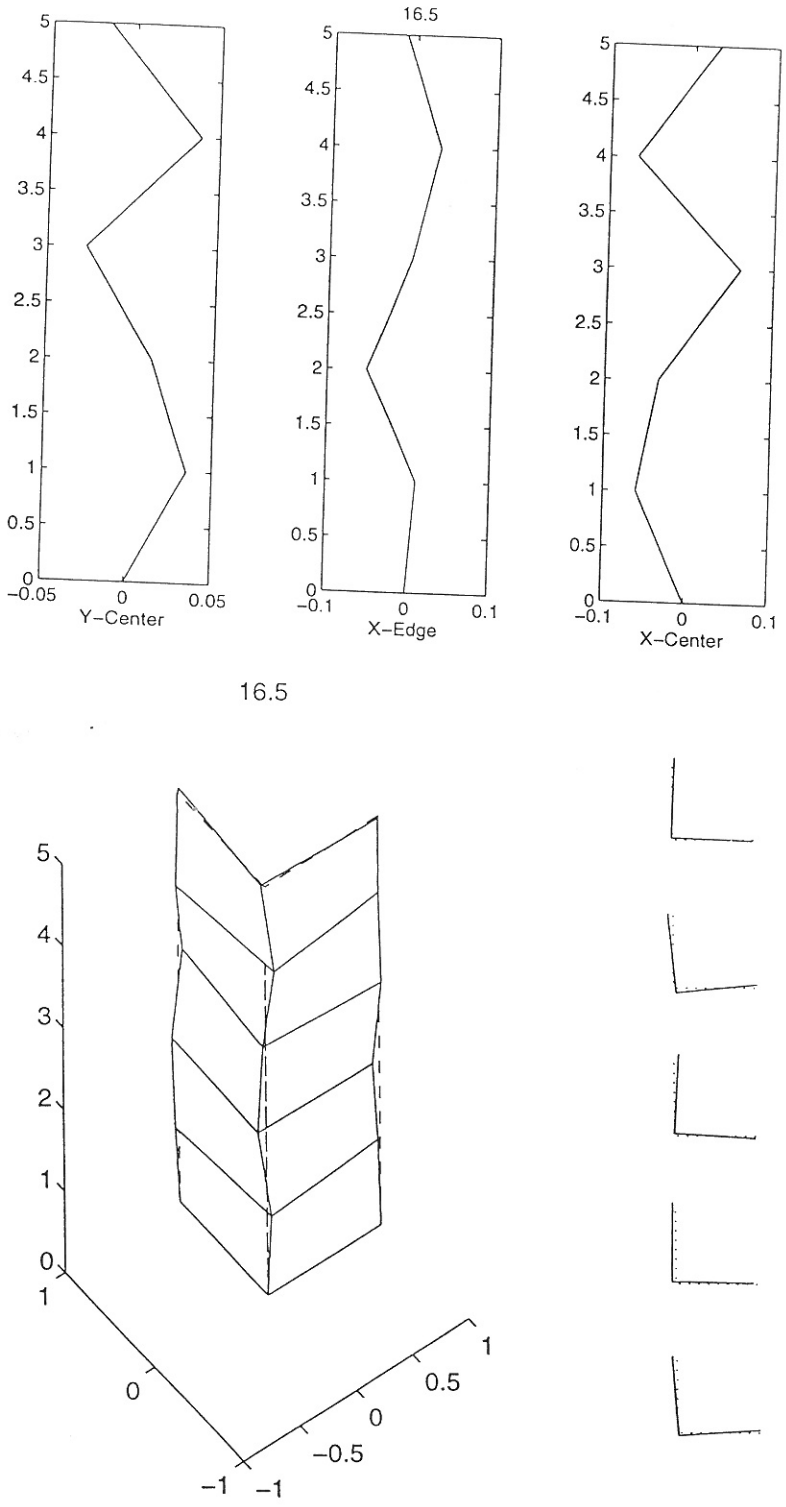

Figure 4.42: 9th mode shape estimated from centre pull-out (FFT).

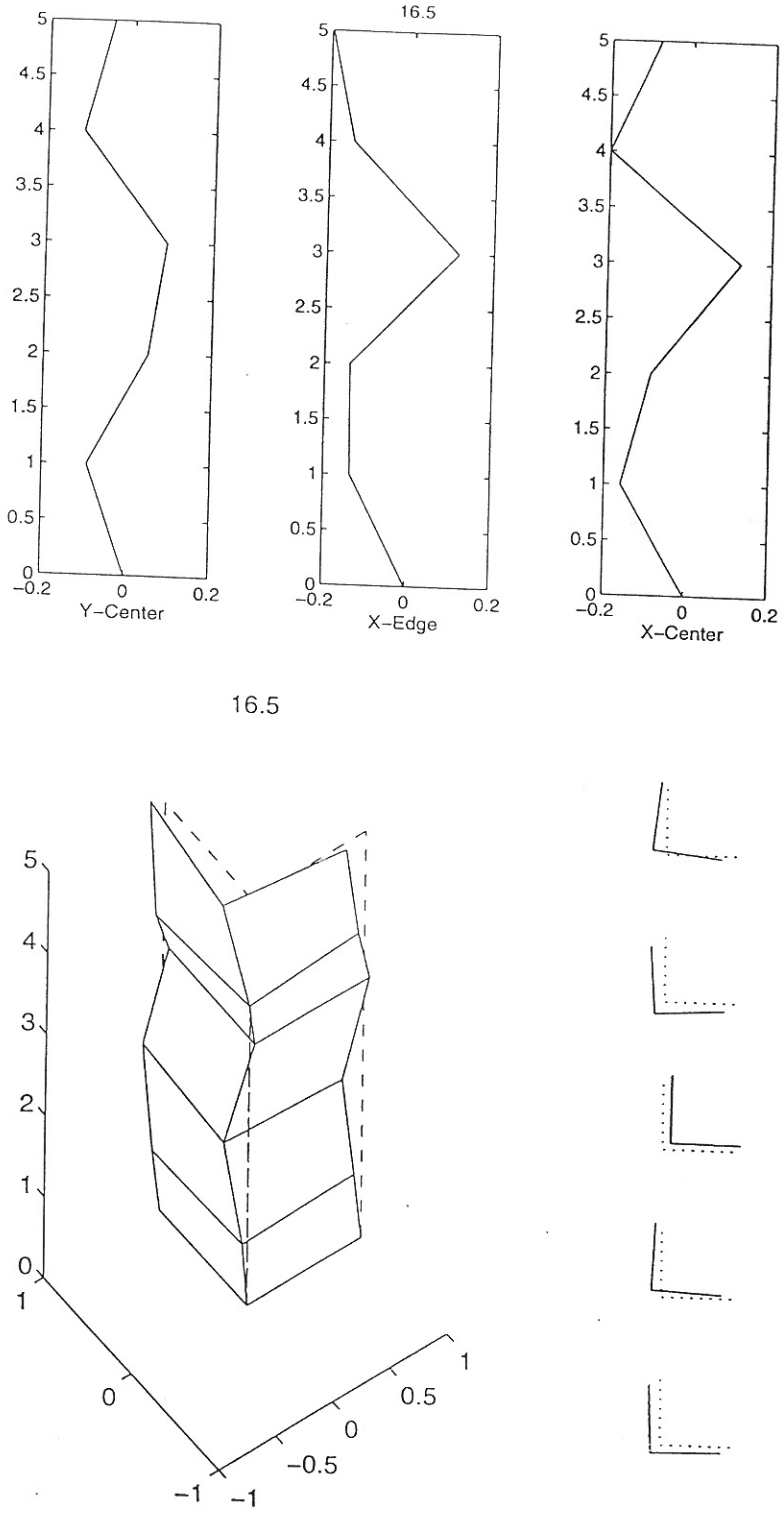

Figure 4.43: 9th mode shape estimated from edge pull-out (FFT).

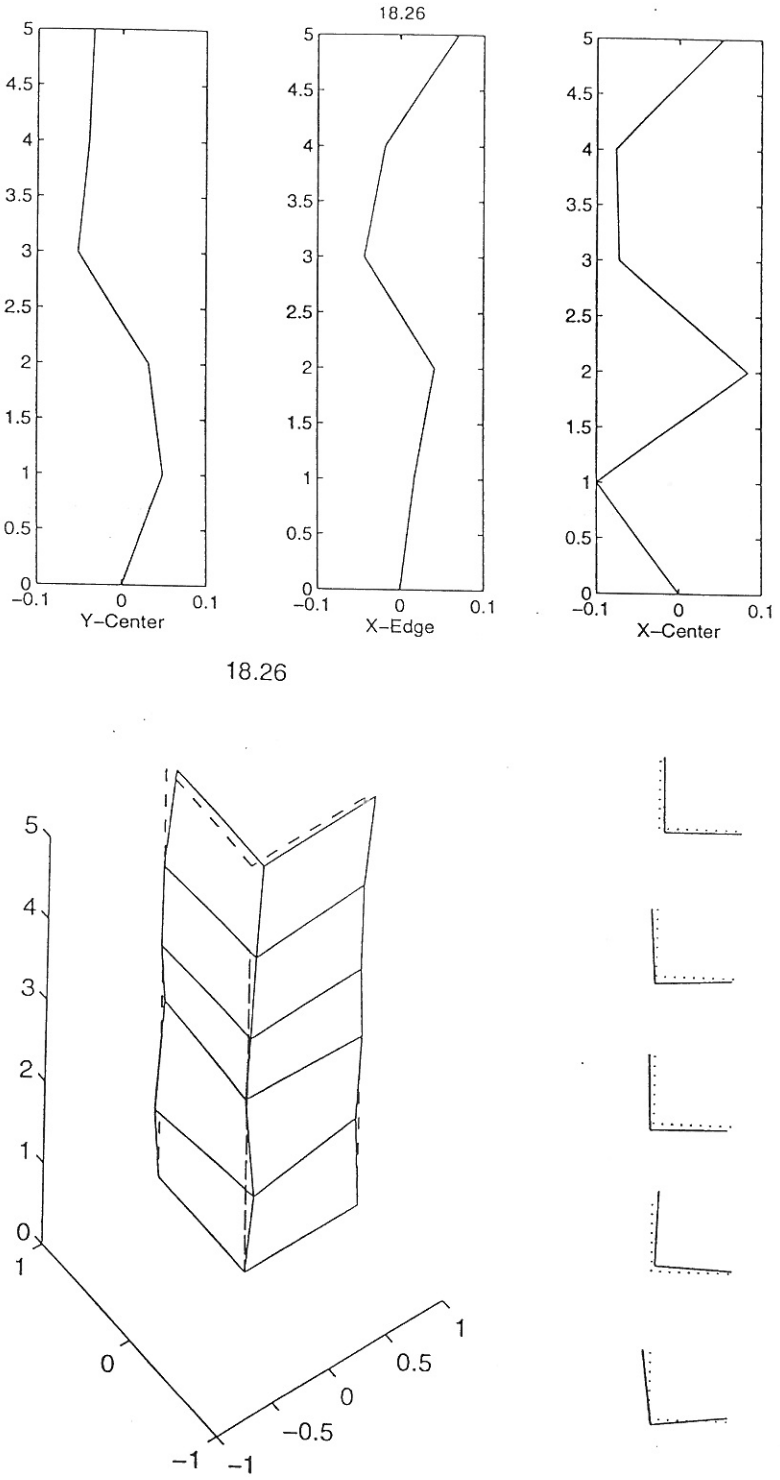

Figure 4.44: 10th mode shape estimated from centre pull-out (FFT).

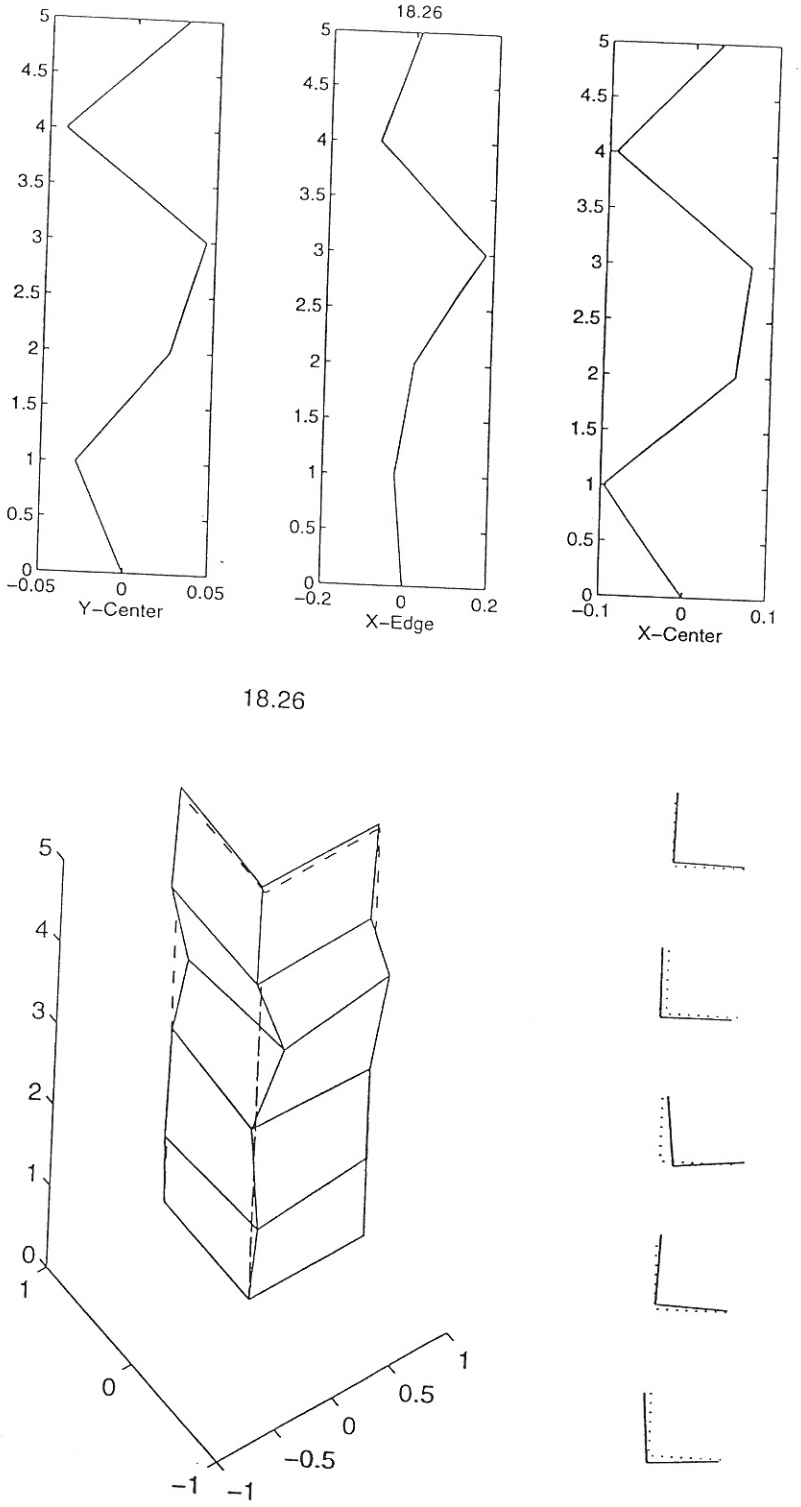

Figure 4.45: 10th mode shape estimated from edge pull-out (FFT).

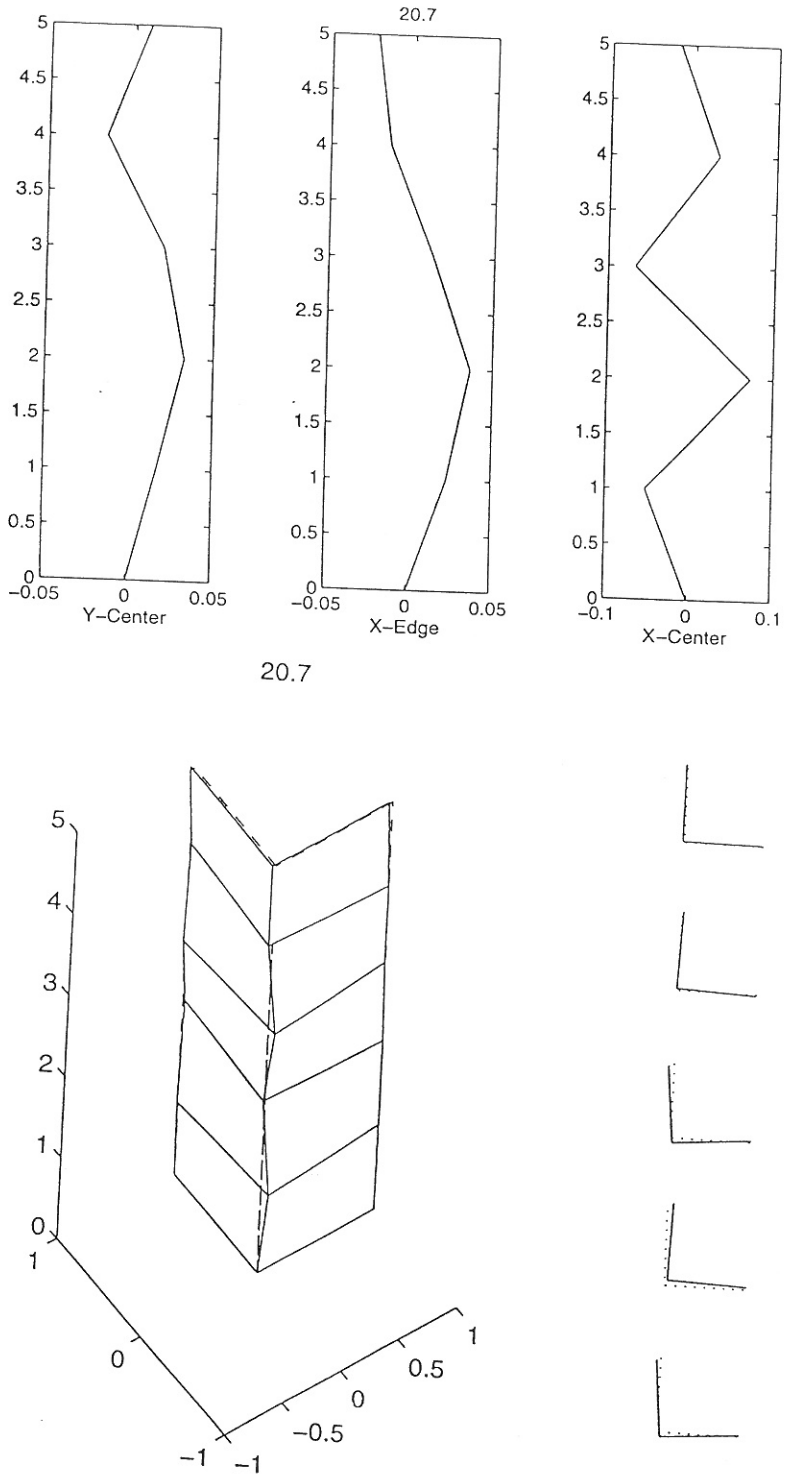

Figure 4.46: 11th mode shape estimated from centre pull-out (FFT).

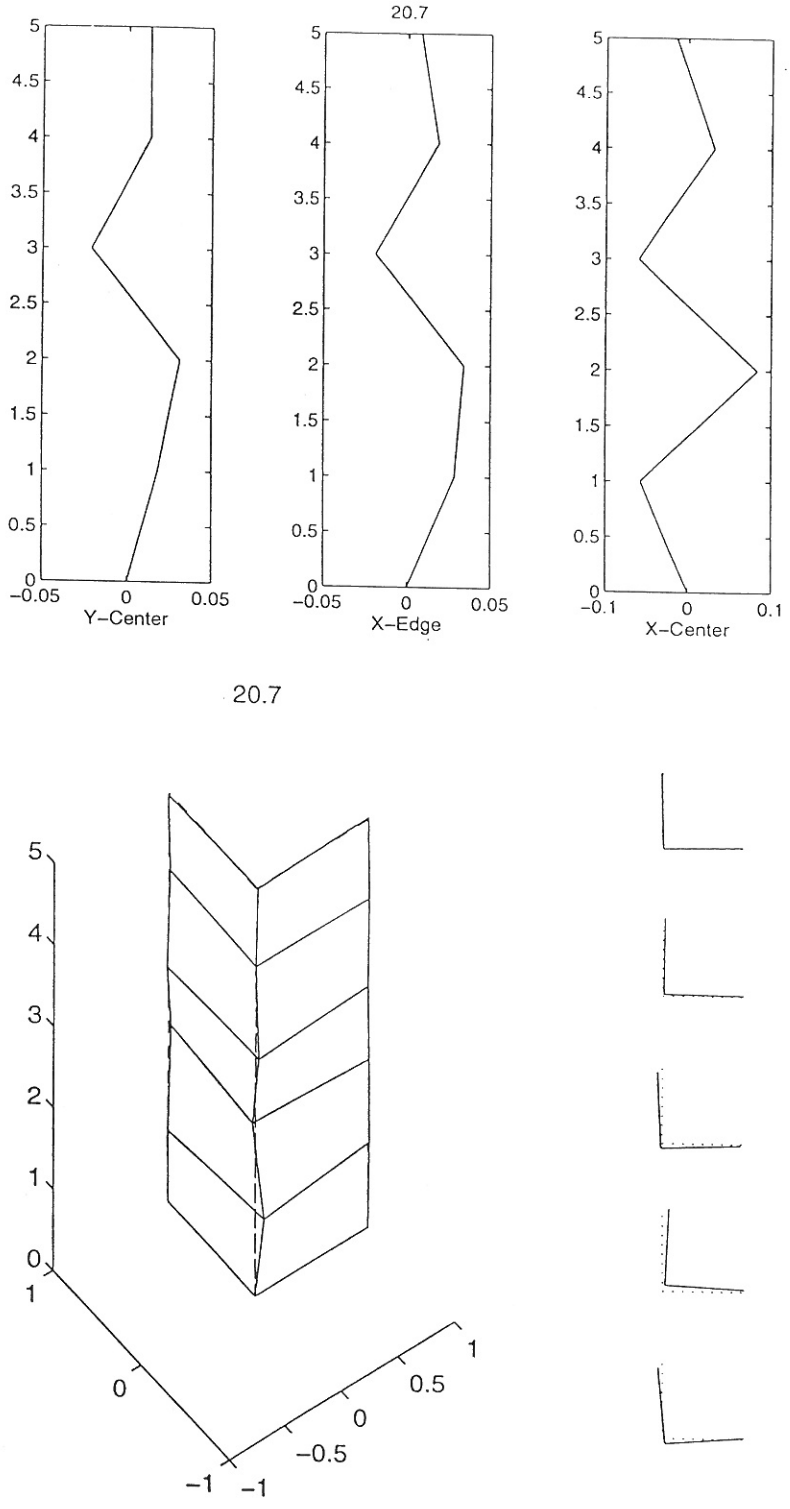

Figure 4.47: 11th mode shape estimated from edge pull-out (FFT).

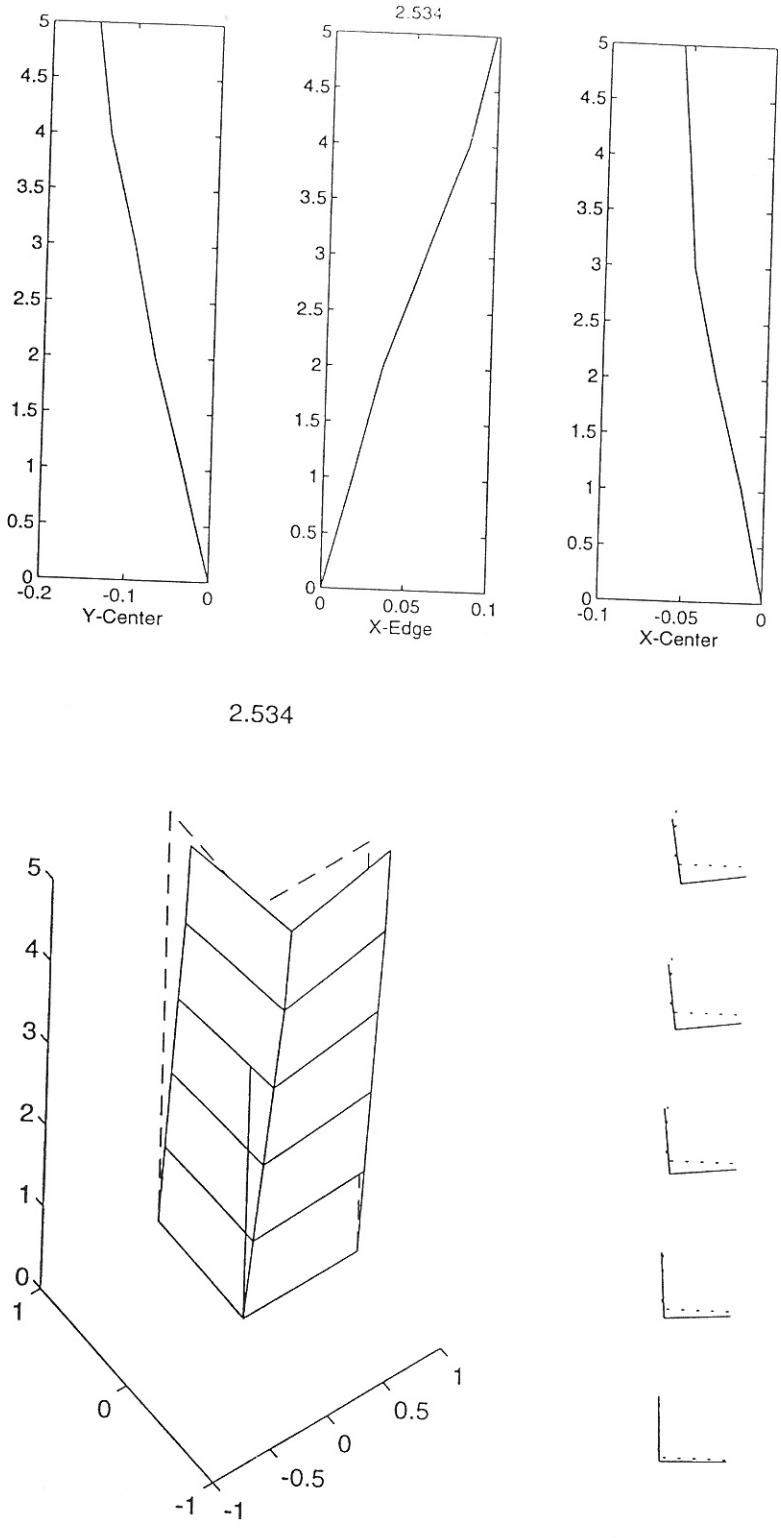

Figure 4.48: 1st mode shape estimated from centre pull-out (ARMAV).

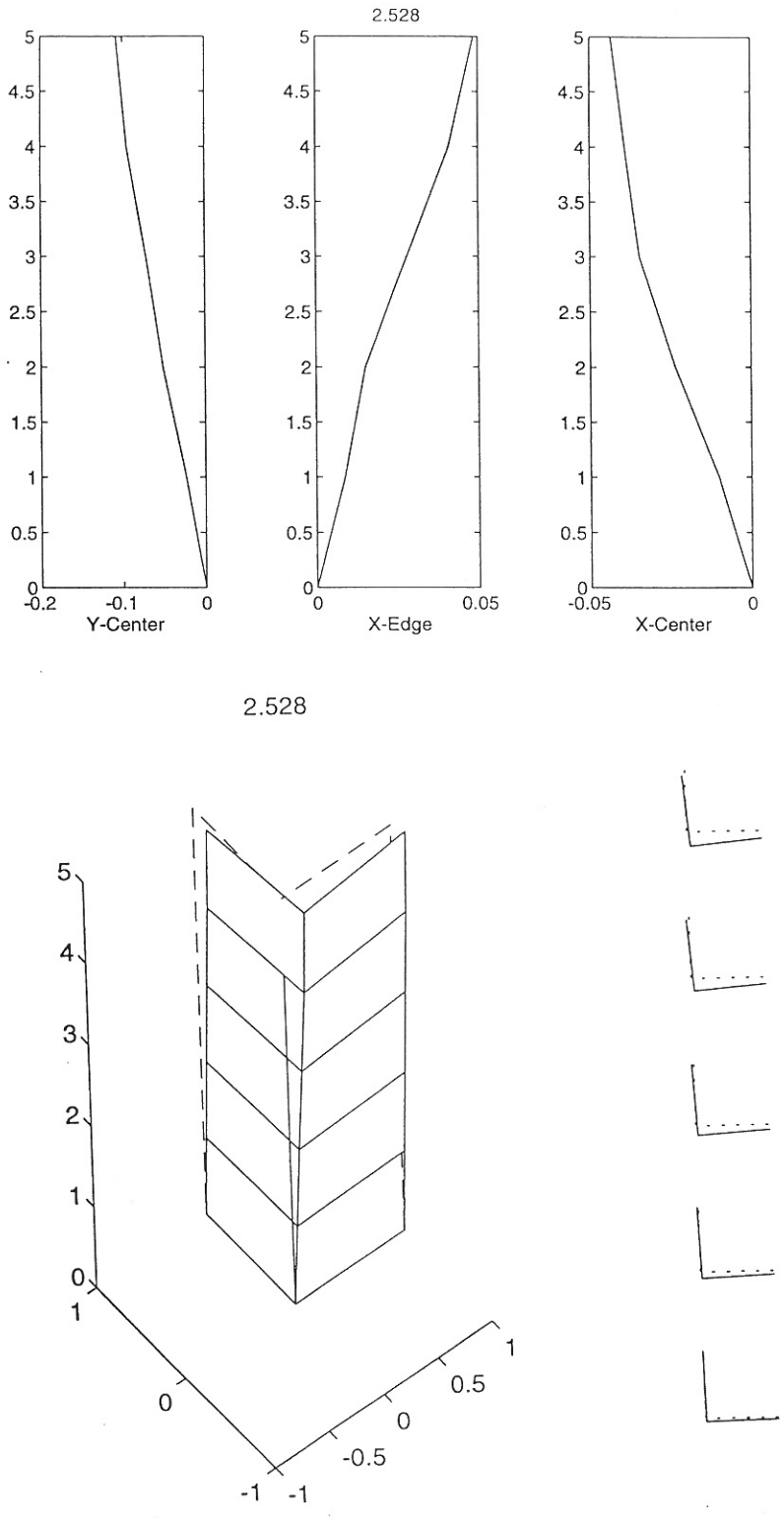

Figure 4.49: 1st mode shape estimated from edge pull-out (ARMAV).

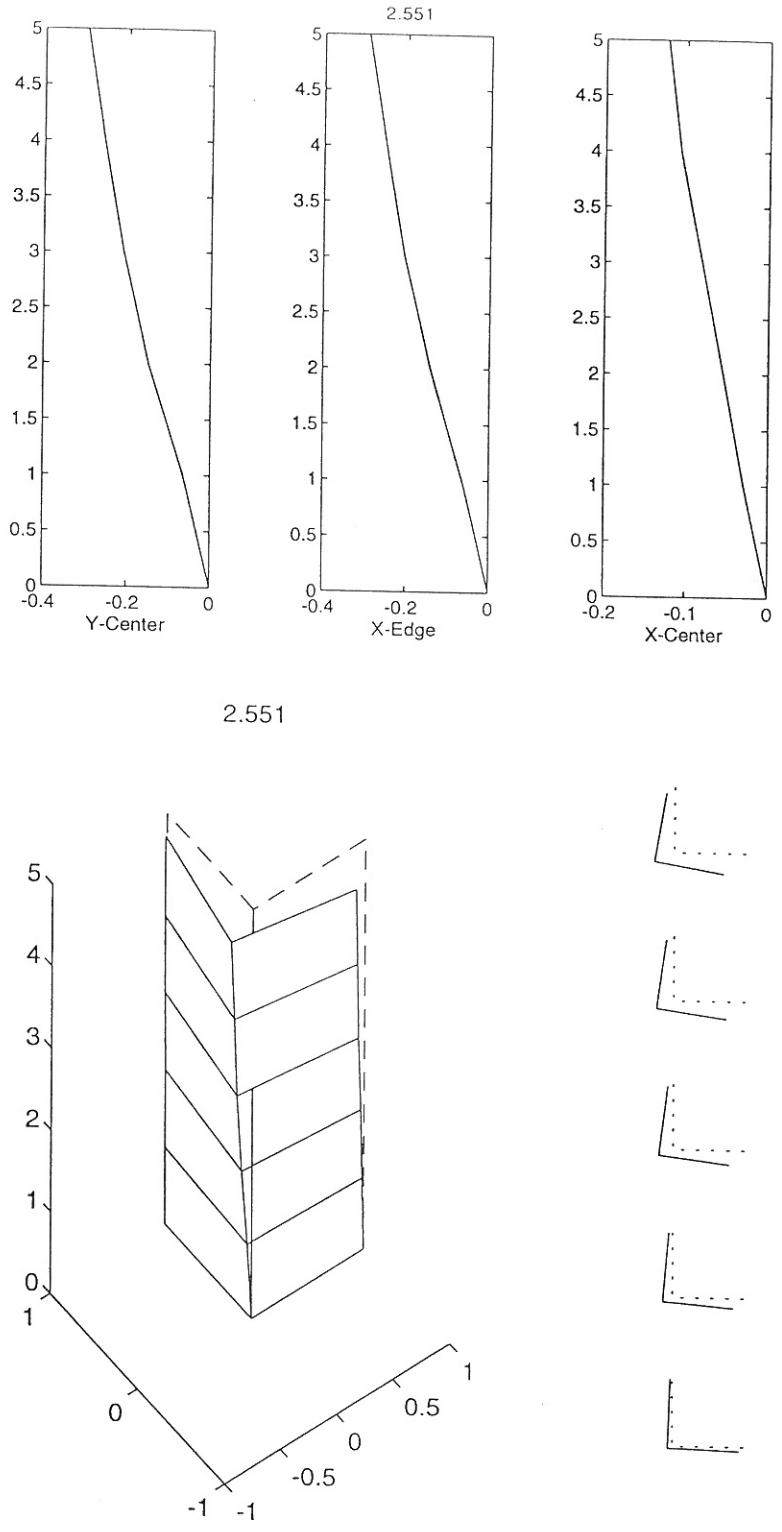

Figure 4.50: 2nd mode shape estimated from centre pull-out (ARMAV).

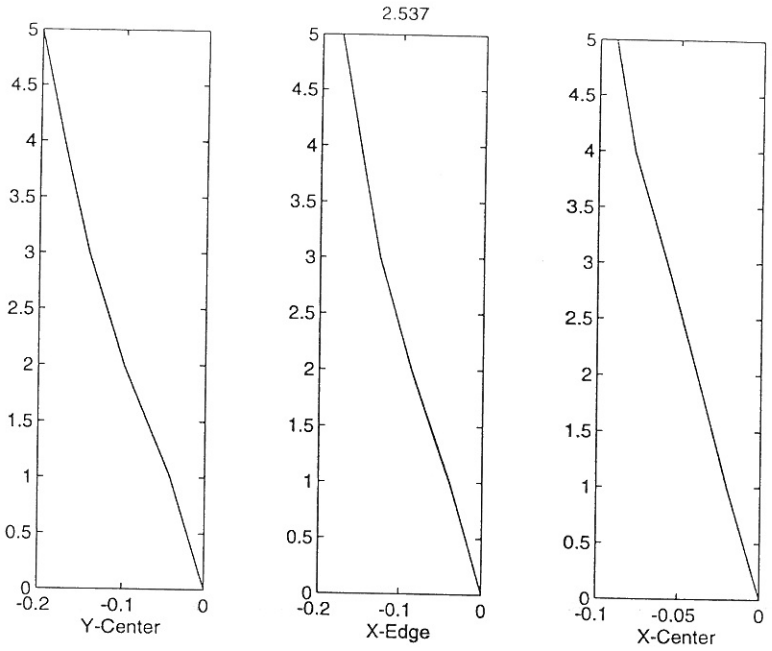

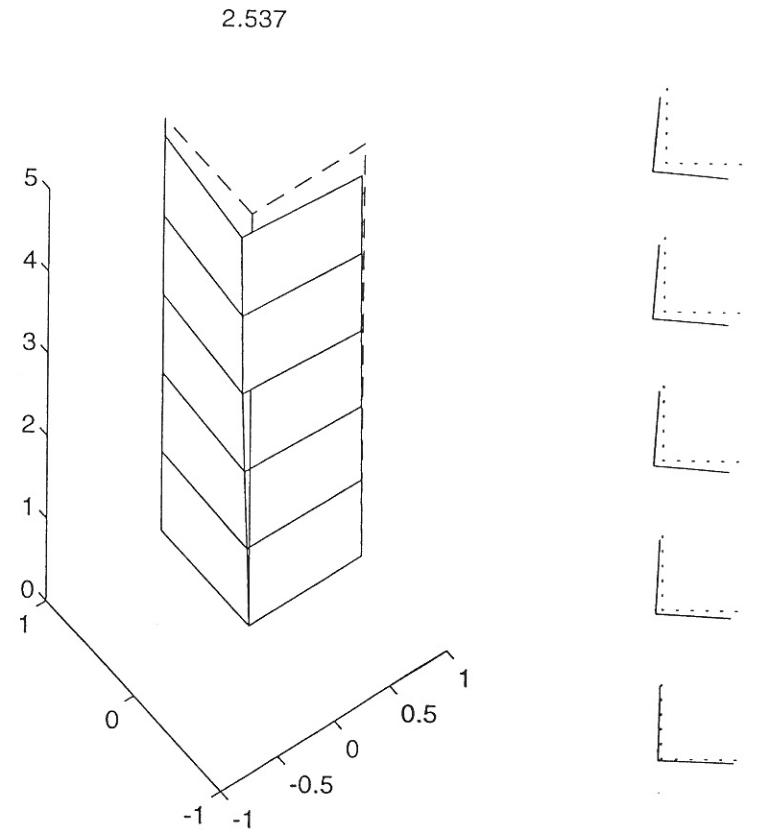

Figure 4.51: 2nd mode shape estimated from edge pull-ou (ARMAV)t.

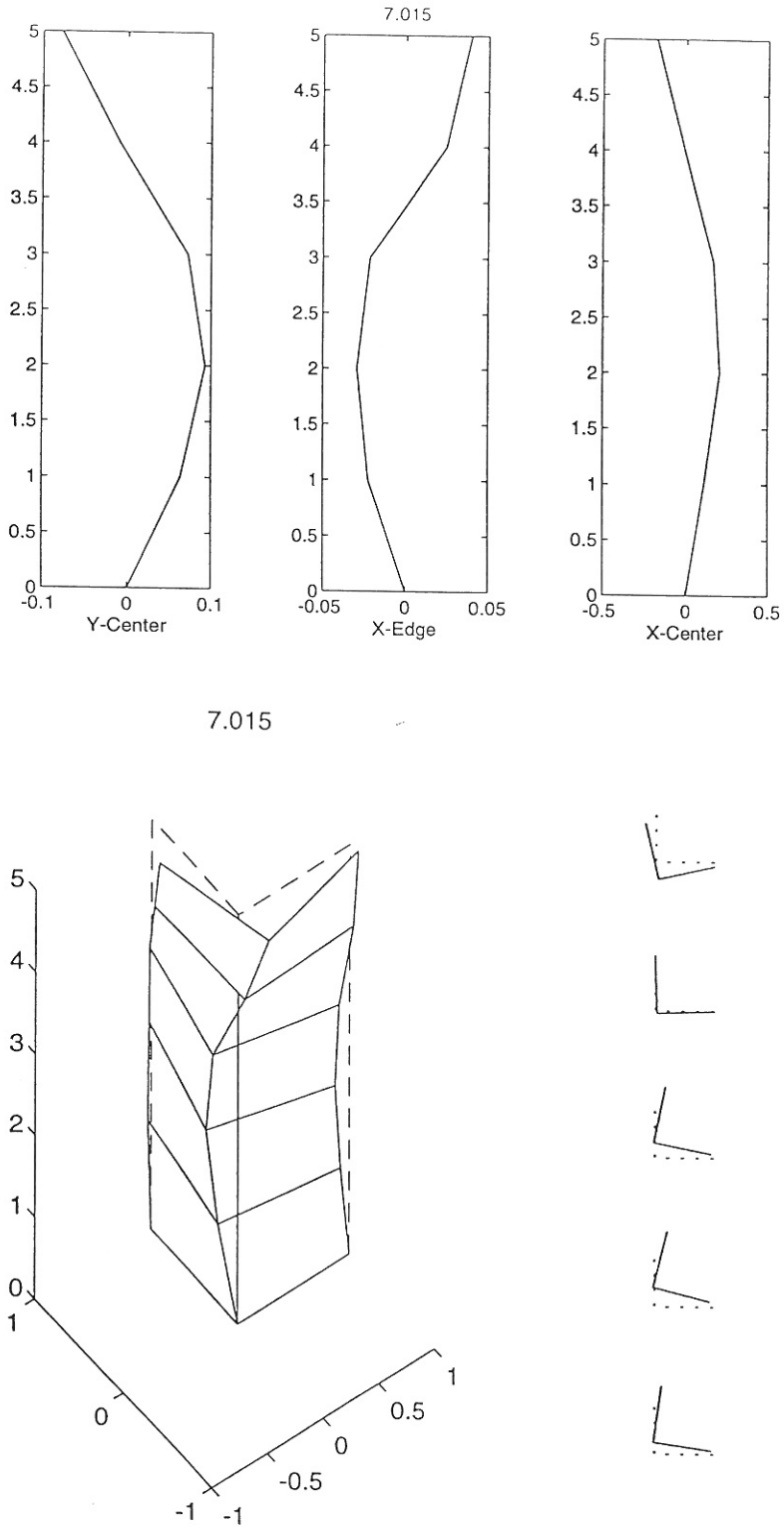

Figure 4.52: 3rd mode shape estimated from centre pull-out (ARMAV).

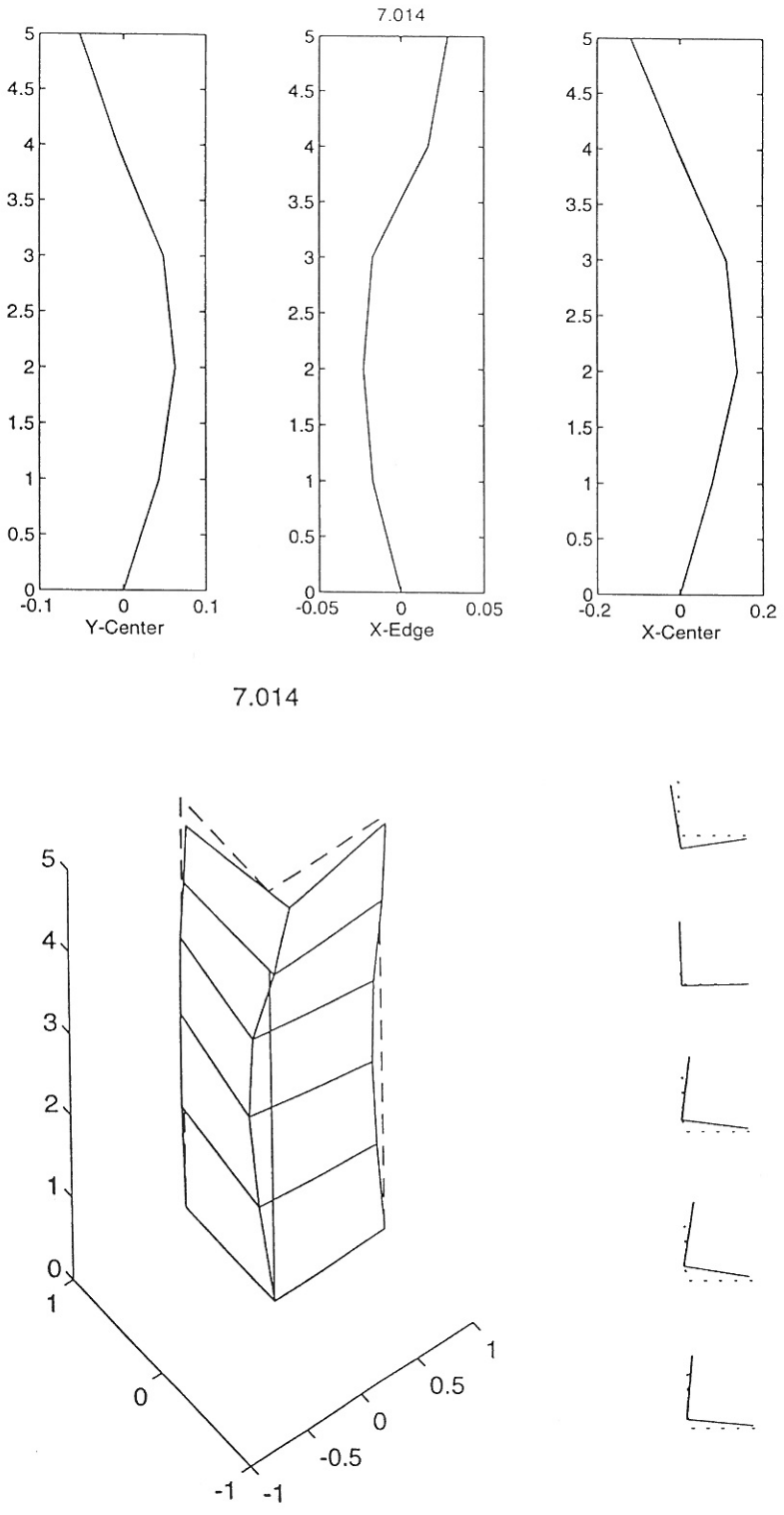

Figure 4.53: 3rd mode shape estimated from edge pull-out (ARMAV).

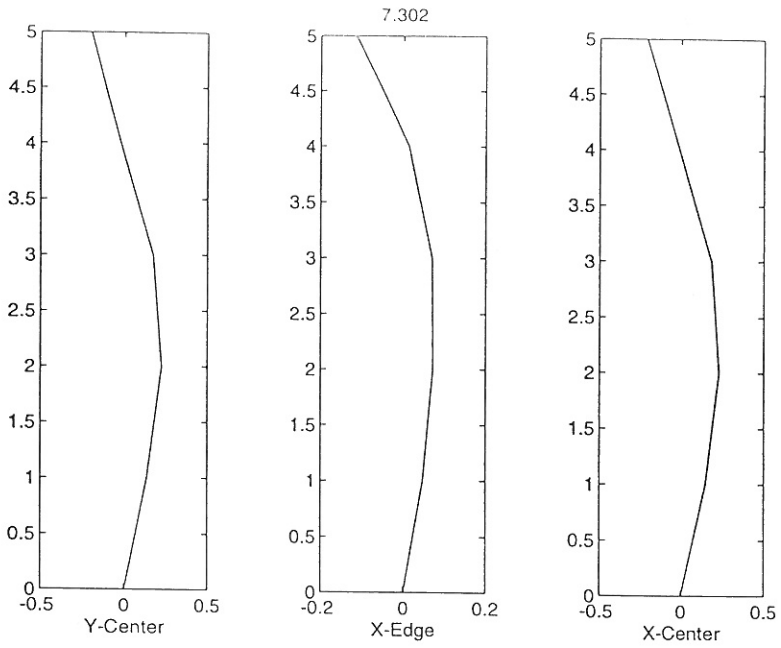

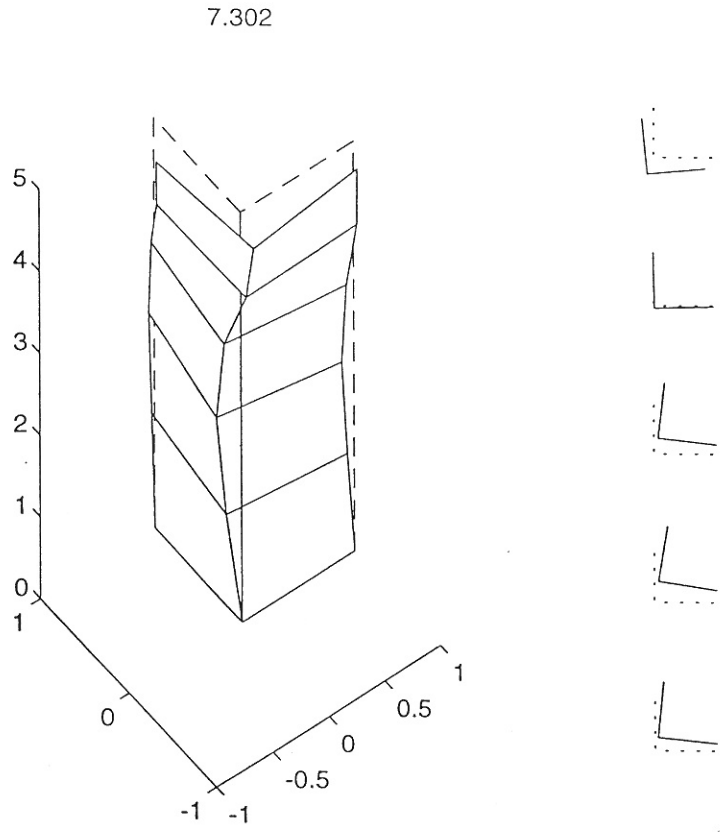

Figure 4.54: 4th mode shape estimated from centre pull-out (ARMAV).

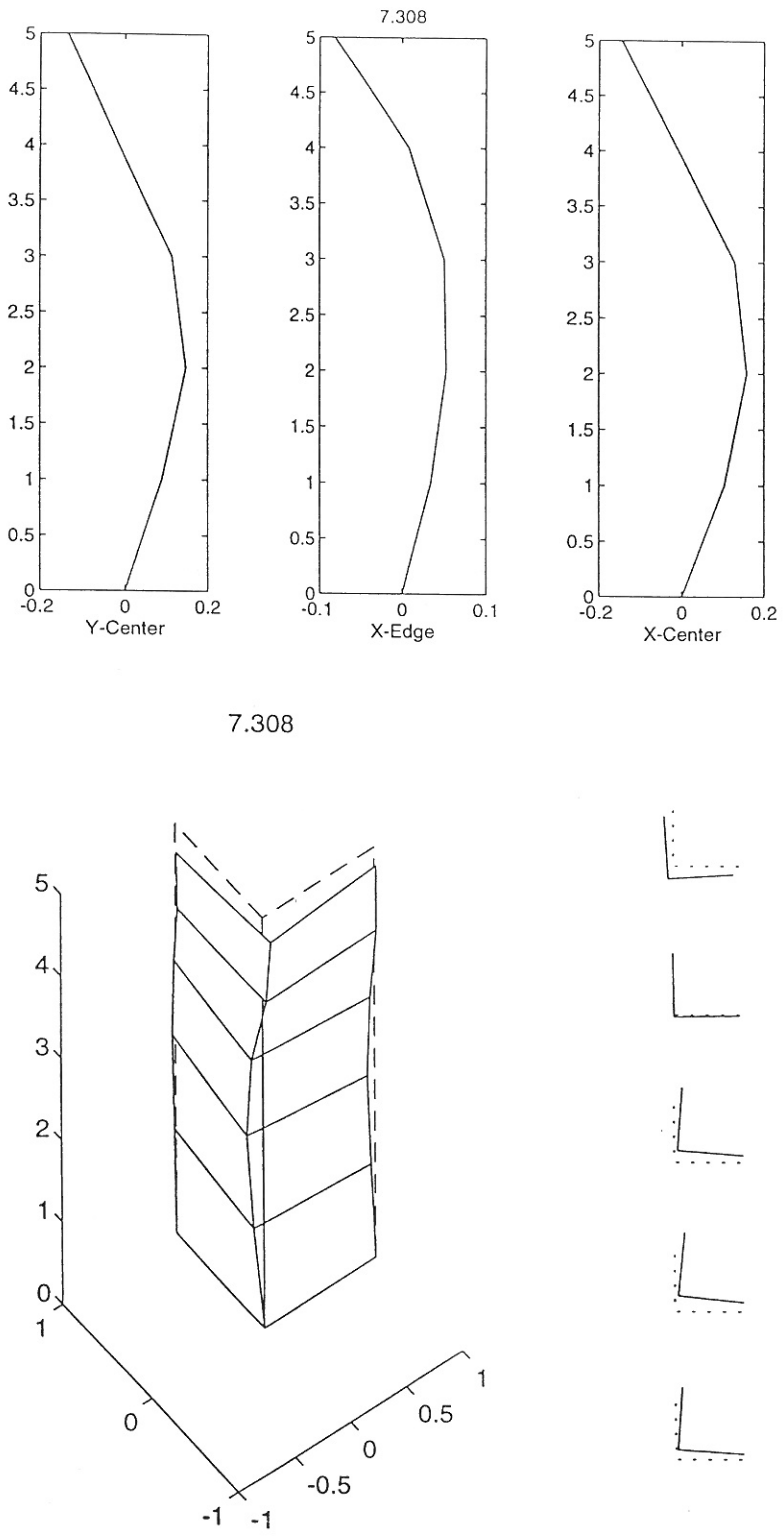

Figure 4.55: 4th mode shape estimated from edge pull-out (ARMAV).

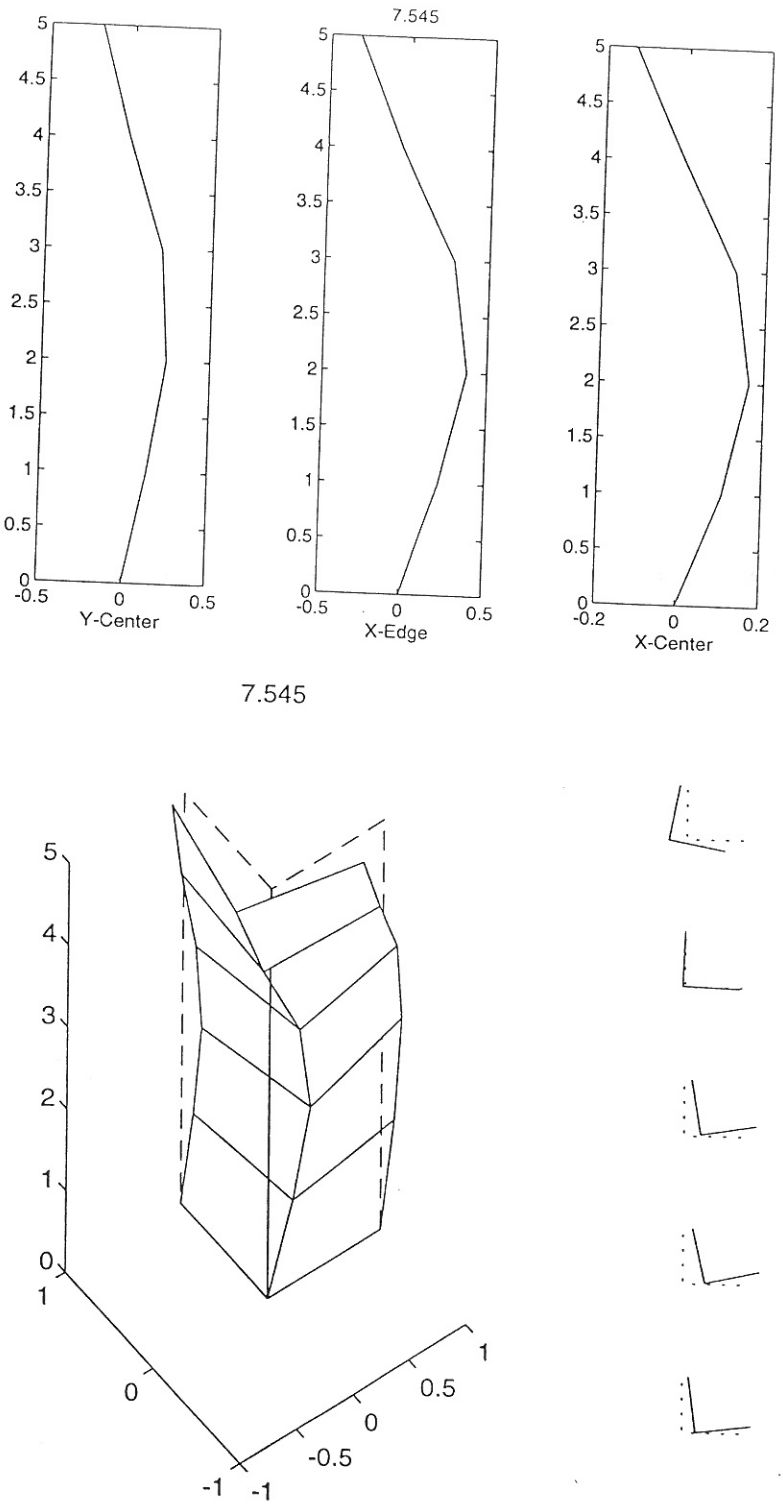

Figure 4.56: 5th mode shape estimated from centre pull-out (ARMAV).

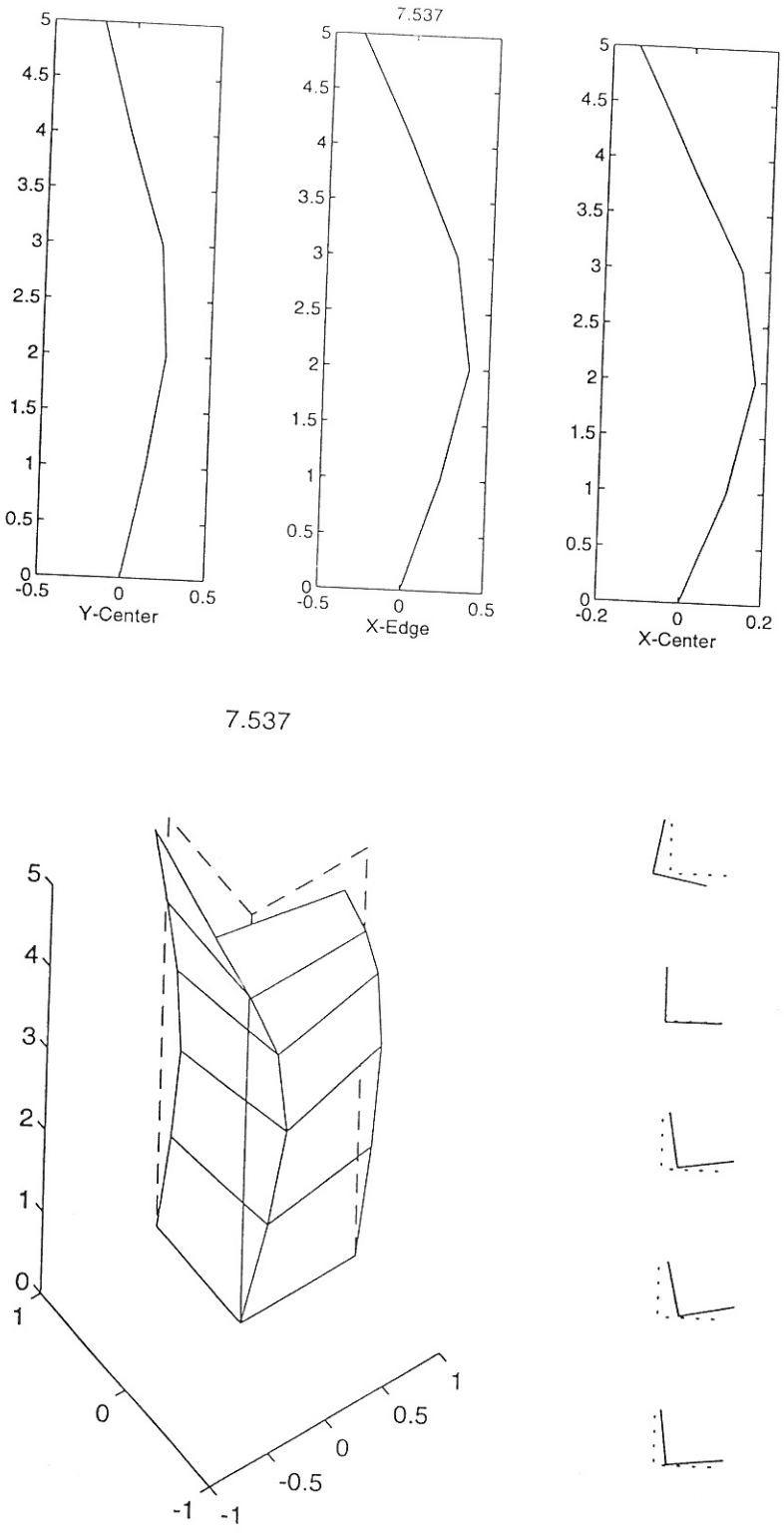

Figure 4.57: 5th mode shape estimated from edge pull-out (ARMAV).

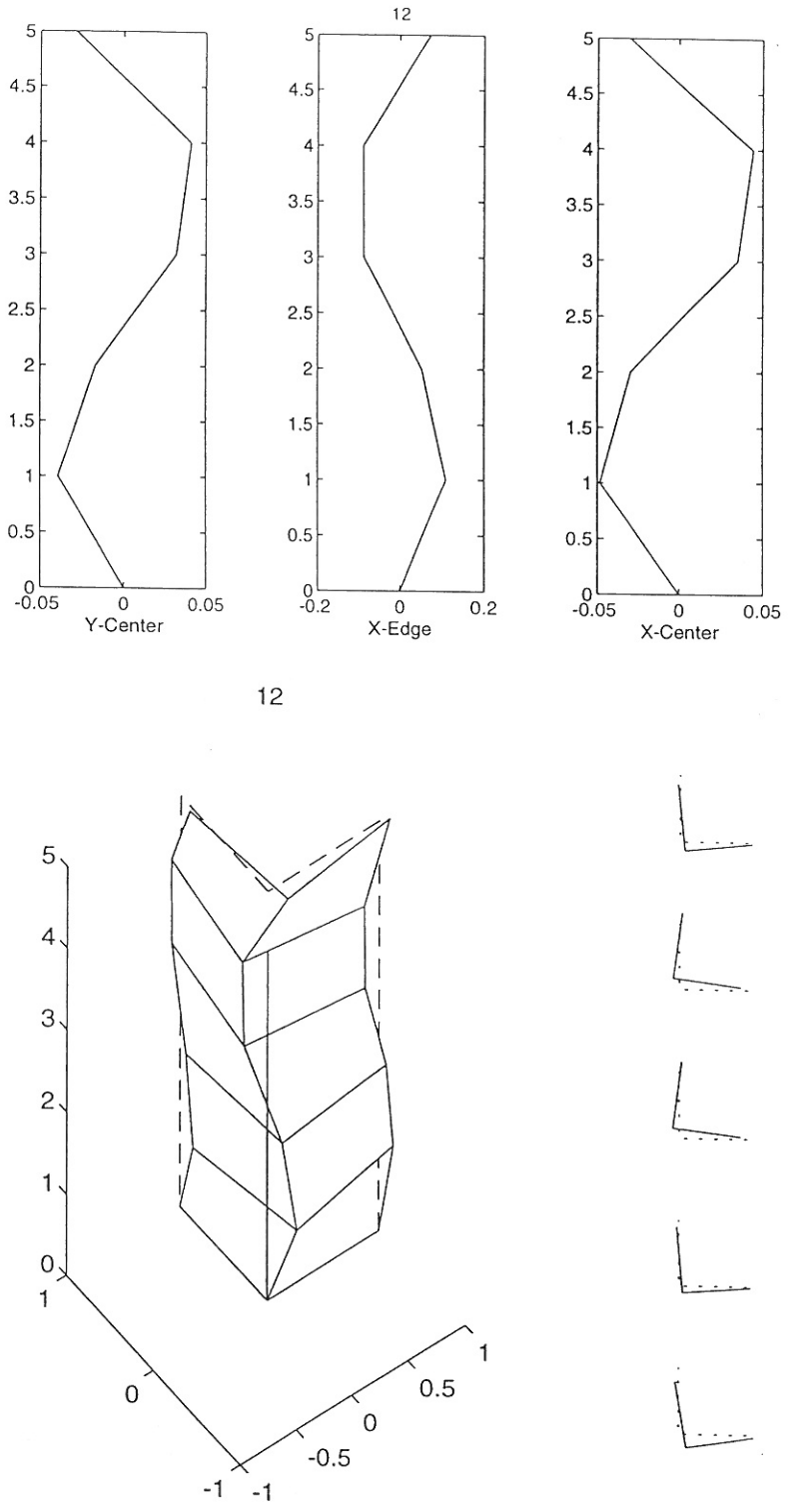

Figure 4.58: 6th mode shape estimated from centre pull-out (ARMAV).

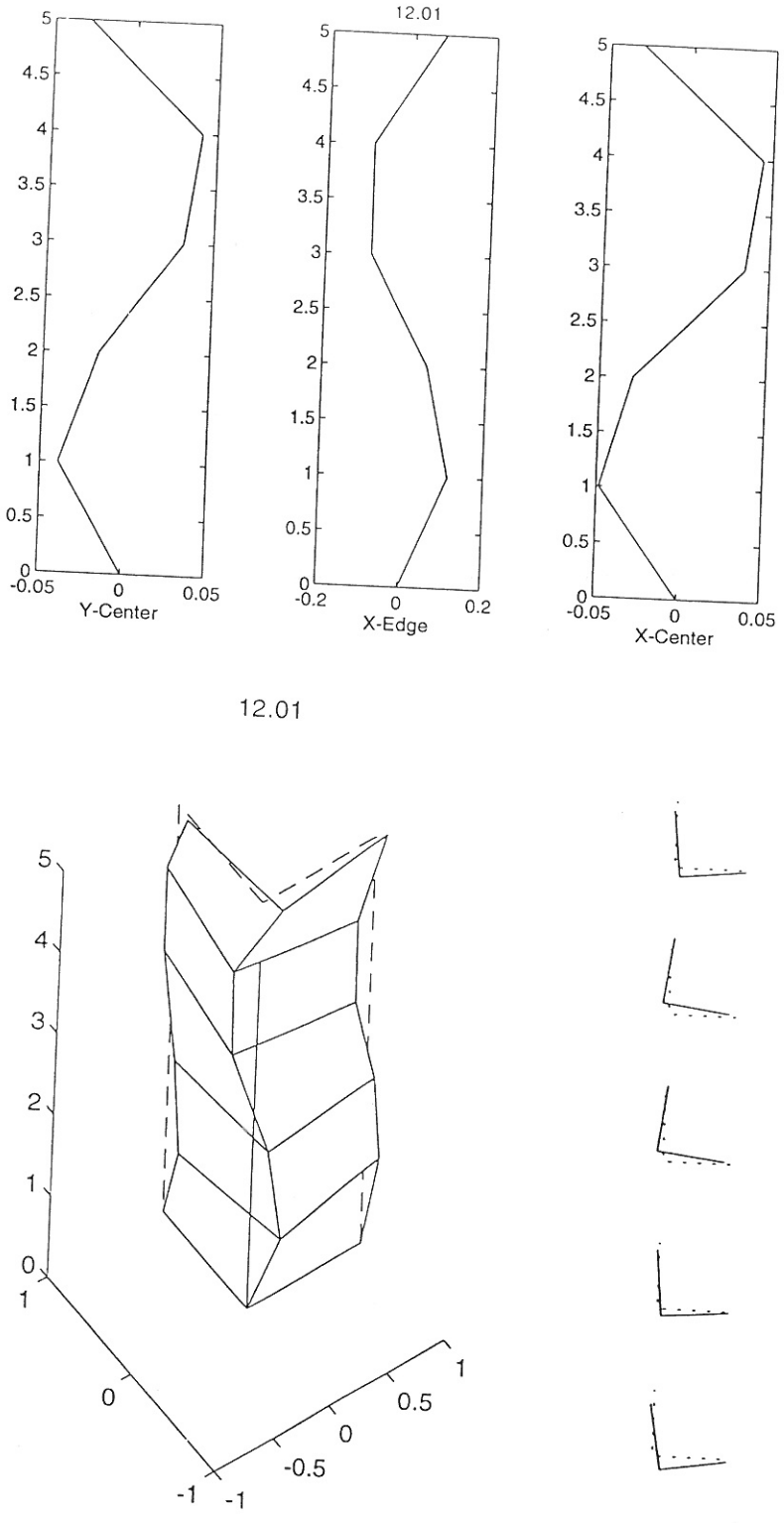

Figure 4.59: 6th mode shape estimated from edge pull-out (ARMAV).

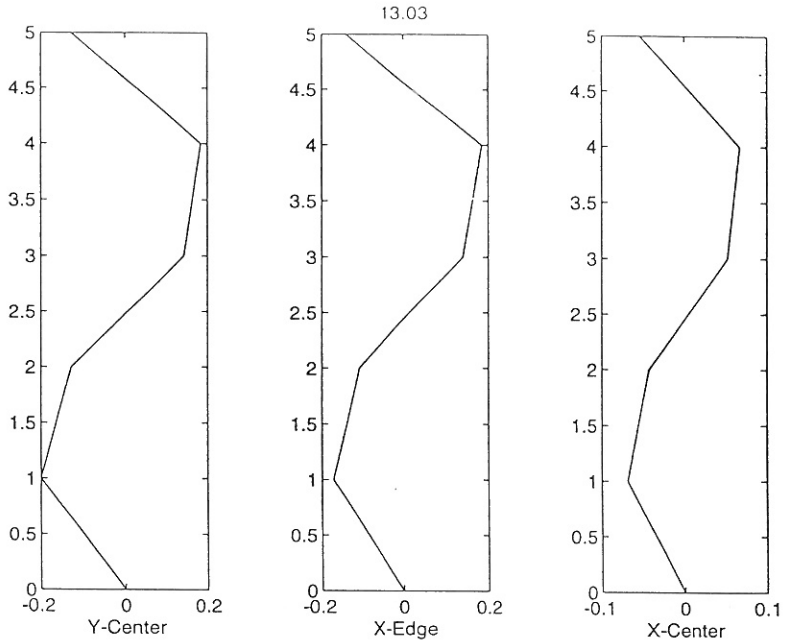

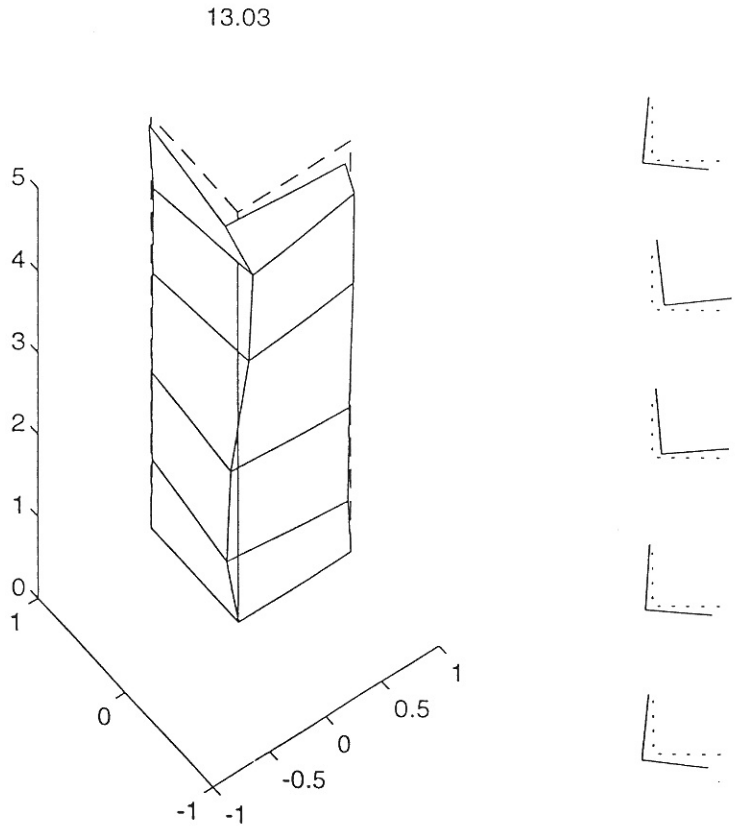

Figure 4.60: 7th mode shape estimated from center pull-out (ARMAV).

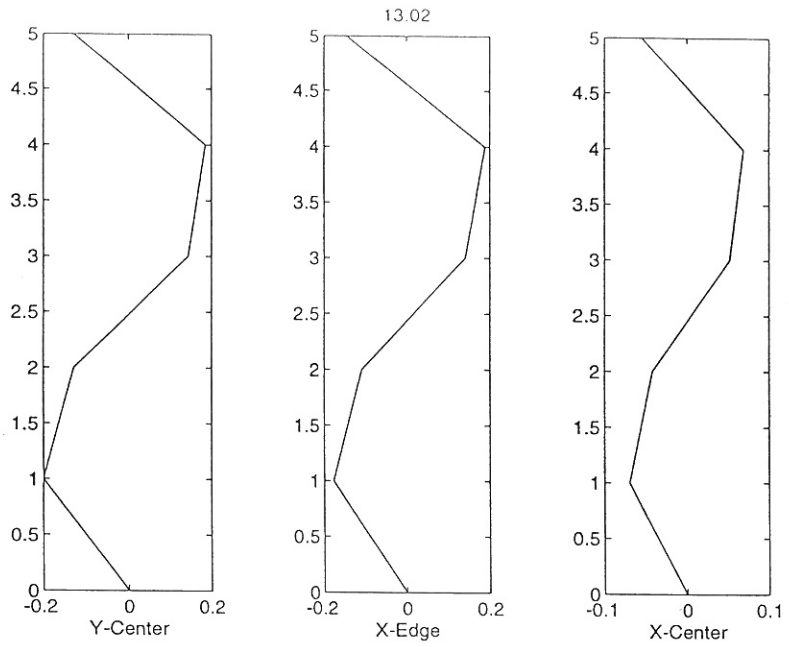

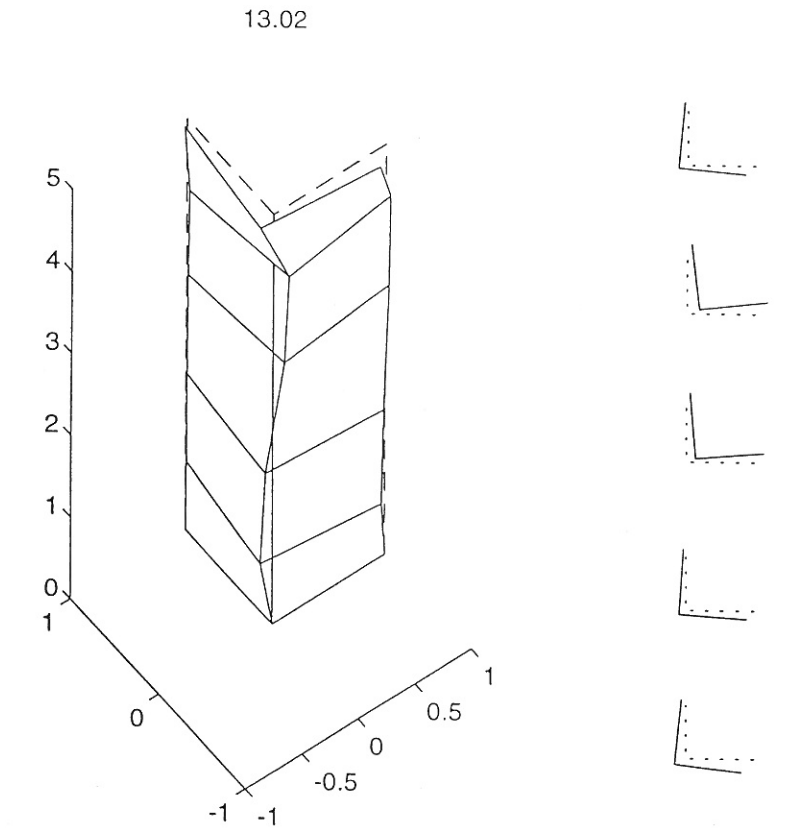

Figure 4.61: 7th mode shape estimated from edge pull-out (ARMAV).

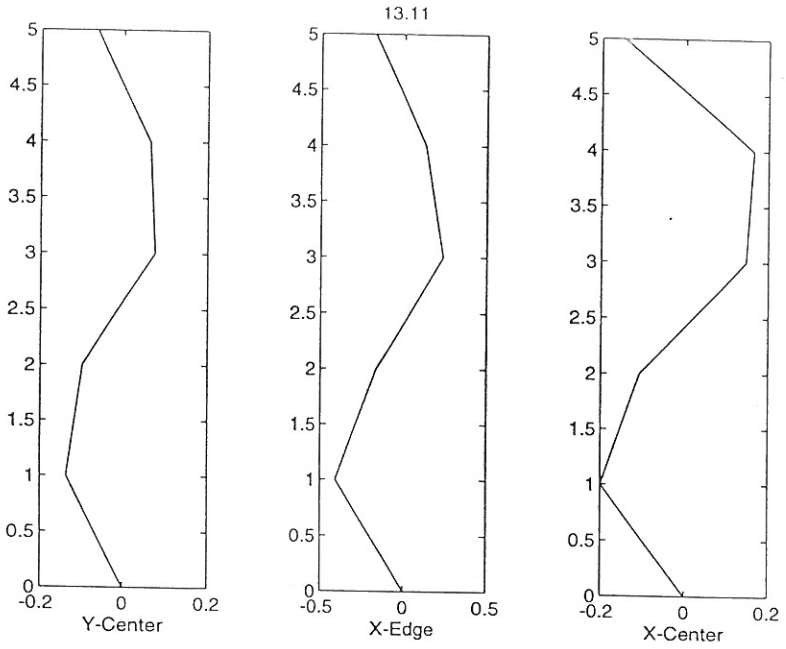

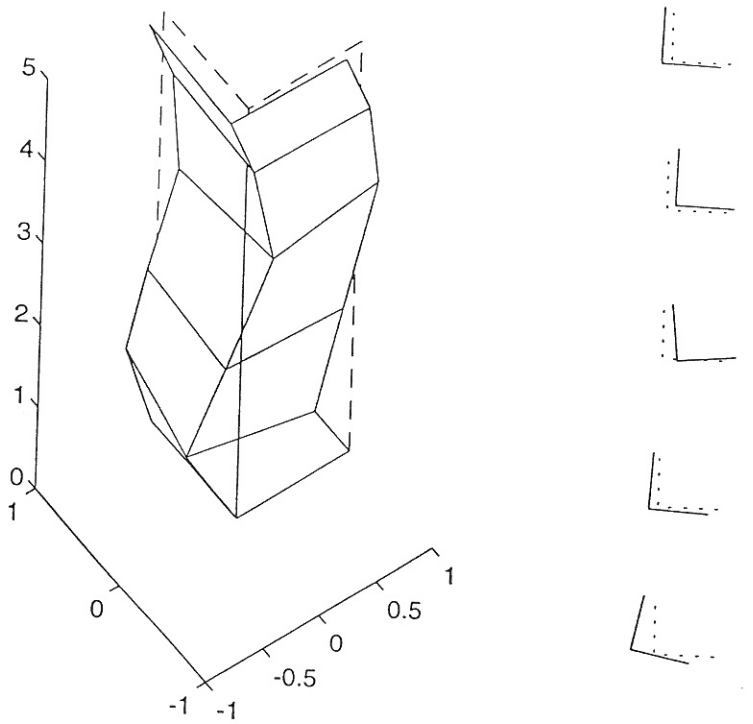

Figure 4.62: 8th mode shape estimated from centre pull-out (ARMAV).

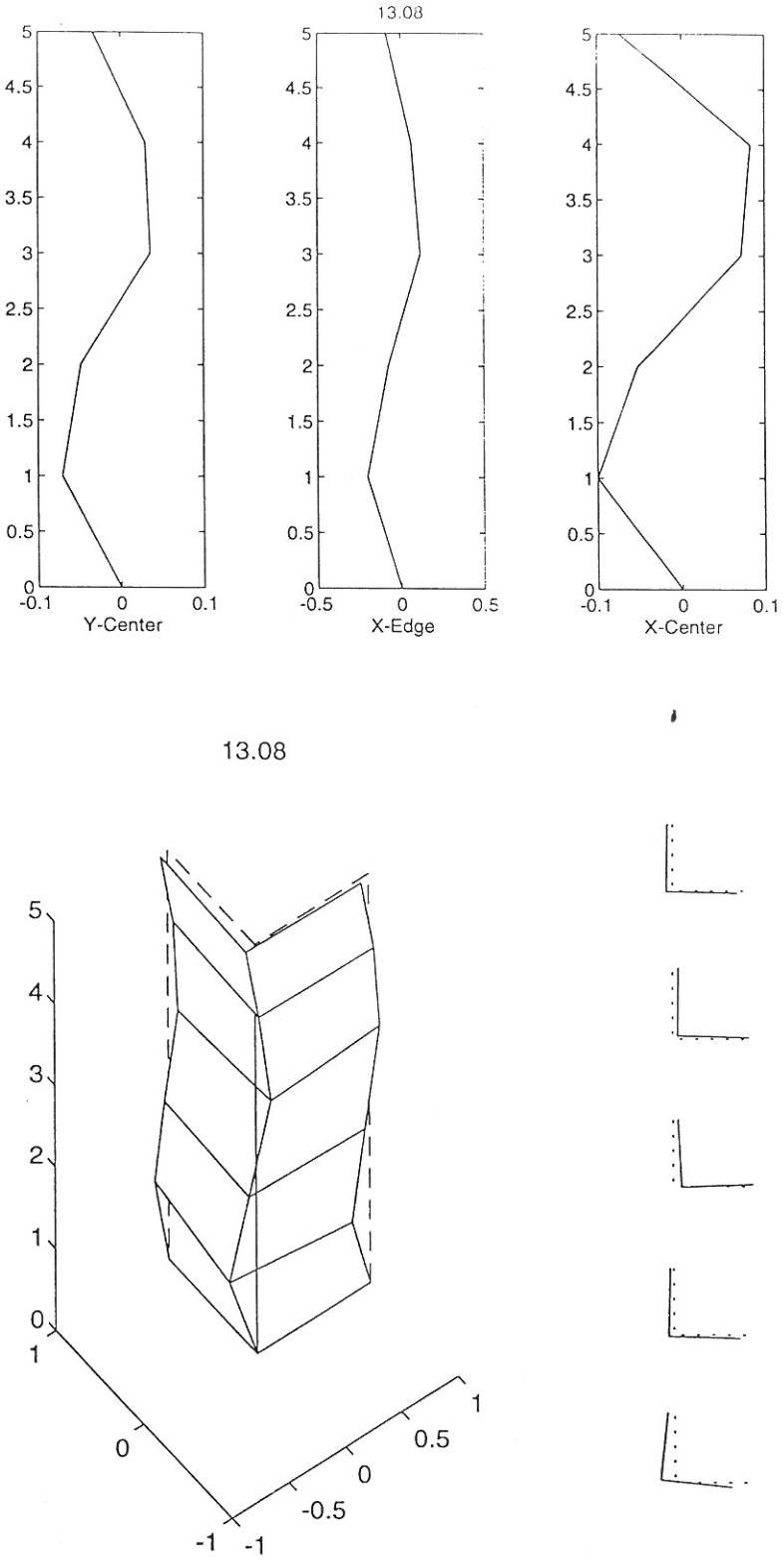

Figure 4.63: 8th mode shape estimated from edge pull-out (ARMAV).

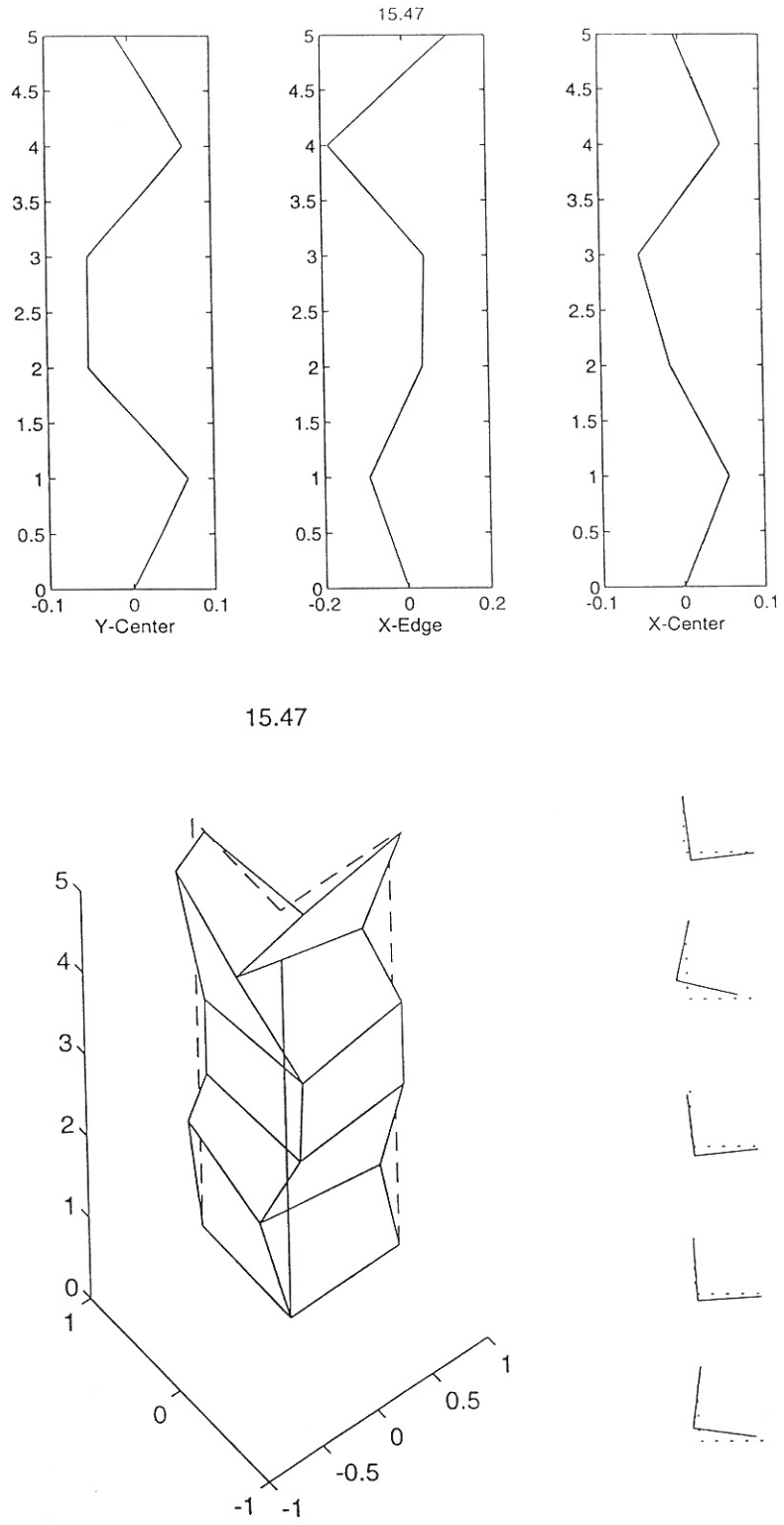

Figure 4.64: 9th mode shape estimated from centre pull-out (ARMAV).

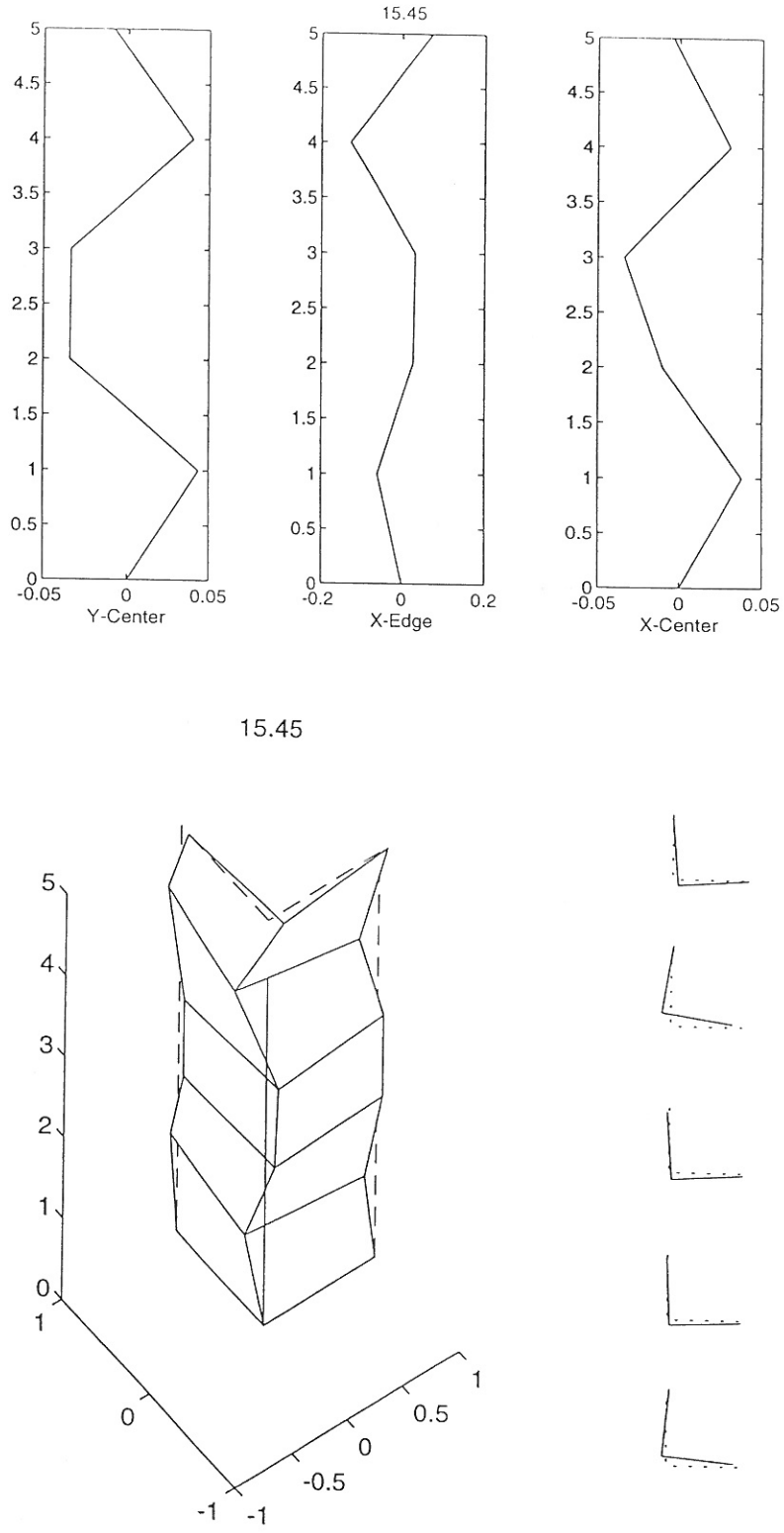

Figure 4.65: 9th mode shape estimated from edge pull-out (ARMAV).

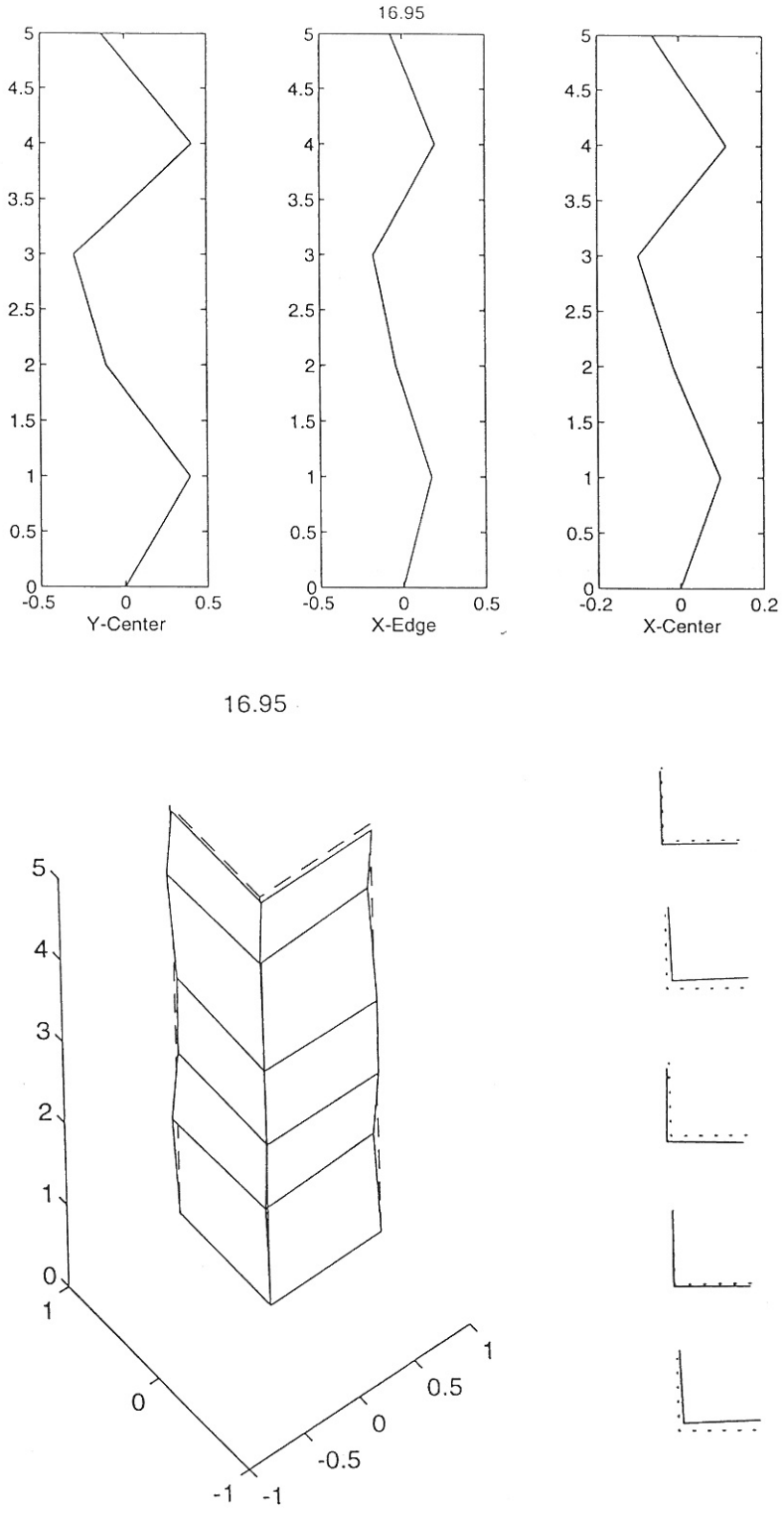

Figure 4.66: 10th mode shape estimated from centre pull-out (ARMAV).

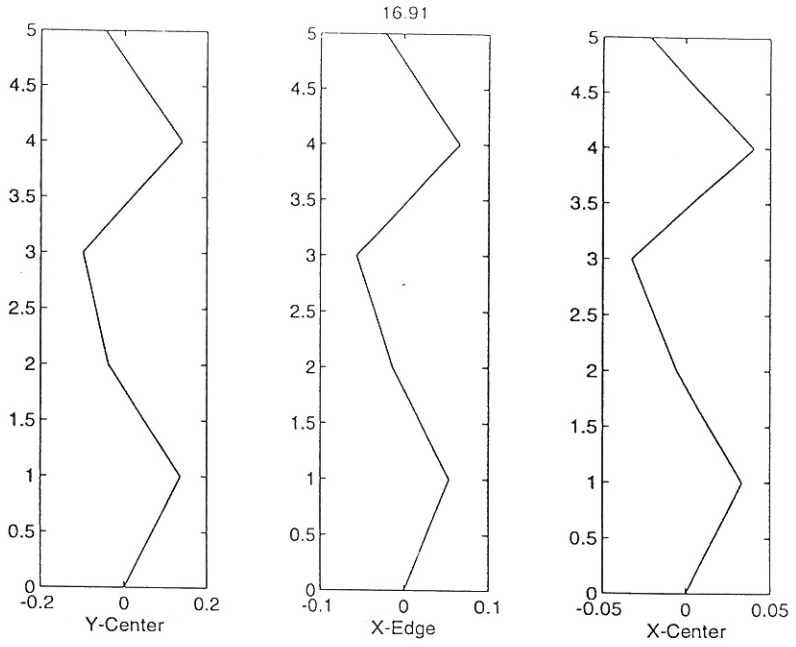

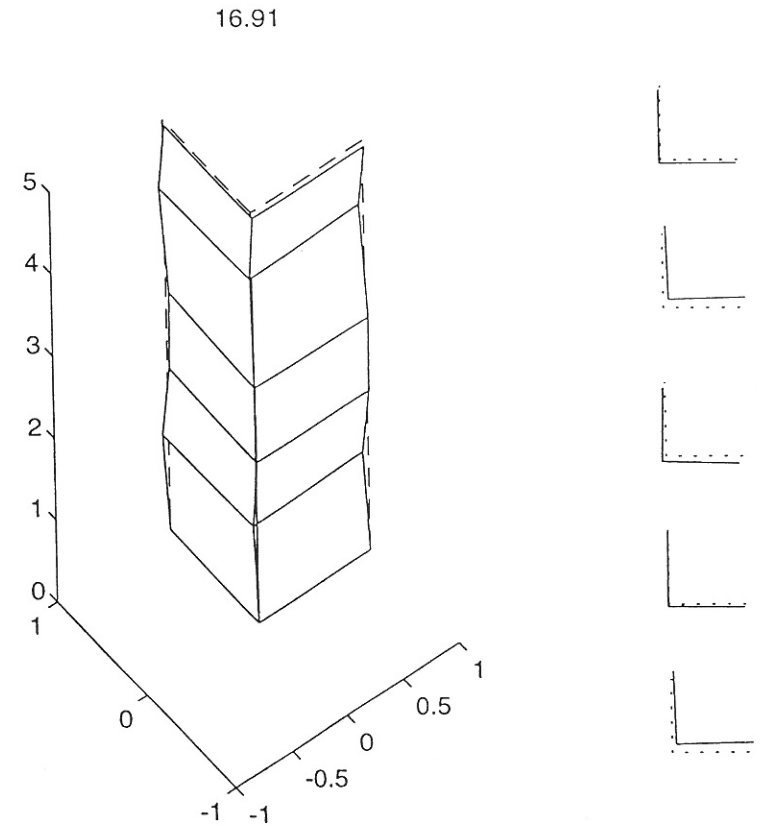

Figure 4.67: 10th mode shape estimated from edge pull-out (ARMAV).

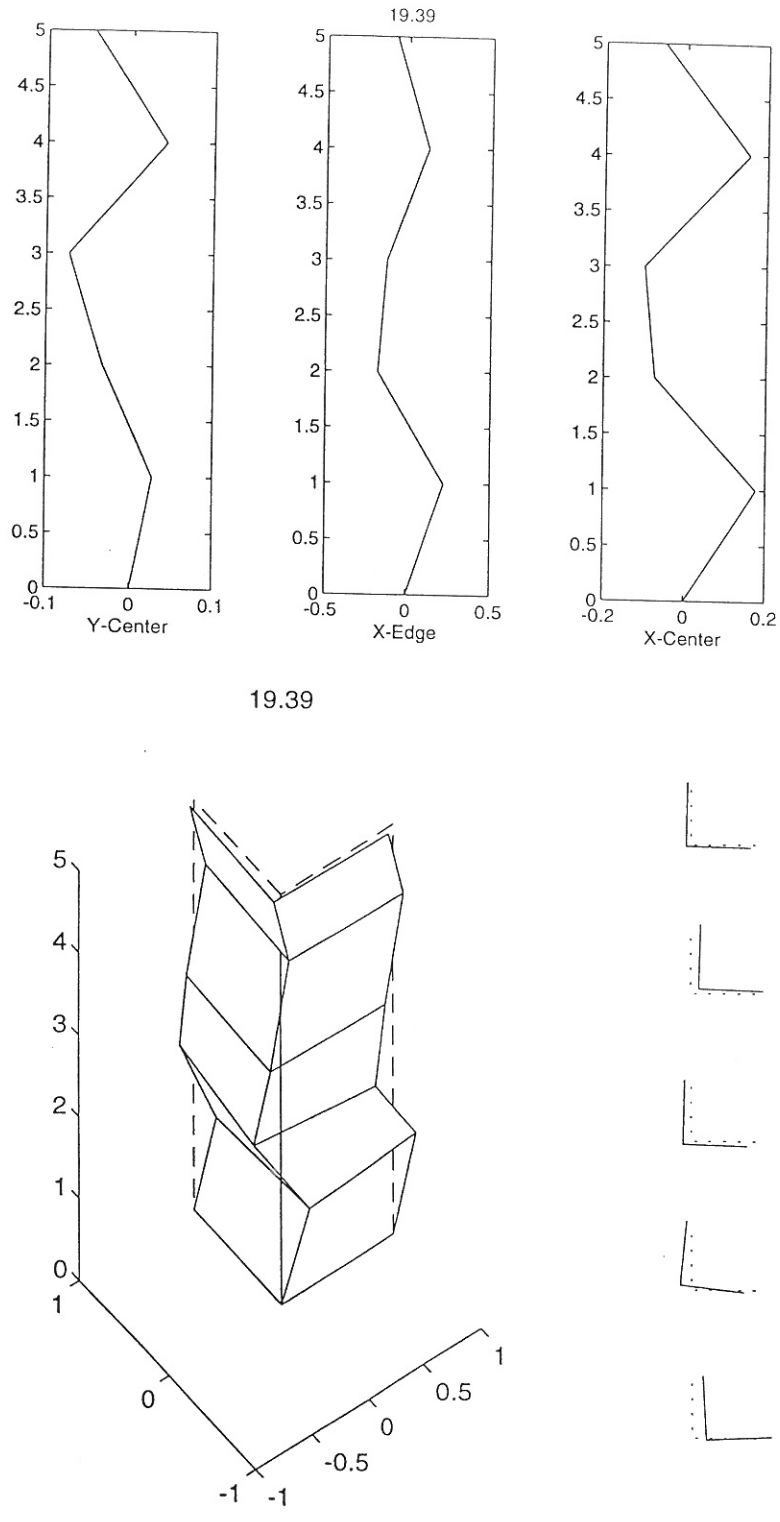

Figure 4.68: 11th mode shape estimated from centre pull-out (ARMAV).

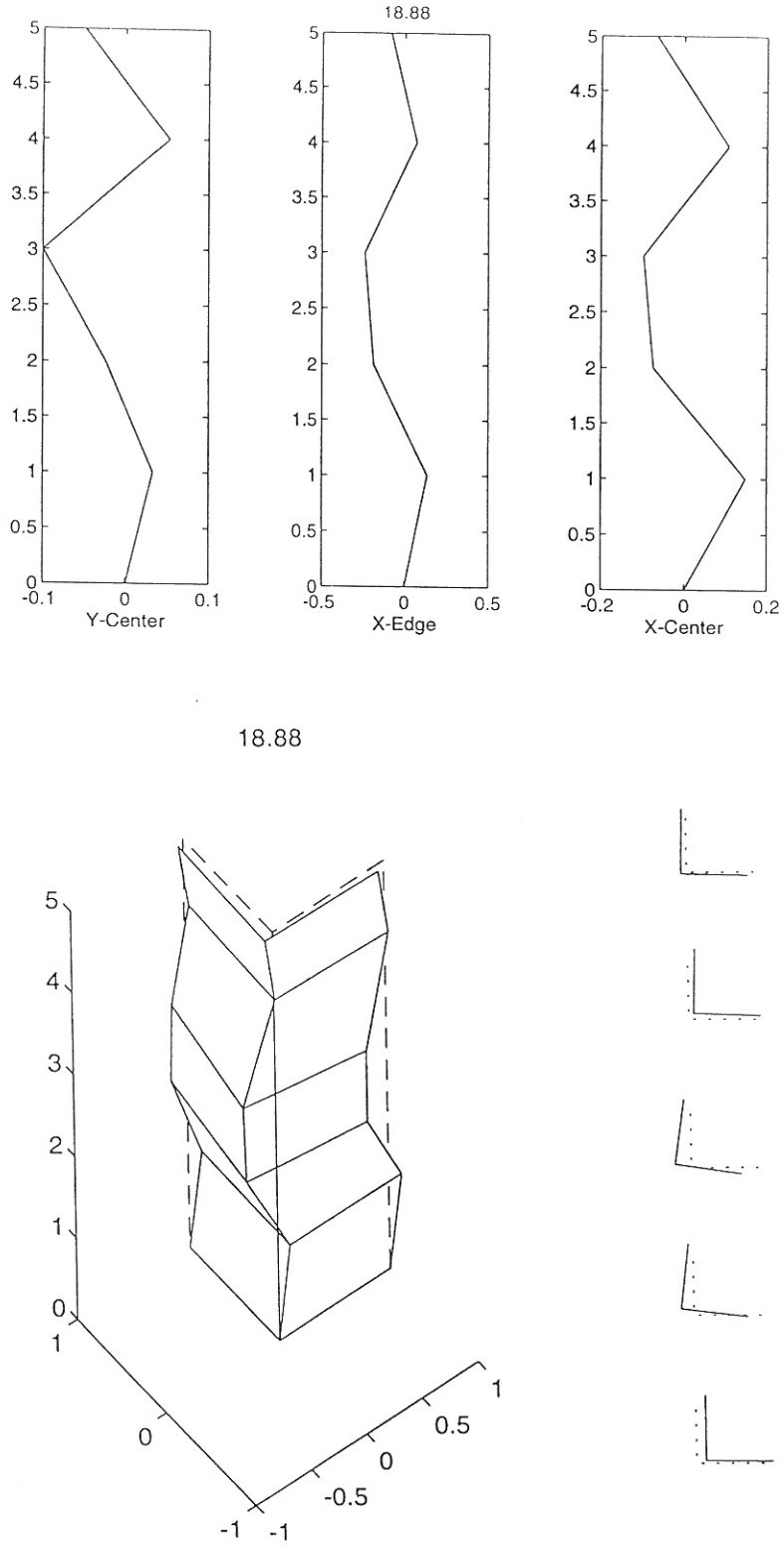

Figure 4.69: 11th mode shape estimated from edge pull-out (ARMAV).

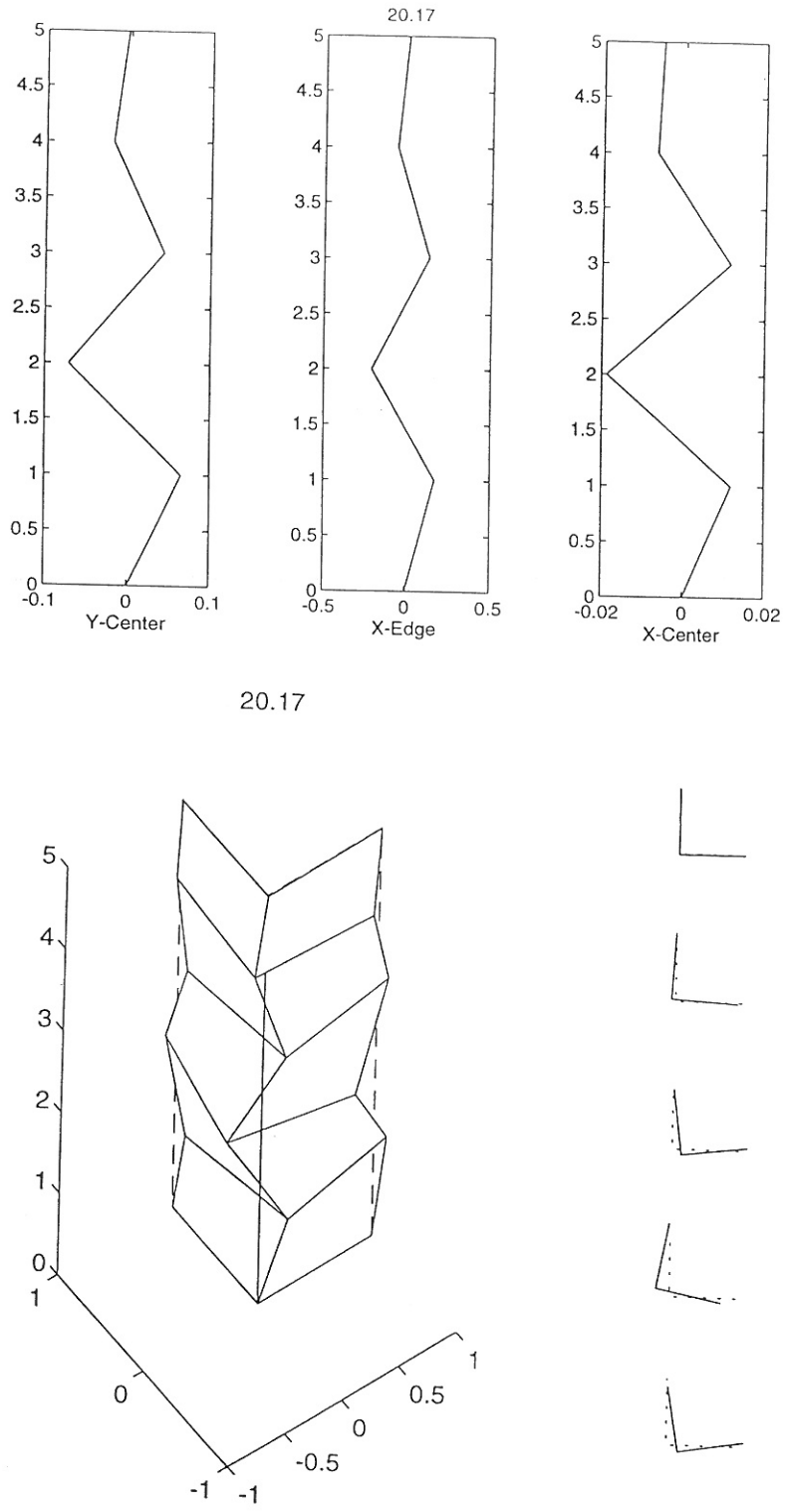

Figure 4.70: 12th mode shape estimated from centre pull-out (ARMAV).

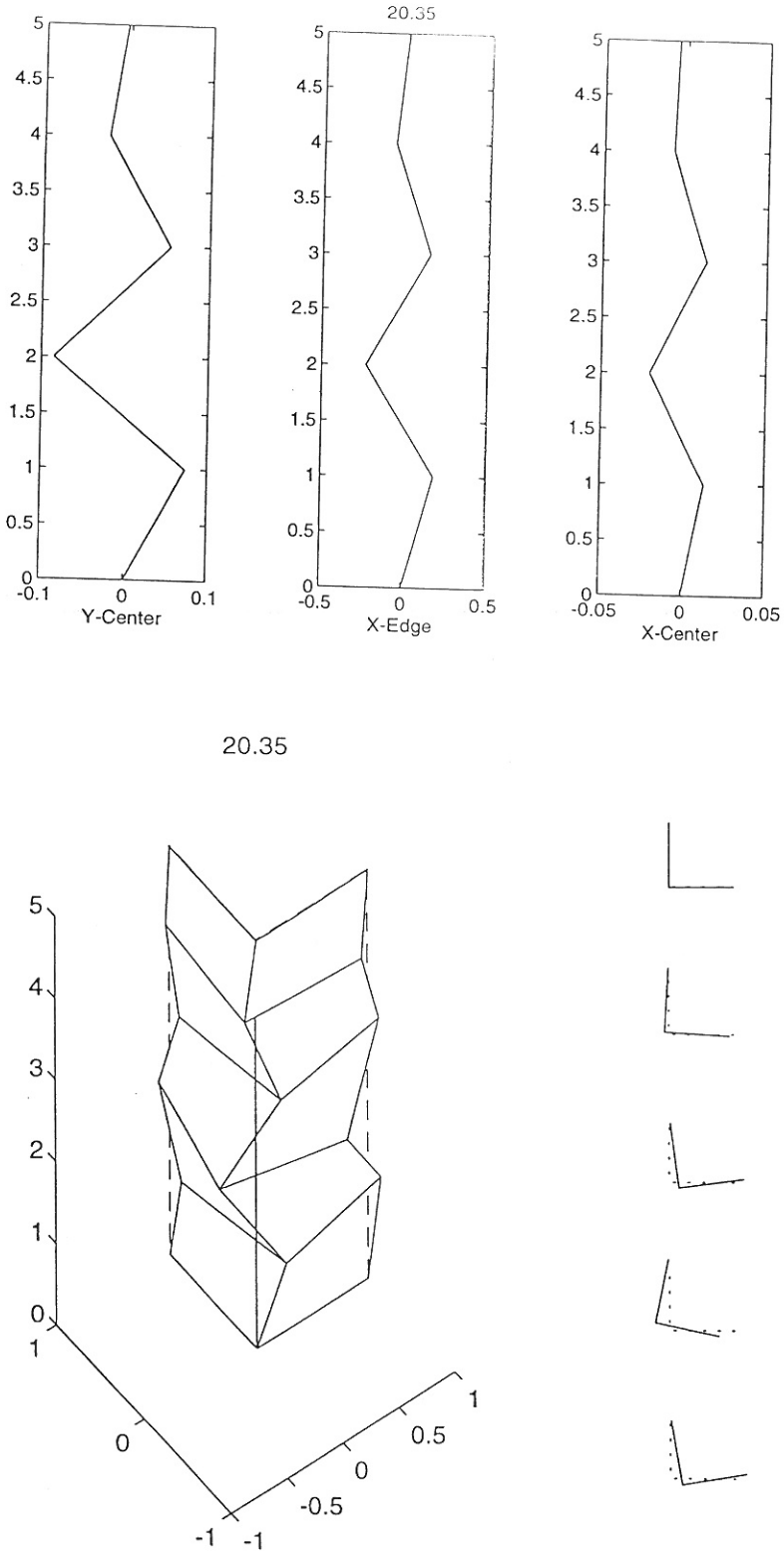

Figure 4.71: 12th mode shape estimated from edge pull-out (ARMAV).

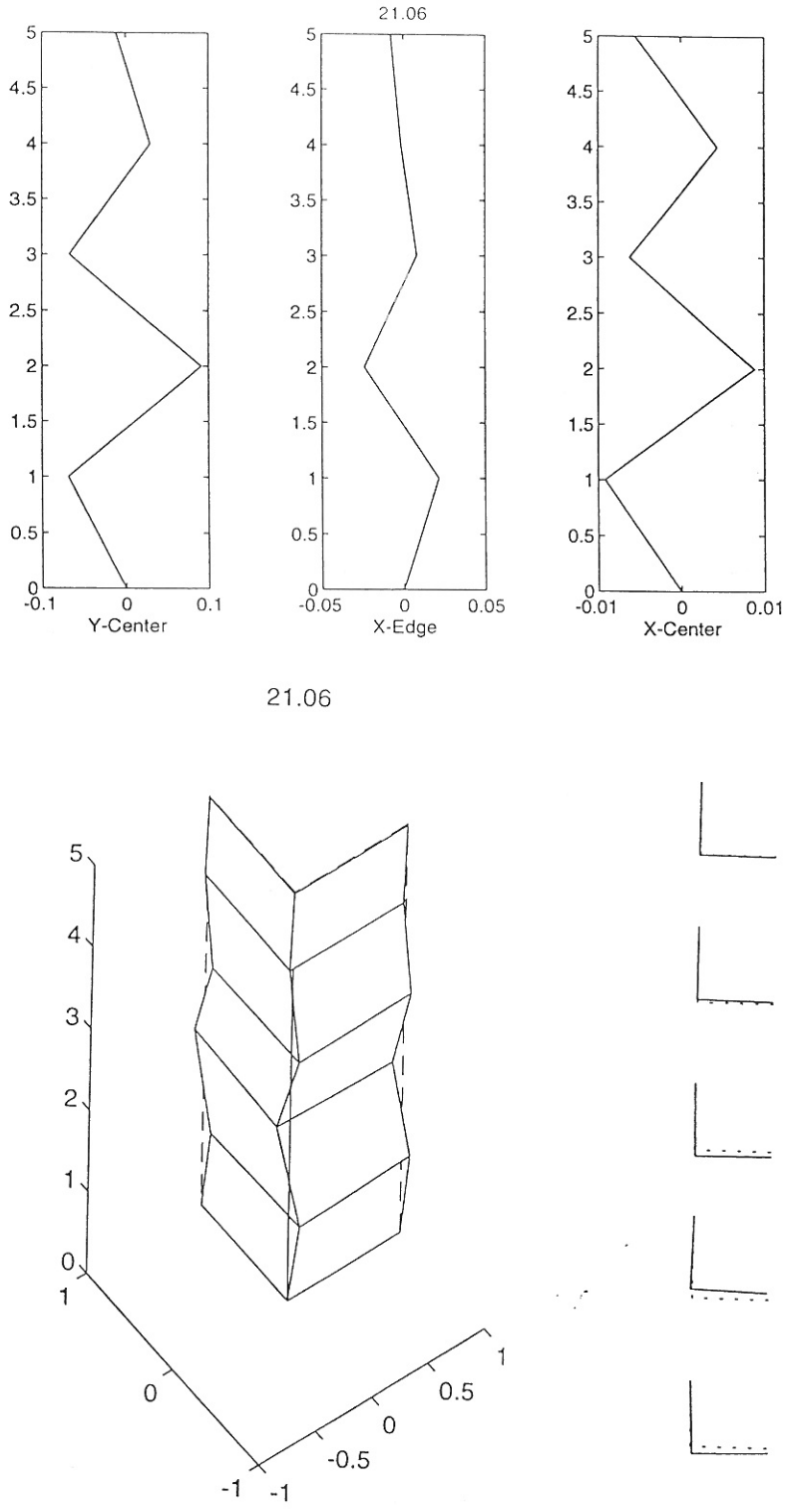

Figure 4.72: 13th mode shape estimated from center pull-out (ARMAV).

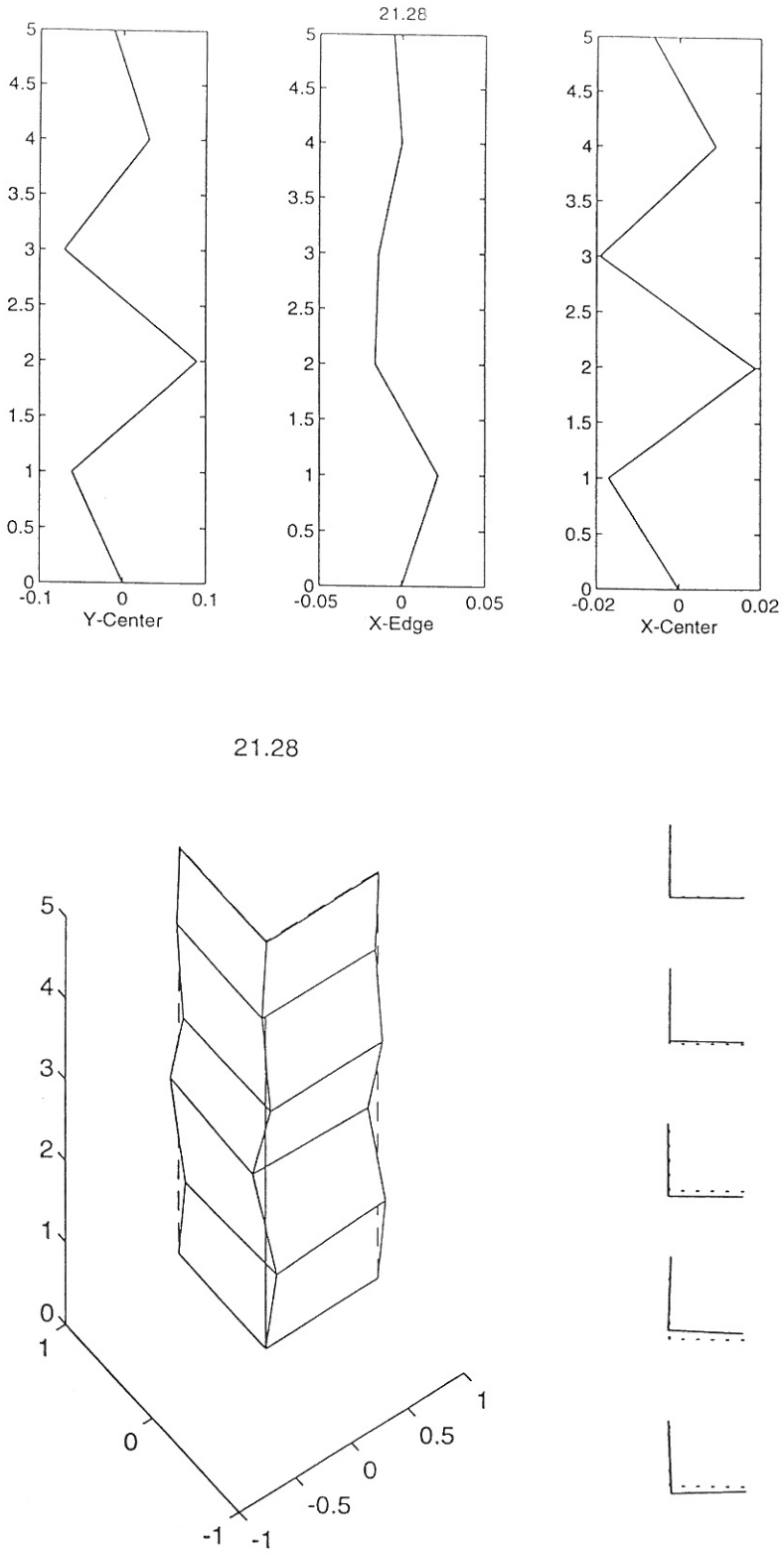

Figure 4.73: 13th mode shape estimated from edge pull-out (ARMAV).

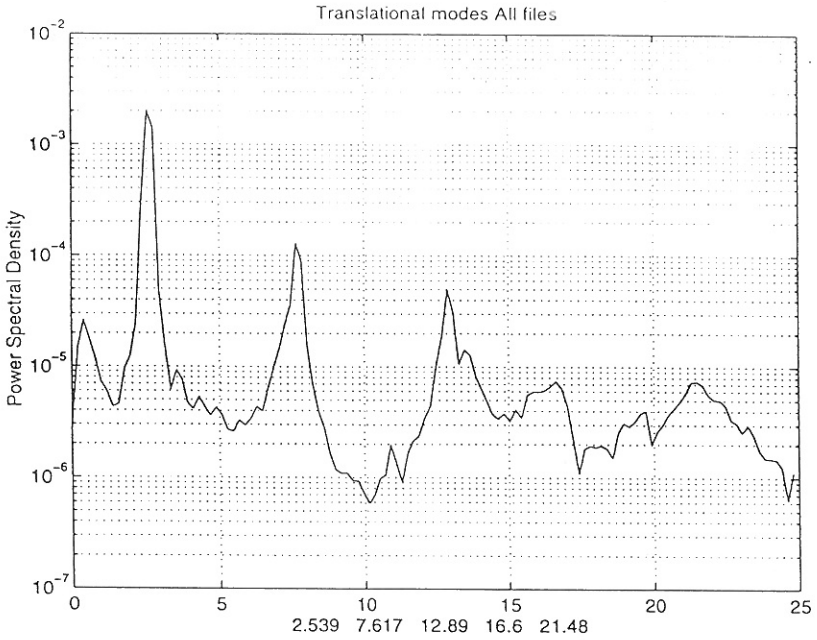

Figure 4.74: Power spectrum of all measurements, translational modes.

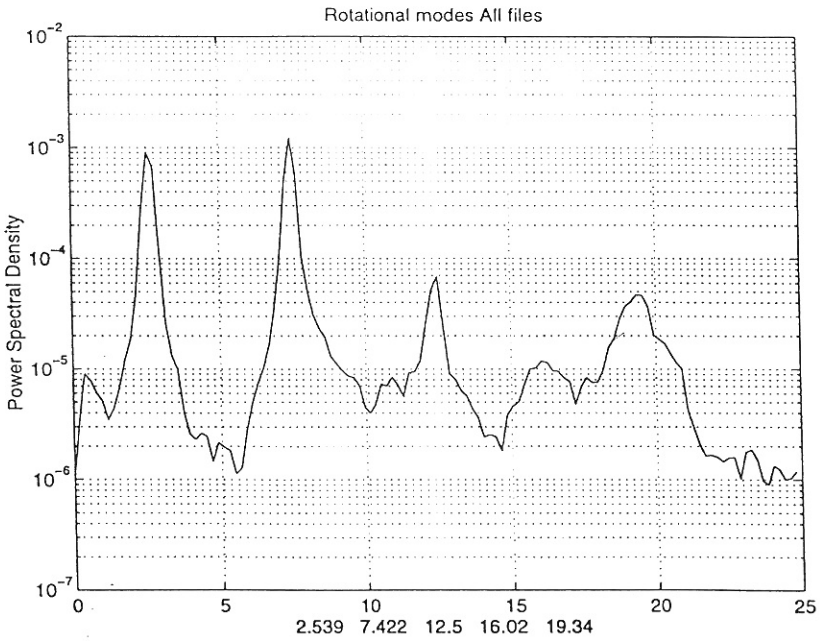

Figure 4.75: Power spectrum of all measurements, rotational modes.

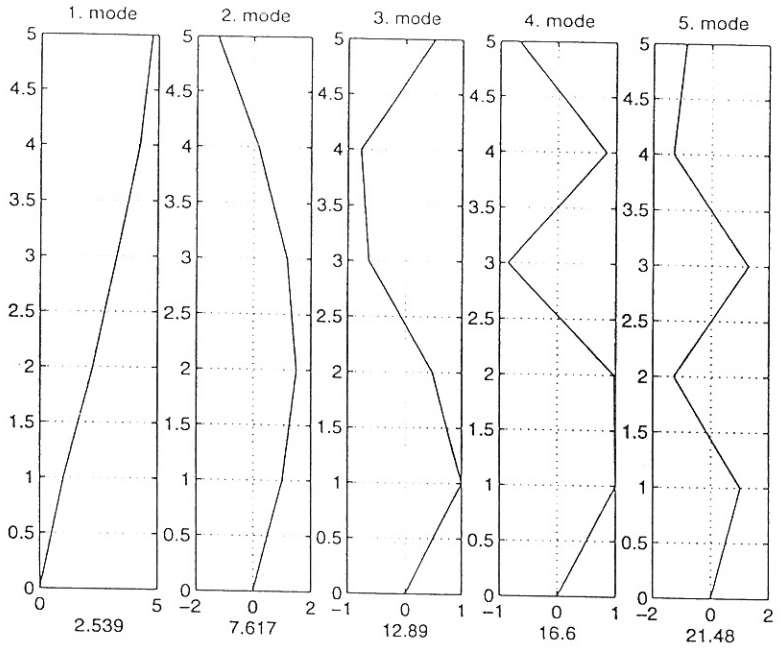

Figure 4.76: Translational mode shapes, magnitude.

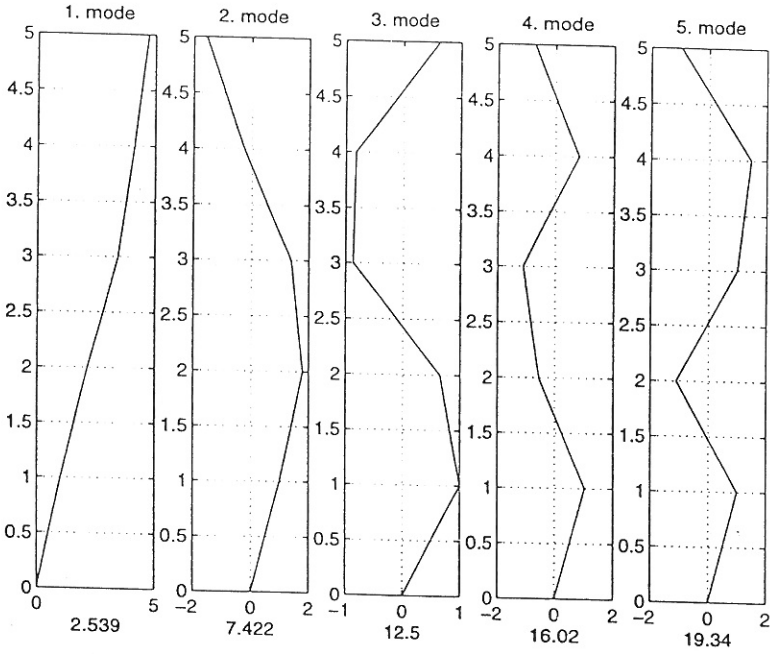

Figure 4.77: Rotational mode shapes, magnitude.

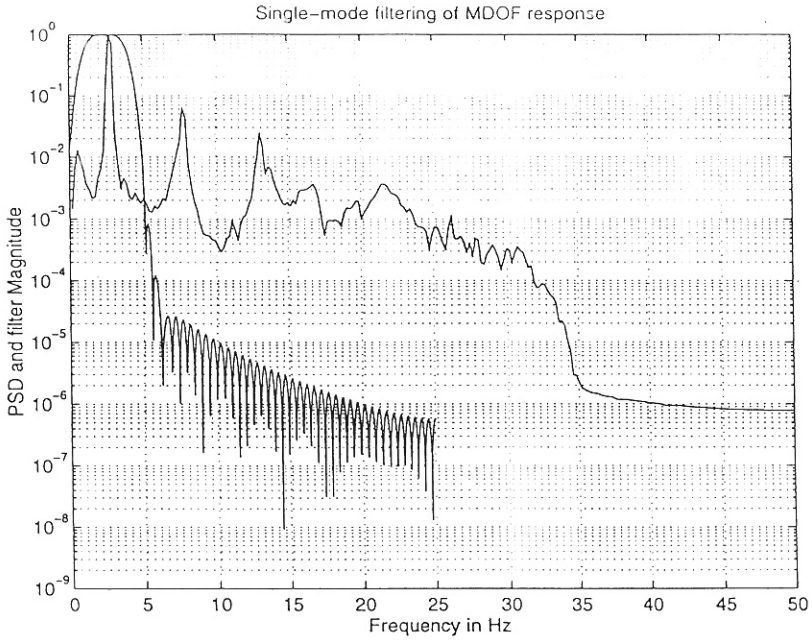

Figure 4.78: Power spectrum of all measurements (translational modes) and the designed filter to pick out the first mode.

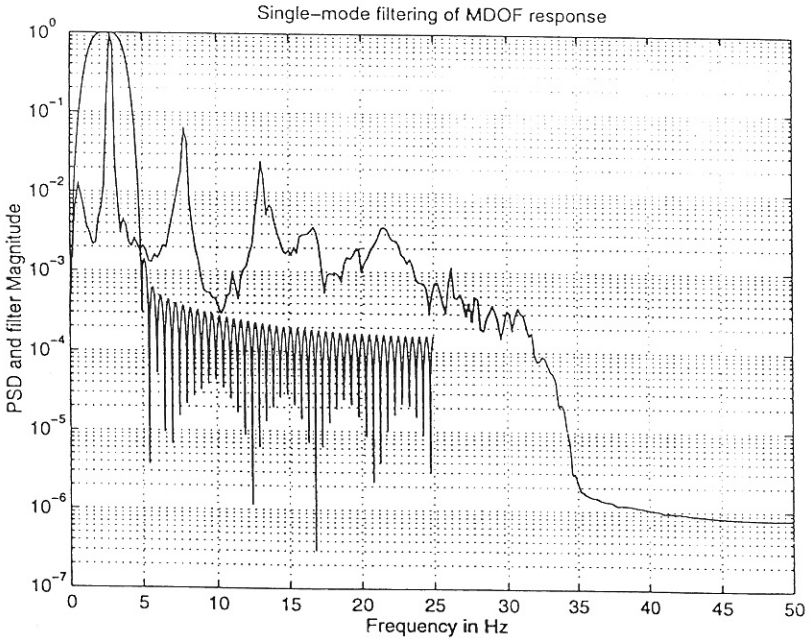

Figure 4.79: Power spectrum of all measurements (rotational modes) and the designed filter to pick out the first mode.

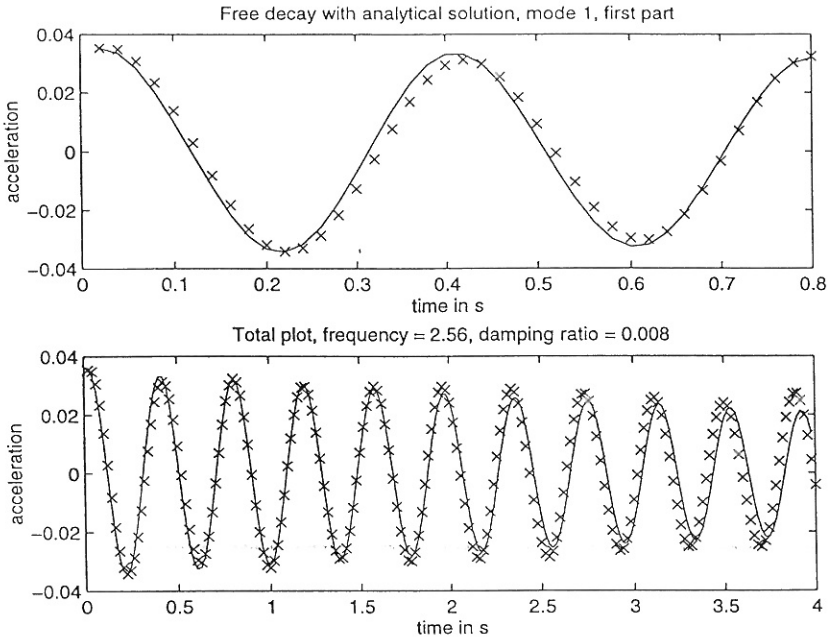

Figure 4.80: Measured and estimated free decay of 1st translational mode.

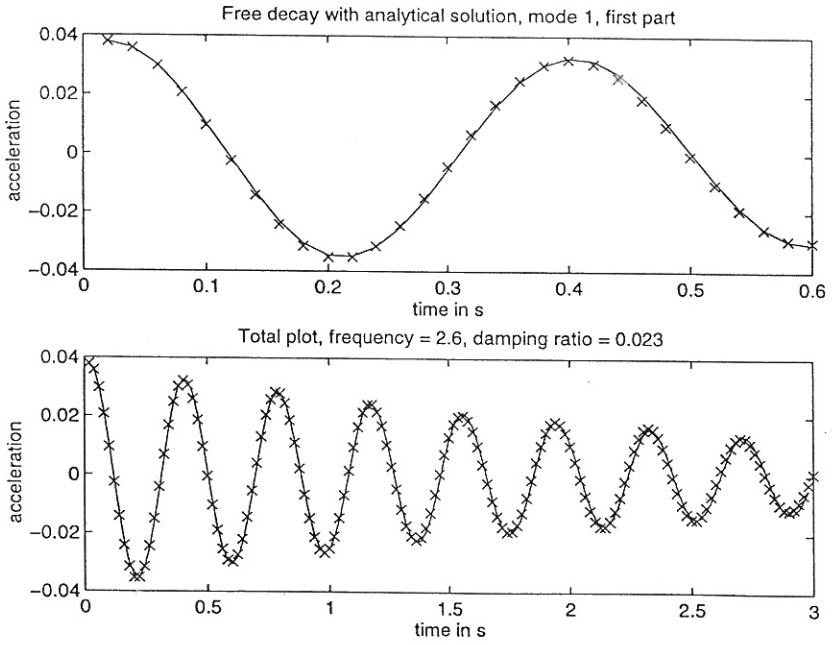

Figure 4.81: Measured and estimated free decay, first rotational mode.

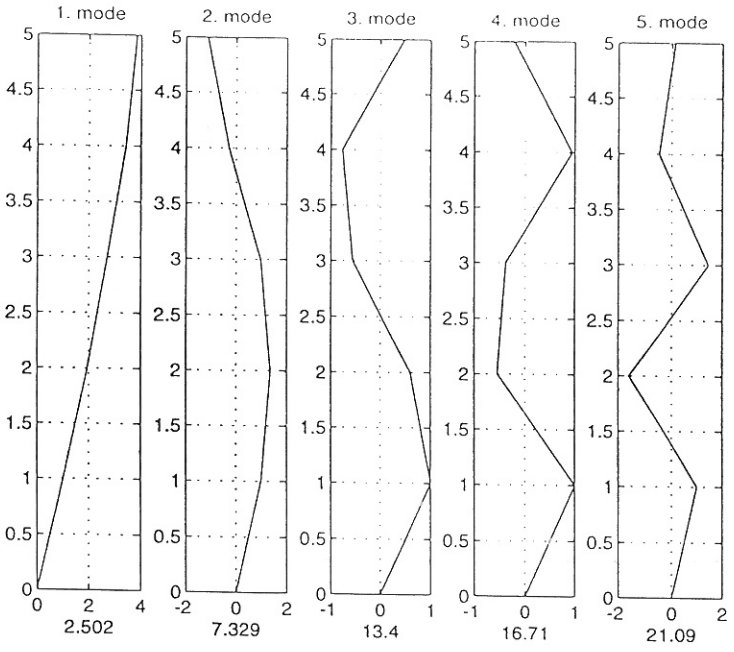

Figure 4.82: Mode shapes of translational modes.

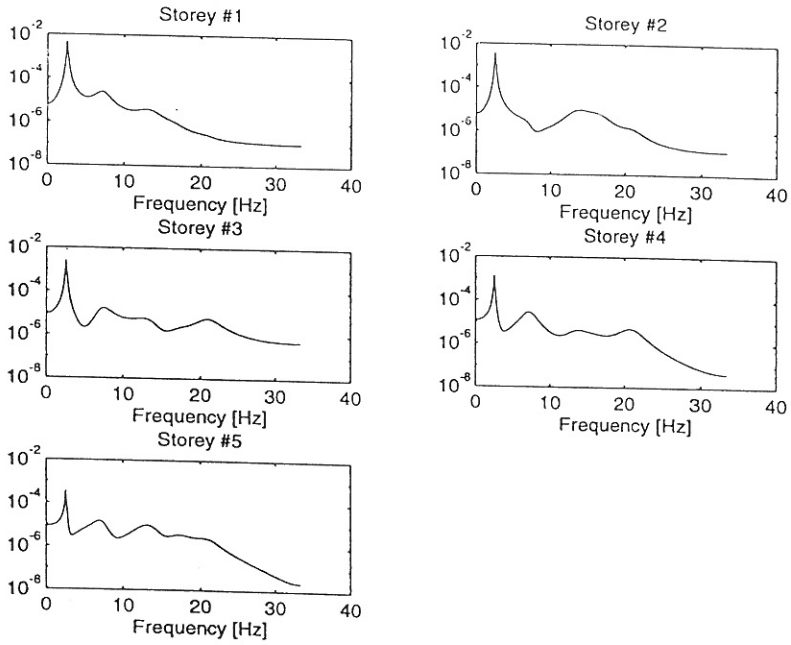

Figure 4.83: Autospectral densities obtained from the model.

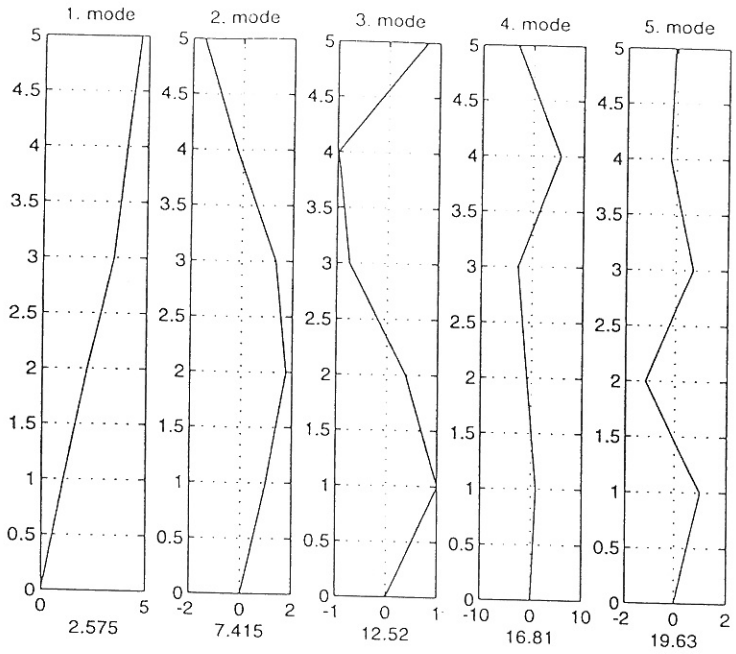

Figure 4.84: Mode shapes of rotational modes.

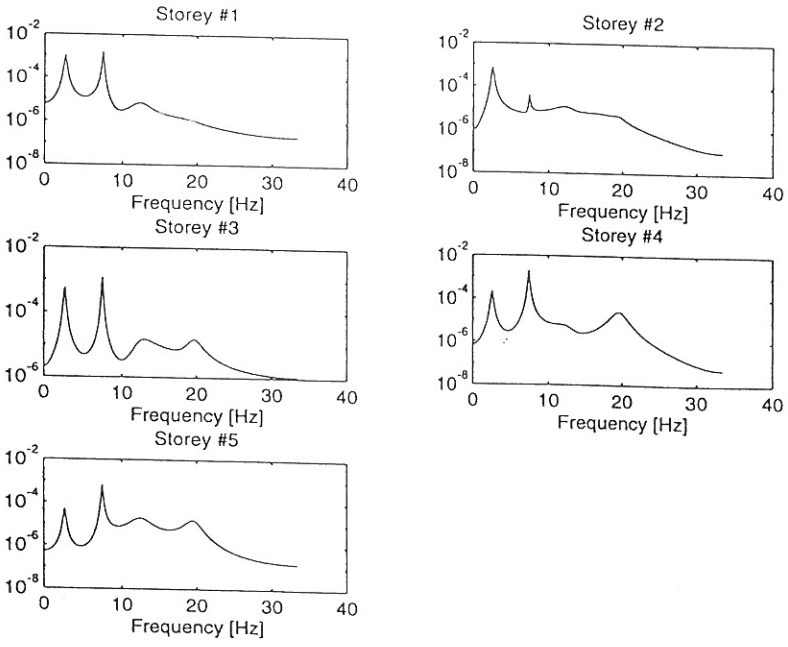

Figure 4.85: Autospectral densities obtained from the model.